Heating and evaporation of droplets of multi-component and blended fuels: A review of recent modelling approaches

Mansour Al Qubeissi [a,b*], Sergei S. Sazhin [c], Nawar Al-Esawi [a,d], Ruslana Kolodnytska [e], Bidur Khanal [b], Mohammed Ghaleeh [d], Ahmed Elwardany [f,g]

[a] *Institute for Future Transport and Cities, Coventry University, Coventry CV1 5FB, United Kingdom*
[b] *School of Mechanical, Aerospace and Automotive Engineering, Faculty of Engineering, Environment and Computing, Coventry University, Coventry CV1 2JH, United Kingdom*
[c] *Advanced Engineering Centre, School of Architecture, Technology and Engineering, University of Brighton, Brighton BN2 4GJ, United Kingdom*
[d] *Faculty of Arts, Science and Technology, University of Northampton, Northampton NN1 5PH, United Kingdom*
[e] *Automotive Engineering Department, Zhytomyr Polytechnic State University, Zhytomyr 10005, Ukraine*
[f] *Fuels and Combustion Engines Laboratory, Energy Resources Engineering Department, Egypt-Japan University of Science and Technology, New Borg El-Arab 21934, Egypt*
[g] *Department of Mechanical Engineering, Faculty of Engineering, Alexandria University, Alexandria 21544, Egypt*

Abstract

In this review, recent models for heating/evaporation of multi-component and blended fuel droplets and their implementation into numerical codes, used for the analysis of the processes in internal combustion engines (ICE), are reviewed. In these models, the diffusion of species, recirculation and temperature gradient inside droplets are considered. The focus of the review is on the group of models based on the implementation of the analytical solutions to the heat transfer and species diffusion equations inside droplets into numerical codes. Four key aspects are summarised: 1) application of the 'Discrete Component (DC)' model and 'Multi-Dimensional Quasi-Discrete model (MDQDM)' to a broad range of fuels, including petrol, Diesel, ethanol and biodiesel fuels and their blends; 2) formulation of fuel surrogates, with a focus on the recently introduced 'Complex Fuel Surrogate Model (CFSM)'; 3) overview of the recently introduced transient algorithm, 'Transient Multi-Dimensional Quasi-Discrete Model (TMDQDM)', for auto-generation of quasi-components; and 4) implementation of the latter into a CFD code for a realistic engineering application to full cycle simulation in internal combustion engines. The original and modified versions of the DC model and MDQDM are evaluated for heating and evaporation of droplets of bio/fossil-fuel (for example, ethanol/petrol/biodiesel/Diesel) blends. These were implemented into commercial CFD software and validated. The feasibility of formulating complex fuel surrogates for fuel blends, their implementation into CFD codes, and their application in the full engine cycle simulation before and after the onset of combustion (autoignition) are described.

Keywords: Biodiesel, Combustion, Diesel, Droplet, Ethanol, Evaporation, Fuel, Heating, Models, Petrol.

Contents

1. Introduction

The sharp increase in demand for energy (mainly from fossil fuels), alongside the worldwide growth in population, is accelerating at 1% annually.[1,2] For instance, combustion engines power 99% of transport sectors, which cause 14% of Greenhouse Gas Emissions (GGE).[1] To reduce GGE and respond to fossil fuel depletion, governments and industries have been shifting the dependency on fossil fuels to renewable energy resources.[3,4] To maintain the use of internal combustion engines (ICE), biofuels (mainly ethanol and biodiesel) can be mixed with, or replace, fossil fuels to reduce GGE.[5,6] Yet, a blend of 10 vol.% ethanol with 90 vol.% petrol (known as E10) fuel can be directly used in petrol (gasoline) engines without the need to tune them.[7] This mixture has also led to a noticeable reduction in CO_2 emissions, and the maintenance of good engine performance.[8] The European Renewable Ethanol Association has defined the reduction in GGE when using E10 in petrol engines as 6%.[9]

Also, the mixture of up to 20% of any variety of biodiesel fuel with Diesel fuels (B20) for direct use in Diesel engines was first regulated in the USA Energy Policy Act of 1992 (EPAct 92).[10] Such mixtures have maintained ICE horsepower, fuel consumption, and torque. Users of B20 fuel, for instance, have not reported any noticeable difference in ICE performance. This blend was found to be economically beneficial and can offer GGE reduction compared with Diesel fuel. These benefits are found to be more meaningful for higher blending ratios with up to 100% biodiesel fuel (B100).[11] Other types of biofuels are also useful for ICE. In accordance with the US federal standards for renewable fuel, E15 (15 vol.% ethanol and 85 vol.% petrol) fuel has been approved as an alternative to petrol fuel since 2001.[12] It is

expected that the increase in ethanol content in the baseline fuel should further reduce the GGE. Likewise, a mixture of 85% Diesel and 15% ethanol can be used in standard Diesel engines with insignificant impact on their performance.[13] In ref 14, a mixture of up to 20% ethanol and 80% Diesel fuel was successfully tested in Diesel engines. Over the last two decades, clear scientific grounds have been established for the appropriate range of bio/fossil-fuel blends to be used in conventional internal combustion engines,[15] which has helped governments to set timely targets for these blends in the baseline fuel. For example, some UK Department for Transport policies have been updated to increase the bio/fossil fuel volume ratios from 4.75% in 2018 to 9.75% in 2020, and to 12.4% in 2032, to meet the required obligations for reducing GGE.[16] Similarly, the US administration has approved the application of E15 in baseline fuels.[17]

The main controlling parameters of mixing different types of fuels are their ignition time and energy release. In a typical internal combustion engine (ICE), the liquid fuel is injected in the form of a spray of droplets into a high pressure ambient air inside a cylinder.[18] The spray is formed due to primary and secondary breakups of these fuel droplets.[15] In the pre-combustion processes, these droplets are heated, evaporated and ignited to release the energy needed to drive the ICE. Fuels are naturally formed of several components. Understanding multi-component fuel droplet heating and evaporation is crucial to the design and optimum operation of ICE.[15,19] These two processes mainly precede the onset of ignition, and can be essential to improving ICE performance.[20] Several issues can be observed when droplets are not heated and evaporated in a timely manner, like incomplete combustion, knocking and high emissions.

Many studies of the modelling of droplet heating and evaporation of multi-component fuels have been presented (e.g., refs. 21–24). However, in most cases, multi-component fuel groups were represented by individual components. For example, petrol fuel was replaced by iso-octane,[25] and Diesel was replaced by n-dodecane.[26,27] Ignoring the presence of multiple components in fuel compositions means that species diffusion during droplet heating and evaporation is ignored or assumed infinitely fast. Also, when dealing with micro-sized droplets, the finite thermal conductivity inside droplets has been ignored in most studies. These assumptions are relied upon to reduce model complexity and central processing unit (CPU) time (e.g., refs. 28,29).

The importance of considering the effects of finite thermal conductivity and species diffusion inside droplets was highlighted in many studies, mainly relying on the 'Effective Thermal Conductivity/Effective Diffusivity (ETC/ED)' models.[30–32] The ETC/ED models accounted for the temperature gradient, species diffusion and recirculating flows inside droplets; these are described in the 'Discrete Component (DC)' model. However, the DC model is computationally expensive when dealing with large numbers of components. Therefore, the DC model was simplified to the 'Quasi-Discrete (QD)'[33,34] model, and 'Multi-Dimensional Quasi-Discrete Model (MDQDM)'[35,36] to account for the contributions of multiple components when attempting to improve the CPU efficiency. Likewise, combustion models were based on the replacement of fuel composition with a certain number of components (described as 'fuel surrogates') to approximate the detailed combustion characteristics of the fuel (e.g., refs. 37,38). These fuel surrogates were commonly used in the models to facilitate the inclusion of unknown chemical mechanisms of middle-chain components and to improve computational efficiency.[39] Most of these studies focused on finding fuel surrogates to mimic the chemical behaviour of realistic multi-component fuels (without considering droplet heating and evaporation) as crucial parameters for the physical delay of fuel combustion and performance of ICE.

Droplet heating and evaporation are the dominant processes preceding the onset of combustion but are complex due to the presence of hundreds of components. Also, the experimental study of these processes is very limited, time consuming and costly. Additionally, the direct numerical simulation of systems with such large numbers of components, including their thermodynamic and transport

properties, are computationally expensive, or impossible to perform. To address this problem, new numerical codes were introduced to implement the analytical solutions to heat transfer and species diffusion equations in the liquid phase (inside droplets) at each time step.[34,35,40,41] The approaches to the development of such codes are summarised in this review, identifying the research gaps, challenges, and where there is room for improvement.

The focus of the review is on the group of models based on the implementation of the analytical solutions to the heat transfer and species diffusion equations inside droplets into numerical codes. These models were originally developed at the University of Brighton (UK),[42] since 2017 these models have been further developed mainly at the University of Coventry (UK) (in collaboration with the University of Brighton (UK)). The review focuses mainly on the results of these developments. These include further developments to the original[30,43] and generalised[44] versions of the DC model, and their applications to the modelling of heating and evaporation of ICE fuels and their bio-fuel blends.[45–47] The original[33–35] and generalised[36] versions of the MDQDM, and the recent advancement in the MDQDM, using the transient algorithm to make it implementable into commercial CFD codes,[41] are presented and discussed. The DC and MDQDM models for the formulation of fuel surrogates,[40,48,49] and the implementation of these models into numerical codes used for combustion simulations are described. A typical example of the full-cycle simulation of the ICE performed using ANSYS Fluent, with the new models implemented into it, is presented.[50] The results are verified and validated, where possible. This review is expected to complement the review published in 2017.[32]

2. Fuel compositions

2.1. Petrol fuel

Petrol is a combination of middle distillate petroleum derivatives, which dominantly consist of C4-C12 hydrocarbons.[51–53] It is a commonly used fuel in the transport sector, mainly in spark ignition ICE (which drive about 80% of passenger vehicles).[38] Therefore, it is essential to fully understand and enhance the combustion characteristics of this fuel. In many previous studies (e.g., refs. 54–57), petrol fuel was replaced with iso-octane for simplicity. Note that commercial petrol fuel consists of hundreds of hydrocarbons.[58] Ignoring this composition of petrol fuel in understanding detailed transient processes, such as multi-component fuel droplet heating and evaporation in ICE, can be crucial in the design of these ICE. Therefore, this review will emphasise the importance of taking into account the effect of this fuel composition.

The results of the studies reviewed in this paper, related to petrol fuel, were based on FACE C (Fuel for Advanced Combustion Engines Type C) petrol fuel. In ref 36, those hydrocarbons with similar thermodynamic and transport properties and the same chemical formulae were replaced by characteristic components, which reduced the original composition of petrol FACE C fuel from 83 (inferred from ref. 38) to 20 components. The composition of petrol fuel was represented by 6 hydrocarbon groups, as shown in Table 1.[36] In our review, the thermodynamic and transport properties of the components of petrol fuel were inferred from ref. 15, while those of ethanol were inferred from refs. 59–61.

Table 1. Molar composition (%) of petrol FACE C fuel.[36]

Carbon no	n-alkanes	iso-alkanes	alkylbenzenes	cycloalkanes	naphthalenes	olefins
C4	3.905	0.092	-	-	-	-
C5	13.87	7.456	-	-	-	-
C6	10.842	2.98	-	-	-	-
C7	-	11.67	-	-	-	-
C8	-	42.17	0.242	1.49	-	-

C9	-	0.137	3.521	-	0.104	0.346
C10	0.01	0.36	0.44	-	-	-
C11	-	0.113	0.055	-	-	-
C12	0.012	-	-	-	-	-
Total %	28.64	64.98	4.26	1.49	0.104	0.346

2.2. Diesel fuel

In ref. 35, similarly to the case of petrol fuel, the full composition of Diesel fuel (containing more than one hundred components, obtained using comprehensive two-dimensional gas chromatography)[62] was simplified to 98 hydrocarbons, based on the overlapping thermodynamic and transport properties. This commercial Diesel fuel conformed to standard European Union fuel (EN590). The simplified fuel composition was formed of 6 groups and 3 characteristic components: tricycloalkane ($C_{19}H_{34}$, with 0.015647 molar fraction), diaromatic ($C_{13}H_{12}$, with 0.01224 molar fraction) and phenanthrene ($C_{14}H_{10}$, with 0.006577 molar fraction). The molar fractions of the components in the 6 hydrocarbon groups of Diesel fuel are presented in Table 2.

Table 2. Molar fraction (%) of Diesel fuel components.[35]

Carbon no	alkanes	cycloalkanes	bicycloalkanes	alkylbenzenes	indanes & tetralines	naphthalenes
C8	0.308	-	-	0.497	-	-
C9	3.032	-	-	3.2357	-	-
C10	5.0541	0.6408	0.6926	5.3584	1.3157	1.9366
C11	3.163	1.8745	1.0524	0.9492	1.3632	2.5290
C12	2.6156	1.6951	0.9753	1.9149	1.1951	1.4012
C13	2.5439	1.2646	0.6611	0.6873	1.0652	0.7692
C14	2.6497	1.3633	0.5631	0.6469	0.8406	0.4879
C15	3.1646	1.2353	0.4314	0.4782	0.7051	0.3843
C16	2.6579	1.0449	0.4921	0.4564	0.6684	0.2854
C17	2.8605	1.0162	0.6529	0.4204	0.5598	0.2072
C18	3.2403	1.2848	0.6554	0.5234	0.5357	0.2358
C19	3.5296	1.3566	0.9901	0.3226	0.3403	0.2151
C20	2.2338	0.9961	0.1965	0.2848	0.3227	0.2256
C21	1.443	0.5374	0.0935	0.2032	0.1638	-
C22	0.799	0.304	0.0701	0.0969	0.0781	-
C23	0.3972	0.109	0.0488	0.0494	-	-
C24	0.1903	0.0755	0.0234	0.0473	-	-
C25	0.0997	0.0445	0.0169	-	-	-
C26	0.0425	0.0214	-	-	-	-
C27	0.0309	0.0155	-	-	-	-
Total %	40.65	14.88	7.62	16.17	9.15	8.68

2.3. Biodiesel fuels

Twenty-two types of 'Fatty Acid Methyl Ester (FAME)' biodiesel fuels were used in refs. 63–65 to investigate heating and evaporation of biodiesel fuel droplets. These were: Rapeseed methyl ester (RME), Soybean methyl ester (SME), Palm methyl ester (PME), Palm kernel methyl ester (PMK), Sunflower methyl ester (SNE), Linseed methyl ester (LNE), Safflower methyl ester (SFE), Hemp-oil methyl ester – Ukrainian (HM1), Hemp-oil methyl ester – European Union (HM2), Waste cooking-oil methyl ester (WCO), Tallow methyl ester (TME), Lard methyl ester (LME), Jatropha methyl ester (JTR)

and Yellow grease methyl ester (YGR), Butter methyl ester (BME), Coconut methyl ester (CME), Peanut methyl ester (PTE), Cottonseed methyl ester (CSE), Corn methyl ester (CNE), Tung methyl ester (TGE), Canola seed methyl ester (CAN), and Camelina methyl ester (CML). The molar fractions of the components of these biodiesel fuels are shown in Tables 3 and 4. The liquid and vapour diffusion coefficients were inferred from refs. 15,44,66.

Table 3. Compositions of FAME biodiesel fuels (the double-bond numbers in each component's structure are indicated after the colon in each FAME code as: 0,1,2,3,4).[63]

FAME	Biodiesel Fuels										
	TME	LME	BME	CME	PMK	PME	SFE	PTE	CSE	CNE	SNE
C8:0	-	-	5.2	6.0	2.6	-	-	-	-	-	-
C10:0	-	-	2.8	8.0	4.0	-	-	-	-	-	-
C12:0	0.2	-	3.4	50.0	50.0	0.3	-	-	-	-	-
C14:0	2.5	1.0	11.0	15.0	17.0	1.3	-	0.5	2.0	1.0	-
C15:0	-	-	-	-	-	-	-	-	-	-	-
C16:0	27.9	26.0	31.7	9.0	8.0	45.1	5.2	8.0	19.0	9.0	5.9
C17:0	-	-	-	-	-	-	-	-	-	-	-
C18:0	23.0	14.0	10.8	3.0	1.7	4.5	2.2	4.0	2.0	2.5	4.2
C20:0	0.4	-	0.4	-	1.5	0.4	-	7.0	-	-	1.4
C22:0	0.4	-	0.4	-	1.5	0.2	-	7.0	-	-	1.4
C24:0	-	-	-	-	-	-	-	-	-	-	-
C16:1	2.5	2.8	2.4	-	0.4	0.2	-	1.5	-	1.5	-
C17:1	-	-	-	-	-	-	-	-	-	-	-
C18:1	40.0	44.0	26.3	7.0	12.0	38.4	76.4	49.0	31.0	40.0	18.5
C20:1	0.3	2.0	1.0	-	-	-	-	-	2.5	1.0	-
C22:1	0.3	2.0	1.0	-	-	-	-	-	2.5	1.0	-
C24:1	-	-	-	-	-	-	-	-	-	-	-
C18:2	2.0	8.0	3.0	2.0	1.3	9.2	16.2	23.0	41.0	44.0	68.3
C20:2	-	-	-	-	-	-	-	-	-	-	-
C18:3	-	-	0.6	-	-	0.2	-	-	-	-	0.3
C20:3	-	-	-	-	-	-	-	-	-	-	-
C18:4	-	-	-	-	-	-	-	-	-	-	-
Others	0.5	0.2	-	-	-	0.2	-	-	-	-	-

Table 4. Biodiesel fuel compositions (continuation of Table 3).

FAME	Biodiesel Fuels										
	TGE	HM1	SME	LNE	HM2	CAN	WCO	RME	CML	JTR	YGR
C8:0	-	-	-	-	-	-	-	-	-	-	-
C10:0	-	-	-	-	-	-	-	-	-	-	-
C12:0	-	-	-	-	-	-	0.2	-	0.4	0.1	0.2
C14:0	-	-	0.3	0.2	-	-	0.7	-	2.6	0.3	0.8
C15:0	-	-	-	-	-	-	-	-	-	-	0.1
C16:0	3.6	6.6	10.9	6.2	6.5	4.5	15.7	4.9	5.8	14.3	16.0
C17:0	-	0.2	-	-	-	0.1	0.2	-	-	0.1	0.1
C18:0	2.6	2.1	4.4	0.6	2.5	2.0	6.1	1.7	2.7	5.9	6.9
C20:0	-	0.5	0.4	-	0.9	0.6	0.4	0.6	1.3	0.2	0.3
C22:0	13.1	0.3	-	-	-	0.4	0.4	-	0.9	0.2	0.4
C24:0	-	0.2	-	-	-	0.2	0.3	-	0.7	2.5	0.2
C16:1	-	0.3	-	-	-	0.4	0.7	-	-	1.0	0.9
C17:1	-	-	-	-	-	-	-	-	-	-	0.1
C18:1	10.1	11.9	24.0	18.0	11.9	59.7	42.8	26.6	15.9	38.9	43.2
C20:1	0.8	0.3	-	-	0.9	1.5	0.6	-	13.7	0.1	0.5
C22:1	-	0.2	-	-	-	0.4	0.2	22.3	2.9	0.1	0.1
C24:1	-	0.2	-	-	-	-	-	0.8	0.2	0.1	4.3
C18:2	13.8	56.6	52.8	16.0	54.7	20.8	29.4	24.8	16.0	34.8	24.3
C20:2	-	-	-	-	-	-	-	-	1.4	-	-
C18:3	51.6	20.6	7.2	59.0	20.1	9.4	2.0	9.7	33.8	0.3	1.1
C20:3	-	-	-	-	-	-	-	-	0.8	-	-
C18:4	-	-	-	-	-	-	-	-	-	-	0.5
Others	4.4	-	-	-	2.5	-	0.3	8.6	0.9	1.1	-

3. Discrete component model

Some of the early developments of the 'Discrete Component (DC)' model were introduced in refs. 43,67,68 to describe the evaporation process in Diesel and petrol fuel droplets. The analyses presented in those studies were based on some simplified solutions to the quasi-steady state equations for heat transfer and species diffusion, which were in turn based on the Effective Thermal Conductivity/Effective Diffusivity (ETC/ED) models (to be described in Sections 3.1 and 3.3). Significant differences were obtained between the predictions of the DC model and those predicted using a 'Single Component (SC)' model. The DC model was applied to the analysis of mixed biodiesel/Diesel fuel droplets.[29] The predictions of ref. 29 showed that increasing the biodiesel fractions in biodiesel/Diesel fuel increased the evaporation time and droplet surface temperature.

In ref. 69, blended Diesel/biodiesel fuel droplet heating and evaporation was analysed using a 'hybrid DC approach', where the continuous thermodynamic model for Diesel fuel and the DC model for biodiesel fuel were used. The study showed that the blended fuel droplet evaporation time increased at higher mass fractions of biodiesel in biodiesel/Diesel fuel blends, which was attributed to the lower volatility of FAME in biodiesel fuel compared to that of hydrocarbons in Diesel fuel. In the same study, the hybrid approach was also applied to the analysis of blended ethanol/petrol fuel droplet heating

and evaporation. It was found that the droplet lifetime of this blend increased at higher mass fractions of ethanol; this was attributed to the higher latent heat of vaporisation of ethanol.

The complete version of the DC model was applied to bi-component fuels.[30] It was used to simulate droplets with 105 components.[45] In ref. 44, the heating and evaporation processes of four types of biodiesel fuel (Soybean, Hemp oil, Rapeseed and Palm), consisting of FAME groups, were analysed using this model. It was found that the approximation of biodiesel fuels by single components led to 5.5% underprediction of droplet lifetime compared to the prediction of the DC model. In ref. 63, the same model was applied to 22 types of biodiesel fuel. Firstly, the detailed DC model was considered, based on the ED/ETC models, taking into account the recirculation, temperature gradient and contribution of all methyl esters in the biodiesel fuels and their diffusion inside droplets. Secondly, the DC model was considered, but the thermal conductivity and species diffusion coefficient were assumed to be infinitely large, based on the 'Infinite Thermal Conductivity/Infinite Diffusivity (ITC/ID)' models.[70] Thirdly, the DC model was used, but the molar fractions were based on the initial fuel composition ignoring diffusion of species, that is using the SC model. The SC model predicted up to 5.5% and 2.4% errors in droplet lifetime and surface temperature, respectively, compared to the prediction of the first (DC) model. The DC model described in this review is the version based on the analytical solutions to the heat transfer and species diffusion equations inside the droplets at each time step, which were implemented into a numerical code.[71,72] The details of this model are described in the following sections.

3.1. Effects of droplet finite thermal conductivity

The heating of spherical moving droplets is described by the transient heat conduction equation:[73–75]

$$\frac{\partial T}{\partial t} = \kappa\left(\frac{\partial^2 T}{\partial R^2} + \frac{2}{R}\frac{\partial T}{\partial R}\right), \tag{1}$$

where $T = T(t, R)$ is the temperature in the liquid phase, t is time, R is the distance from the centre of the droplet, and κ is the effective thermal diffusivity:[76,77]

$$\kappa = k_{\text{eff}}/c_l\rho_l, \tag{2}$$

k_{eff} is the Effective Thermal Conductivity (ETC), c_l is the liquid specific heat capacity, ρ_l is the liquid density. The ETC is defined as:[78]

$$k_{\text{eff}} = \chi k_l, \tag{3}$$
$$\chi = 1.86 + 0.86\tanh\left[2.225\log_{10}\left(\text{Pe}_{d(l)}/30\right)\right], \tag{4}$$

$\text{Pe}_l = \text{Re}_{d(l)}\text{Pr}_l$ is the Peclet number, $\text{Pr}_l = \frac{c_l\mu_l}{k_l}$ is the liquid phase Prandtl number, $\text{Re}_{\text{d}(l)} = \frac{2\rho_l U_s R_d}{\mu_l}$ is the liquid phase Reynolds number, $U_s = \frac{1}{32}\Delta U\left(\frac{\mu_g}{\mu_l}\right)\text{Re}_d C_F$ is the maximum liquid surface velocity inside the droplet, $\Delta U = \left|U_g - U_d\right|$ is the relative velocity between the gas flow and droplet velocities, $C_F = \frac{12.69}{\text{Re}_d{}^{2/3}(1+B_M)}$ is the skin friction drag coefficient, Re_d is the Reynolds number in the gas phase based on the droplet diameter, B_M is the Spalding mass transfer number defined by Expression (15),[31] μ_l and k_l are the dynamic viscosity and thermal conductivity in the liquid phase, respectively. In the case of stationary droplets, χ in Equation (4) reduces to 1. The model based on the concept of Effective Thermal Conductivity is commonly called the 'Effective Thermal Conductivity' (ETC) model.

The initial and boundary conditions for Equation (1) are:

$$\left.\begin{aligned} T(t=0) &= T_{d0}(R) \\ h\left(T_g - T_s\right) &= k_{\text{eff}}\left.\frac{\partial T}{\partial R}\right|_{R=R_d-0} \end{aligned}\right\}, \tag{5}$$

where $T_s = T_s(t)$ is the droplet surface temperature, $T_g = T_g(t)$ is the ambient gas temperature, R_d is the droplet radius, and $h = h(t)$ is the convective heat transfer coefficient inferred from the Nusselt number (Nu) as:

$$h = \mathrm{Nu}\, k_g / 2R_d, \tag{6}$$

k_g is the thermal conductivity of ambient gas. In boundary condition (5) only the contribution of convective heating was considered.

Assuming that the droplet is an opaque and non-reflective (emissivity equal to 1) sphere and taking into account the effects of evaporation and radiation, the boundary condition at the droplet surface (5) can be generalised to:

$$k_{\mathrm{eff}} \left.\frac{\partial T}{\partial R}\right|_{R=R_d-0} = \rho_l L \frac{dR_d}{dt} + h\left(T_g - T_s\right) + \sigma T_{\mathrm{rad}}^4, \tag{7}$$

where $\frac{dR_d}{dt} = \dot{R}_{dE}$ is the rate of droplet radius change due to evaporation (see Expression (32)), L is the latent heat of evaporation, σ is the Stefan-Boltzmann constant (σ =5.6703 10^{-8} W m^{-2}K^{-4}), T_{rad} is the radiative temperature, which is assumed equal to the gas temperature in the case of optically thick gas, and to the external temperature in the case of optically thin gas.

The analyses considered in this review focused on the case of optically thin gas, where the maximal impact of thermal radiation is expected under engine-like conditions. The emitted radiation from the droplet to the ambient gas (σT_d^4) was ignored, compared with the strong external radiation flux (e.g., from remote flames) to the droplet $\sigma T_{\mathrm{rad}}^4$.

The analytical solution to Equation (1) at the end of each time step ($t = t_1$) was obtained as:[42]

$$T(R,t) = \frac{R_d}{R} \sum_{n=1}^{\infty} \begin{Bmatrix} q_n \exp[-\kappa_R \lambda_n^2 t] - \frac{\sin\lambda_n}{\|v_n\|^2 \lambda_n^2} \mu_0(0) \exp[-\kappa_R \lambda_n^2 t] \\ -\frac{\sin\lambda_n}{\|v_n\|^2 \lambda_n^2} \int_0^t \frac{d\mu_{0(\tau)}}{d\tau} \exp[-\kappa_R \lambda_n^2 (t-\tau)] d\tau \end{Bmatrix} \sin\left(\lambda_n \frac{R}{R_d}\right) + T_{\mathrm{eff}}(t), \tag{8}$$

where $\|v_n\|^2 = \frac{1}{2}\left(1 - \frac{\sin 2\lambda_n}{2\lambda_n}\right) = \frac{1}{2}\left(1 + \frac{h_{0T}}{h_{0T}^2 + \lambda_n^2}\right)$, $q_n = \frac{1}{R_d \|v_n\|^2} \int_0^{R_d} \tilde{T}_0(R) \sin\left(\lambda_n \frac{R}{R_d}\right) dR$, $\tilde{T}_0(R) = R\, T_{d0}(R)/R_d$, $k_R = \frac{k_{\mathrm{eff}}}{c_l \rho_l R_d^2}$, $\mu_0(t) = \frac{h T_g(t) R_d}{k_{\mathrm{eff}}}$, $h_{l0} = \left(\frac{h R_d}{k_{\mathrm{eff}}}\right) - 1$. The eigenvalues λ_n, $n > 0$ ($\lambda = 0$ is excluded), were found from the solution to the following relationship:

$$\lambda \cos\lambda + h_{l0} \sin\lambda = 0, \tag{9}$$

The effective temperature T_{eff} was calculated, taking into account the effects of radiation and droplet evaporation, as:

$$T_{\mathrm{eff}} = T_g + \frac{\rho L \frac{dR_d}{dt}}{h} + \frac{\sigma T_{\mathrm{rad}}^4}{h}. \tag{10}$$

Within each time step Δt, R_d is constant and updated at the end of Δt, as $R_{d(new)} = R_{d(old)} + \dot{R}_d \Delta t$, where the value of $\dot{R}_d$ takes into account the droplet evaporation rate and thermal swelling. In the limit $k_{\mathrm{eff}} \to \infty$, Expression (8) reduces to that of the 'Infinite Thermal Conductivity' (ITC) model.[27] Nu was calculated for an isolated moving droplet, as:[76]

$$\mathrm{Nu}_{\mathrm{iso}} = 2 \frac{\ln(1+B_T)}{B_T} \left[1 + \frac{(1+\mathrm{Re_d Pr_d})^{1/3} \max\{1, \mathrm{Re_d}^{0.077}\} - 1}{2\, F(B_T)}\right], \tag{11}$$

where $F(B_T) = (1+B_T)^{0.7} \frac{\ln(1+B_T)}{B_T}$, B_T is the Spalding heat transfer number:

$$B_T = \frac{C_{pv}(T_g - T_s)}{L_{\mathrm{eff}}}, \tag{12}$$

c_{pv} is the specific heat capacity of the fuel vapour at constant pressure, L_{eff} is the effective latent heat of evaporation, calculated as:

$$L_{\text{eff}} = L + \frac{Q_L}{\dot{m}_d} = \sum_i \epsilon_i L_i + \frac{Q_L}{\sum_i \dot{m}_i}, \quad (13)$$

$\epsilon_i = \epsilon_i(t)$ are the evaporation rates of species i, $\dot{m}_i = \epsilon_i \, \dot{m}_d$ ($\dot{m}_d = \sum_i \dot{m}_i$), and Q_L is the power spent on heating the droplet. The interactions between droplets are ignored; they were discussed in refs. 77,79,80.

3.2. Effects of droplet evaporation

The total evaporation rate of a multi-component fuel droplet is weakly dependent on the individual species diffusion rates from the droplet surface to the gas phase.[30,79] Therefore, it is not always necessary to consider the relative diffusion among individual species in the gas phase.[32,43] The total evaporation rate of an isolated droplet ($\dot{m}_d$) was calculated as:[15]

$$\dot{m}_d = -2\pi R_d D_v \rho_{\text{total}} B_M \, \text{Sh}_{\text{iso}}, \quad (14)$$

where $\dot{m}_d \leq 0$, D_v is the coefficient of binary vapour diffusion in ambient gas, $\rho_{\text{total}} = \rho_g + \rho_v$ is the total mixture density, summed up, of the vapour (ρ_v) and gas (ρ_g) densities, the Spalding mass transfer number (B_M) is calculated as:[81]

$$B_M = \frac{\rho_{vs} - \rho_{v\infty}}{1 - \rho_{vs}} = \frac{Y_{vs} - Y_{v\infty}}{1 - Y_{vs}}, \quad (15)$$

ρ_{vs} and $\rho_{v\infty}$ are the densities of fuel vapour in the vicinity of the droplet surface and far from it, respectively, Y_v is the mass fraction of fuel vapour, the Sherwood number for isolated droplets (Sh_{iso}) is calculated as:[76]

$$\text{Sh}_{\text{iso}} = 2\frac{\ln(1+B_M)}{B_M}\left[1 + \frac{(1+\text{Re}_\text{d}\text{Sc}_\text{d})^{1/3}\max\{1, \text{Re}_\text{d}^{0.077}\} - 1}{2\,F(B_M)}\right], \quad (16)$$

Sc_d is the gas phase Schmidt number, $F(B_M)$ is the same as in (11) but with B_T replaced by B_M.[82] B_T and B_M are linked by the following relationship:[76]

$$B_T = (1 + B_M)^{\varphi} - 1, \quad (17)$$

$$\varphi = \left(\frac{c_{pv}}{c_{pa}}\right)\left(\frac{\text{Sh}^*}{\text{Nu}^*}\right)\frac{1}{\text{Le}}, \quad (18)$$

$\text{Le} = k_g/\left(c_{pa}\,\rho_g\,D_v\right)$ is the Lewis number. The modified Sherwood number Sh^* and the modified Nusselt number Nu^* are determined from:[83]

$$\text{Sh}^* = 2\left[1 + \frac{(1+\text{Re}_d\text{Sc}_d)^{1/3}\max\{1,\text{Re}_d^{0.077}\} - 1}{2F(B_M)}\right], \quad (19)$$

$$\text{Nu}^* = 2\left[1 + \frac{(1+\text{Re}_d\text{Pr}_d)^{1/3}\max\{1,\text{Re}_d^{0.077}\} - 1}{2F(B_T)}\right]. \quad (20)$$

For stationary droplets $\frac{\text{Sh}^*}{\text{Nu}^*} = 1$. For slowly moving droplets, this ratio was also sometimes assumed equal to 1 (e.g., refs. 43,84). Such an assumption was invalid in some cases.[83] Hence, in our recent models, Expressions (19) and (20) were used to estimate φ based on Equation (18).

When calculating the rate of change in droplet radius ($\dot{R}_d$), both thermal swelling and droplet evaporation were accounted for during each time step:[85]

$$\dot{R}_d = \dot{R}_{dT} + \dot{R}_{dE}, \quad (21)$$

where $\dot{R}_{dT}$ is the rate of change in droplet radius due to thermal expansion or contraction:[85]

$$\dot{R}_{dT} = \frac{R_d(T_{av,0})}{\Delta t}\left[\left(\frac{\rho_l(T_{av,0})}{\rho_l(T_{av,1})}\right)^{1/3} - 1\right], \quad (22)$$

$T_{av,0}$ and $T_{av,1}$ are average droplet temperatures at the timestep beginning ($t = t_0$) and end ($t = t_1$). The rate of change in droplet radius caused by evaporation ($\dot{R}_{dE}$) is determined as:[43]

$$\dot{R}_{dE} = \frac{\dot{m}_d}{4\pi R_d^2 \rho_l}. \quad (23)$$

3.3. Effects of species diffusion

In moving droplets, the species mass fractions in the liquid phase $Y_{li} \equiv Y_{li}(t, R)$ are described by the following species diffusion equations:[30]

$$\frac{\partial Y_{li}}{\partial t} = D_{\text{eff}}\left(\frac{\partial^2 Y_{li}}{\partial R^2} + \frac{2}{R}\frac{\partial Y_{li}}{\partial R}\right), \quad (24)$$

where i is the species index, D_{eff} is the effective species diffusion coefficient in the liquid phase, calculated as:[86]

$$D_{\text{eff}} = \chi_Y D_l, \quad (25)$$

$$\chi_{\text{Y}} = 1.86 + 0.86\tanh\left[2.225\log_{10}\left(\text{Re}_{\text{d}(l)}\text{Sc}_l/30\right)\right], \quad (26)$$

D_l is the liquid diffusion coefficient, v_l is the liquid kinematic viscosity, $\text{Sc}_{\text{d}(l)} = \frac{v_l}{D_l}$ is the Schmidt number in the liquid phase, and $\text{Re}_{\text{d}(l)}$ is the Reynolds number in the liquid phase, as in Expression (4). In the case of a stationary droplet, χ_{Y} reduces to 1. The set of Equations (24)-(26) describe the Effective Diffusivity (ED) model.[19,76] The following boundary conditions are applied to solve Equations (24):[43]

$$\alpha(\epsilon_i - Y_{lis}) = -D_{\text{eff}}\frac{\partial Y_{li}}{\partial R}\Big|_{R=R_d-0}, \quad (27)$$

where $Y_{lis} = Y_{lis}(t)$ are liquid component mass fractions at the droplet surface, and:

$$\alpha = \left|\dot{R}_{dE}\right|. \quad (28)$$

Assuming that the ambient gas is a dry air (without vapour species), the values of ϵ_i are obtained from refs. 30,87,88, as:

$$\epsilon_i = \frac{Y_{vis}}{\sum_i Y_{vis}}. \quad (29)$$

The initial condition for mass fractions of species was presented as $Y_{li}\ (t = 0) = Y_{li0}(R)$, leading to the analytical solution to Equation (24):[30,43]

$$Y_{li} = \epsilon_{\text{i}} + \frac{1}{R}\left\{\begin{array}{l}\left[\exp\left[D_{\text{eff}}\left(\frac{\lambda_0}{R_d}\right)^2 t\right][q_{i0} - \epsilon_i Q_0]\sinh\left(\lambda_0\frac{R}{R_d}\right) + \\ \sum_{\text{n}=1}^{\infty}\left[\exp\left[-D_{\text{eff}}\left(\frac{\lambda_n}{R_d}\right)^2 t\right][q_{in} - \epsilon_i Q_n]\ \sin\left(\lambda_n\frac{R}{R_d}\right)\right.\end{array}\right\}, \quad (30)$$

where λ_0 and λ_n are calculated from equations $\tanh\lambda_0 = -\lambda_0/h_{0Y}$ and $\tanh\lambda_n = -\lambda_n/h_{0Y}$ (for $\text{n} \geq 1$), respectively, $h_{0Y} = -\left(1 + \frac{\alpha R_d}{D_{\text{eff}}}\right)$,

$$Q_n = \left\{\begin{array}{ll} -\frac{1}{\|v_o\|^2}\left(\frac{R_d}{\lambda_0}\right)^2(1 + h_0)\sinh\lambda_0 & \text{when}\ \ n = 0 \\ \frac{1}{\|v_n\|^2}\left(\frac{R_d}{\lambda_n}\right)^2(1 + h_{0Y})\sin\lambda_n & \text{when}\ \ n \geq 1 \end{array}\right\}, \quad (31)$$

$\|v_n\|^2 = \frac{1}{2}\left(1 - \frac{sin\ 2\lambda_n}{2\lambda_n}\right) = \frac{1}{2}\left(1 + \frac{h_{0Y}}{h_{0Y}^2 + \lambda_n^2}\right)$, and:

$$q_{in} = \left\{ \begin{array}{ll} \frac{1}{\|v_0\|^2} \int_0^{R_d} R\, Y_{li0}(R) \sinh\left(\lambda_0 \frac{R}{R_d}\right) dR & \text{when } n = 0 \\ \frac{1}{\|v_n\|^2} \int_0^{R_d} R\, Y_{li0}(R) \sin\left(\lambda_n \frac{R}{R_d}\right) dR & \text{when } n \geq 1 \end{array} \right\}. \quad (32)$$

Solution (30) was incorporated into the numerical code, which was used in the analysis of droplet heating and evaporation.[89] The calculations of fuel properties in the liquid phase were based on the average droplet temperatures $\left(T_{av} = \frac{3}{R_d^3} \int_0^{R_d} R^2 T(R)\, \mathrm{d}R\right)$. The calculations of fuel properties in the vapour phase were based on the reference temperature $\left(T_r = \frac{2}{3} T_s + \frac{1}{3} T_g\right)$. The ideal gas law was used for the calculation of ambient gas density. The calculations of latent heat of evaporation and vapour pressure at saturation point were performed at the surface temperature of the droplet T_s.

3.4. Effects of activity coefficient

The activity coefficient (AC) is a controlling parameter in determining the vapour molar fractions of individual species at the surface of a droplet (X_{vis}). The latter is estimated as:

$$X_{vis} = \gamma_i \frac{X_{lis}\, p_{is}^{\mathrm{sat}}}{\varphi_i p}, \quad (33)$$

where X_{lis} is the molar fraction of the i^{th} species in the liquid phase at the droplet surface, γ_i is the AC of the i^{th} species, p_{is}^{sat} is the saturated pressure at the droplet surface of the i^{th} species (determined in the absence of other species), φ_i is the fugacity coefficient (or the ratio of fugacity/pressure), and p is the total ambient pressure. For the parameters used in this review, it can be assumed that the fugacity coefficient is $\varphi_i = 1$ due to the ideal gas phase assumption.[54]

Ref. 90 emphasised that it was necessary to calculate the AC. This suggestion was made in contrast to several previous publications (e.g., refs. 35,36,63,91,92) in which it was assumed that $\gamma_i = 1$, which reduces (33) to Raoult's law. The UNIFAC model was implemented in ref. 90 for the calculation of AC, which could then be applied to a broad range of fuel blends, including 21 components of ethanol/petrol, 114 components of biodiesel/Diesel, and 119 components of E85-Diesel fuel blends. The UNIFAC model takes into account the contributions of the combinatorial (C) and residual (R) terms, to account for the excess entropy and excess enthalpy, respectively. The excess entropy was based on the shapes and sizes of molecules and their atomic functional groups, and the excess enthalpy was based on the interactions among molecules, or among the molecular groups.[93,94] The AC of the i^{th} species in a multi-component mixture was calculated using the following UNIFAC equation:[95]

$$\ln \gamma_{\mathrm{i}} = \ln \gamma_{\mathrm{i}}^{\mathrm{C}} + \ln \gamma_{\mathrm{i}}^{\mathrm{R}} \quad (34)$$

where the combinatorial part is $\ln \gamma_{\mathrm{i}}^{\mathrm{C}} = \ln \frac{\Phi_i}{X_i} + \frac{z}{2} q_i \ln \frac{\theta_i}{\Phi_i} + l_i - \frac{\Phi_{\mathrm{i}}}{X_i} \sum_{\mathrm{j}} X_j l_j$, the residual part is $\ln \gamma_i^R = \sum_k v_k^i (\ln \Gamma_k - \ln \Gamma_k^i)$, v_k^i is the number of groups in the i^{th} molecule, $\theta_i = \frac{q_i X_i}{\sum_j q_j X_j}$ is the area fraction of each molecule in the mixture, $\theta_m = \frac{Q_m X_m}{\sum_n Q_m X_m}$ is the area fraction of group m molecules, $l_i = \frac{Z}{2}(r_i - q_i) - (r_i - 1)$, $Z = 10$, $r_i = \sum_k v_k^i R_k$ is the volume parameter, $q_i = \sum_k v_k^i Q_k$ is the surface parameter, $\Phi_i = \frac{r_i X_i}{\sum_j r_j X_j}$ is the volume fraction of each molecule, $\ln \Gamma_k = Q_k \left[1 - \ln(\sum_m \theta_m \psi_{mk}) - \sum_m \frac{\theta_m \psi_{km}}{\sum_n \theta_n \psi_{nm}}\right]$, X_i is the molar fraction of the i^{th} liquid component (identical to X_{lis} in Equation (33)), X_m is the molar fraction of group m molecules, $\psi_{mn} = e^{-\left(\frac{a_{mn}}{T}\right)}$ is the interaction coefficient, T is the interface temperature, a_{mn} is the group-interaction parameter between groups m and n, R_k are the van der Waals volumes, and Q_k are the van der Waals surface areas.[94,95] Both R_k and Q_k are dependent on the characteristics of the group; e.g., bonding angles, bonding distances, shapes, and contact

distances.[96] The van der Waals values, R_k and Q_k, and the interaction parameters a_{mn} were calculated in ref. 90 for selected molecular groups in fuels, as shown in Tables 5 and 6, respectively.

Table 5. Van der Waals volumes (R_k) and surface areas (Q_k) for various fuel chemical groups.[90]

Chemical group	m-group	R_k	Q_k
alkanes	1	0.9011	0.848
		0.6744	0.540
		0.4469	0.228
olefin	2	1.3454	1.176
benzene	3	0.5313	0.400
alkylbenzenes	4	1.2663	0.968
		1.0396	0.660
		0.8121	0.348
ethanol	5	1.0000	1.200
methyl ester	11	1.6764	1.188

Table 6. Interaction parameters (a_{mn}) between m and n groups, used in the UNIFAC model.[90]

m-group	a_{mn} (in K) for each n-group number					
	n = 1	2	3	4	5	11
1	0.0	86.02	61.13	76.50	986.5	232.11
2	−35.36	0.0	38.81	74.15	524.1	37.85
3	−11.12	3.446	0.0	167.0	636.1	5.994
4	−69.70	−113.6	−146.8	0.0	803.2	5688
5	156.4	457.0	89.6	25.82	0.0	101.1
11	114.8	132.1	85.84	−170.0	245.4	0.0

It was emphasised in ref. 90 that the same values of R_k and Q_k and structures of groups as those presented in Tables 5 and 6 apply to other fuel types and blends (e.g., E85-Diesel fuel blends) that consist of the same molecules. If different molecules are detected, the structures of these molecules are approximated by the structures for which R_k and Q_k can be defined.[90] Such approximation, originally suggested in ref. 47, is useful for the prediction of the ACs of all components of fuels and fuel blends. In the case of ethanol/petrol fuel blends, the mixture is non-ideal. Therefore, the partial vapour pressure was corrected with AC, using the UNIFAC model. In some studies (e.g., ref. 97), however, this model was found to be complicated, and alternative approaches, such as the Wilson equation, were used to calculate the ACs. The Wilson equation was found to be simple to implement but it had limited applicability, to binary components alone. Hence, the UNIFAC model was believed to be the most attractive approach for the calculation of ACs of multi-component fuel droplets.[93,98]

An example of the saturated vapour pressures calculated using the UNIFAC model at different mass fractions of ethanol in ethanol/petrol fuel $\left(\text{mass}_{\text{eth}}/\left(\text{mass}_{\text{eth}}+\text{mass}_{\text{petrol}}\right)\right)$ at 296 K and 350 K was presented in ref. 90, and is reproduced in Figure 1. In this figure, a comparison is made between the predictions of the UNIFAC model and the classical approach (assuming AC = 1) based on the validity of Raoult's law.

One can see from Figure 1 that the non-unity ACs of the ethanol/petrol fuel blends, calculated using the UNIFAC model, have significant influence on the accuracy of the predicted p^{sat}. This influence is more noticeable for the balanced mixture, where the inter-molecular forces are low due to breaks in the hydrogen bonds, which leads to higher p^{sat}.[99] For the least balanced molecules (i.e. mixtures with either the lowest or highest concentrations of ethanol) and at low p^{sat}, the hydrogen bonds become stronger and more influential. The predictions obtained using the UNIFAC model were found to be compatible with the experimental data reported in refs. 100–102 (see Section 3.5).

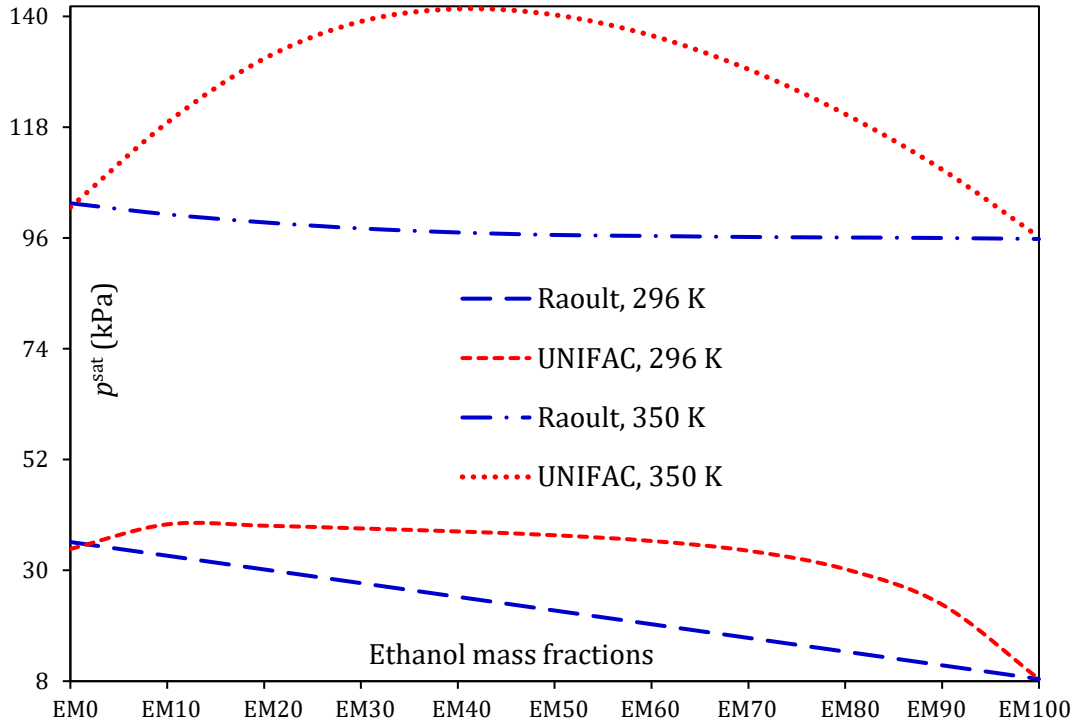

Figure 1. Total saturated vapour pressure (p^{sat}) versus ethanol mass fractions for the whole range from EM0 to EM100 $\left(\text{EM\#} = \text{mass}_{\text{eth}}/\left(\text{mass}_{\text{eth}} + \text{mass}_{\text{petrol}}\right)\right)$, predicted based on: the calculated AC of multi-component fuel, using the UNIFAC model, and the classical assumption that AC = 1, using Raoult's law, at ambient temperatures $T = 296$ K and 350 K. Reproduced with modifications from International Communications in Heat and Mass Transfer 98, 177–182, "The impacts of the activity coefficient on heating and evaporation of ethanol/petrol fuel blends," by Al-Esawi et al., copyright Elsevier (2018).

Following the successful implementation of the transient UNIFAC model into the DC model,[90] a further investigation was made focused on the validation of its predictions. In ref. 103, the droplet heating and evaporation were analysed for various ethanol/petrol (including E0 (pure petrol), E5, E20, E30, E50, E85 and E100 (pure ethanol)) fuel blends under a broad range of ambient conditions. It was shown that the errors attributed to using Raoult's law were up to 5.7% and 0.4% for the predictions of droplet lifetimes and surface temperatures, respectively.

3.5. Model validation

The DC model was applied to the analysis of ethanol/petrol (a combination of iso-octane and heptane) fuel droplet evaporation, and the results were validated against experimental data,[104] as shown in Figure 2. The following mixtures were investigated: EW30 (in EWX, X% refers to the mass fraction of ethanol and $(100 - \text{X})\%$ is the remaining mass fraction of petrol), EW70, and EW100. The mass fractions in EW70 and EW30 fuel blends are equivalent to the volume fractions of 67% ethanol/33% petrol and 27% ethanol/73% petrol, respectively. The blended fuel droplets were assumed to have initial radii equal to 23.6 μm, initial temperatures equal to 280.15 K, and they were suspended in stationary dry air of 1 atm ambient pressure.

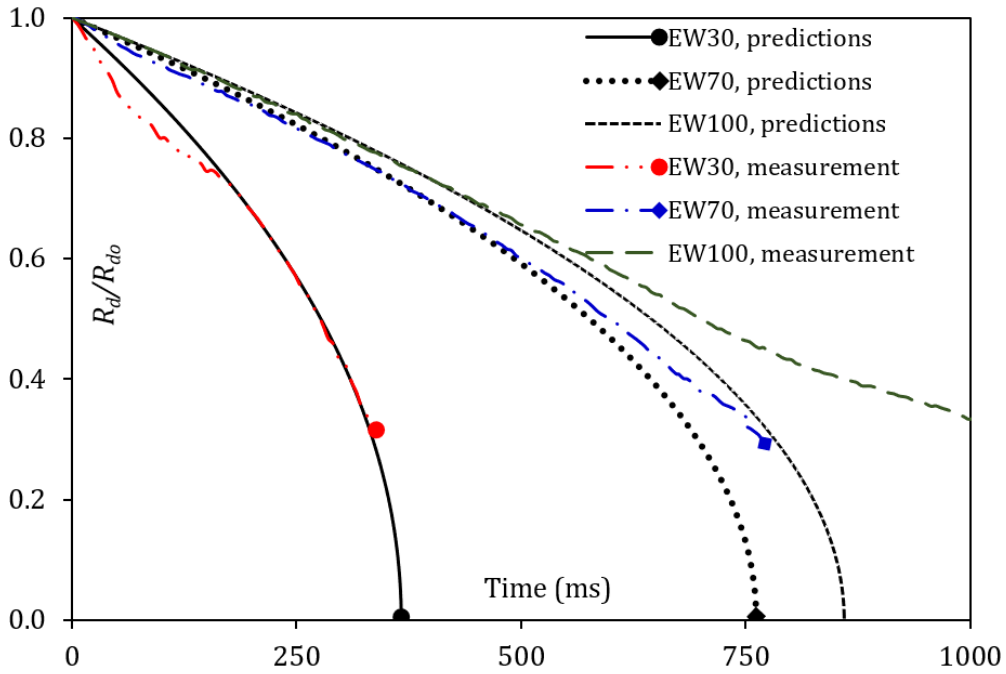

Figure 2. Normalised radii (R_d/R_{do}) of EW30, EW70 and EW100 droplets inferred from predicted (in ref. 103) and experimental (see ref. 104) data. Reprinted with modifications with permission from Energy & Fuels, 32, Pages 6498–506, "Ethanol/gasoline droplet heating and evaporation: Effects of fuel blends and ambient conditions," by Al Qubeissi et al., copyright (2018) American Chemical Society.

One can see from Figure 2 that the initial evolutions of predicted droplet radii were in close agreement with those obtained from experimental data.[104] At later stages of droplet evaporation, however, the differences between the plots were more noticeable. The difference was more significant for higher mass fractions of ethanol (e.g., EW70–EW100); hence, modelling results near the end of these droplet lifetimes are less reliable. These noticeable differences were attributed to the experimental set-up used in ref. 104, in which steam condenses from the ambient gas to the fuel droplets during the experiment. The justification and impact of such measurement uncertainty was made clear in ref. 103.

In refs. 47,90,103, the validation of the DC model, applied to the analysis of evaporation of Diesel fuel droplets, was investigated. Also, the results were verified against the data predicted by other numerical analyses. Following previous studies,[105,106] the authors of refs. 47,90,103 approximated Diesel fuel by the following 6 hydrocarbons with mass fractions: 11% decane ($C_{10}H_{22}$), 21% dodecane ($C_{12}H_{26}$), 8% toluene (C_7H_8), 27% tetradecane ($C_{14}H_{30}$), 16% octadecane ($C_{18}H_{38}$) and 17% hexadecane ($C_{16}H_{34}$). In refs. 105,106, the initial diameters of Diesel fuel droplets were assumed equal to 0.84 mm (for ambient gas temperature $T_g = 723$ K) and 0.86 mm (for $T_g = 523$ K). The initial fuel temperature was equal to 300 K. The droplets were suspended from a quartz fibre tip. The relative velocity of droplets was about 0.3 m/s (constant) and they were placed in a chamber at 1 atm ambient pressure.

In ref. 47, the evolutions of droplet diameters were predicted using the DC model with analytical solutions to the heat transfer and species diffusion equations, and compared with the predictions of this model using the numerical solutions to the same equations obtained in ref. 105. These predictions were validated using the experimental data of ref. 106. The result of these comparisons is presented in Figure 3. Note that it was stated in ref. 105 that "the droplet temperature and composition were assumed to be uniform", which contradicted the principle of using the ETC/ED models in the same paper. In refs. 47,90,103, this statement was assumed to be a typographical error, and it was intentionally ignored.

As follows from Figure 3, the predictions of the DC model in ref. 47 are very close to the numerical and experimental data. The total vapour pressures of ethanol/petrol (E0–E100) blends, predicted using

the UNIFAC model (Section 3.4), were validated against the experimental data.[102] The comparison of the results of ref. 107 and the results of measurements presented in ref. 102 are shown in Figure 4. The difference between the predicted, using the UNIFAC model, and the experimentally measured vapour pressures was insignificant. These minor differences, however, were partly attributed to the differences between the fuel used in ref. 107 (petrol FACE C) and the New Zealand regular grade unleaded petrol fuel used in the experiments of ref. 102. It was found in ref. 107 that the physical properties of these fuels were reasonably close.

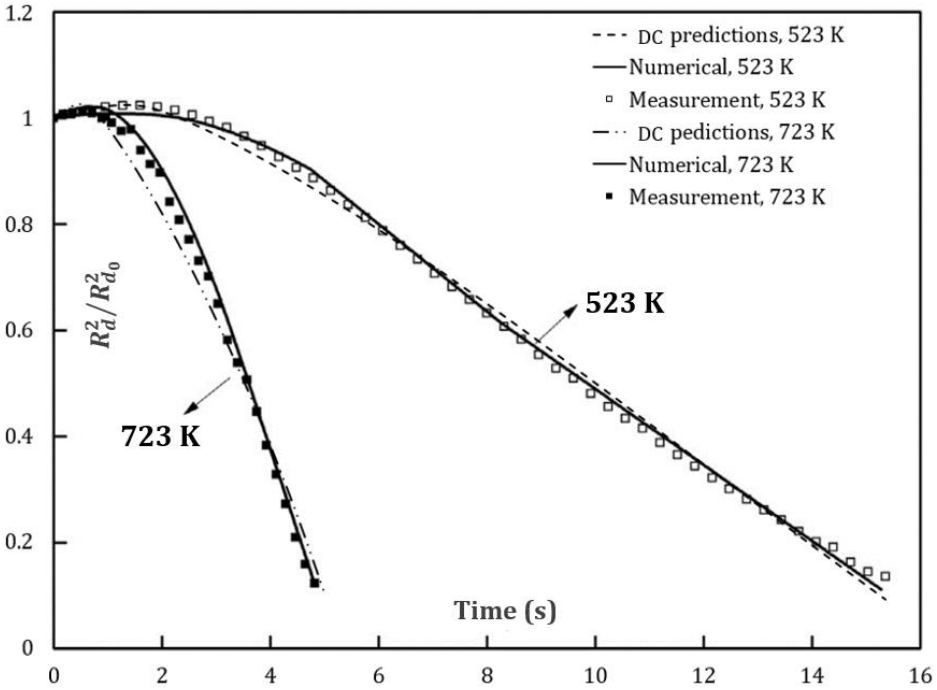

Figure 3. Normalised squared radii ($R_d^2/R_{d_0}^2$) of Diesel fuel droplets versus time, predicted by the DC model based on analytical solutions (DC predictions),[47] the numerical algorithm described in ref. 105 (Numerical) and the measurement results reported in ref. 106 (Measurement) at ambient temperatures of 523 K and 723 K (indicated near the curves). Reprinted with permission from Energy & Fuels, Vol. 33, Pages 2477–2488, "Blended E85–Diesel fuel droplet heating and evaporation," by Al Qubeissi et al., copyright (2019) American Chemical Society.

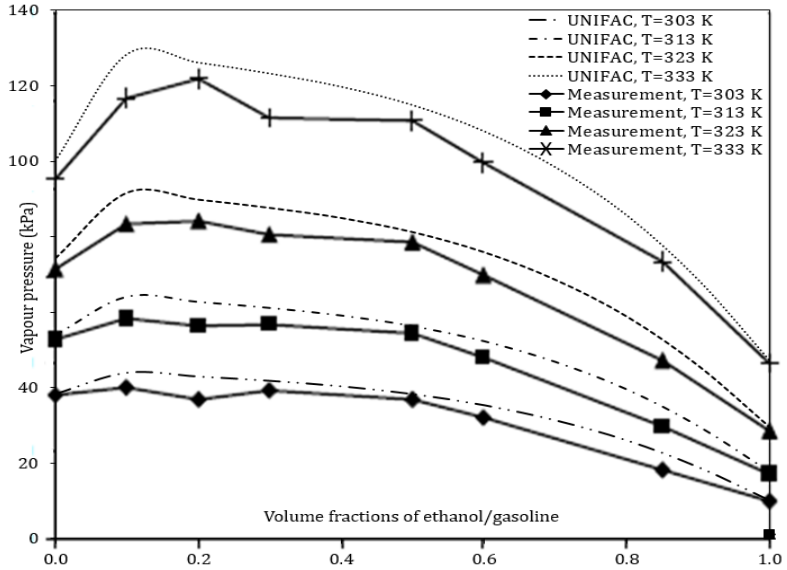

Figure 4. Total vapour pressures of ethanol/petrol predicted by UNIFAC,[90] and those experimentally measured,[102] at 303 K, 313 K, 323 K and 333 K. Reprinted from International Communications in Heat and Mass Transfer, Vol. 98, Pages 177-182, "The impacts of the activity coefficient on heating and evaporation of ethanol/gasoline fuel blends," by Al-Esawi et al., copyright Elsevier (2018).

3.6. Ethanol/petrol fuel blends

In this section, the major effects of the input parameters (including blending ratios, ambient and radiative temperatures, and ambient pressures) on ethanol/petrol fuel droplet heating and evaporation are reviewed. Many investigations have been performed with mixtures of petrol and ethanol.[54,104,108] In refs. 90,103, the DC model was applied to the analysis of droplets of petrol FACE C, ethanol and their blends. It was shown that petrol can be mixed with up to 10% ethanol with minimal impact on engines.[12] In accordance with the UK Department for Transport, increasing ethanol volume fractions from 5% to 10% in ethanol/petrol fuels is equivalent to taking 35,000 cars off the road in terms of emissions.[16,109] In this section, the impacts of ethanol (a typical biofuel that can be blended with petrol) on petrol droplet heating and evaporation are reviewed, accounting for several in-cylinder conditions. The analyses took into account the vapour-liquid equilibrium of the blend, using the UNIFAC model to calculate the non-unity activity coefficient. It is worth noting that ethanol is a polar liquid, unlike petrol fuel. The assumption that the value of the activity coefficient is unity, using Raoult's law, was shown to be invalid for predicting the vapour pressures of such fuel blends (see Section 3.4).[110]

3.6.1. Impacts of fuel blends

In what follows, the results of investigations into the effects of various fractions of ethanol in ethanol/petrol fuel blends on droplet heating and evaporation are reviewed. In ref. 103, the impacts of the following molar fractions of ethanol in ethanol/petrol fuel blends were investigated: 100% (pure ethanol, indicated as EM100), 85% (indicated as EM85), 50% (indicated as EM50), 20% (indicated as EM20), 5% (indicated as EM5) and 0% (pure petrol, indicated as EM0). These were converted to the following volume factions for comparable industrial understanding of the mixtures: 70% vol. ethanol/30% vol. petrol for EM85, 29% vol. ethanol/71% vol. petrol for EM50, 9% vol. ethanol/91% vol. petrol for EM20, and 2% vol. ethanol/98% vol. petrol for EM5. The contributions of all 21 components in ethanol/petrol FACE C fuel blends were considered. The blended fuel droplet radii R_d and surface temperatures T_s were presented versus time, as shown in Figure 5.

The authors of ref. 103 assumed that the initial droplet radius was $R_{do} = 12$ μm. This was inferred from the measured Sauter mean diameter (SMD).[36] The droplet, at T_{d0} = 296 K (initial temperature), was assumed to be moving at constant velocity $U_d = 24\ \mathrm{m \cdot s^{-1}}$. The ambient (in-cylinder) temperature and pressure were equal to $T_g = 545$ K and p_g = 9 bar, respectively. In Figure 5, the petrol fuel (EM0) droplet lifetime was shorter than those of the ethanol/petrol blends. The droplet lifetimes increased for the higher ethanol fractions in the ethanol/petrol blends. A similar trend was previously reported in refs. 104,108. The droplet lifetime was 33.9% longer for EM100, compared with that of EM0. This was attributed to the difference in the thermodynamic and transport properties of both fuels. The longer droplet lifetime of ethanol (EM100) was also related to its lower droplet surface temperature, which was about 24.3% lower than that of EM0. This was due to the fact that the critical temperature of EM100 (514 K) and its boiling temperature (351.5 K) were both lower than those of any of the petrol FACE C components; for example, the critical and boiling temperatures of C_8H_{18} are 543.9 K and 372.4 K, respectively. The compositions of the blends were the main influence on these trends. In Figure 6, the evolutions of surface mass fractions of some components of the EM20 fuel blend are illustrated following ref. 103.

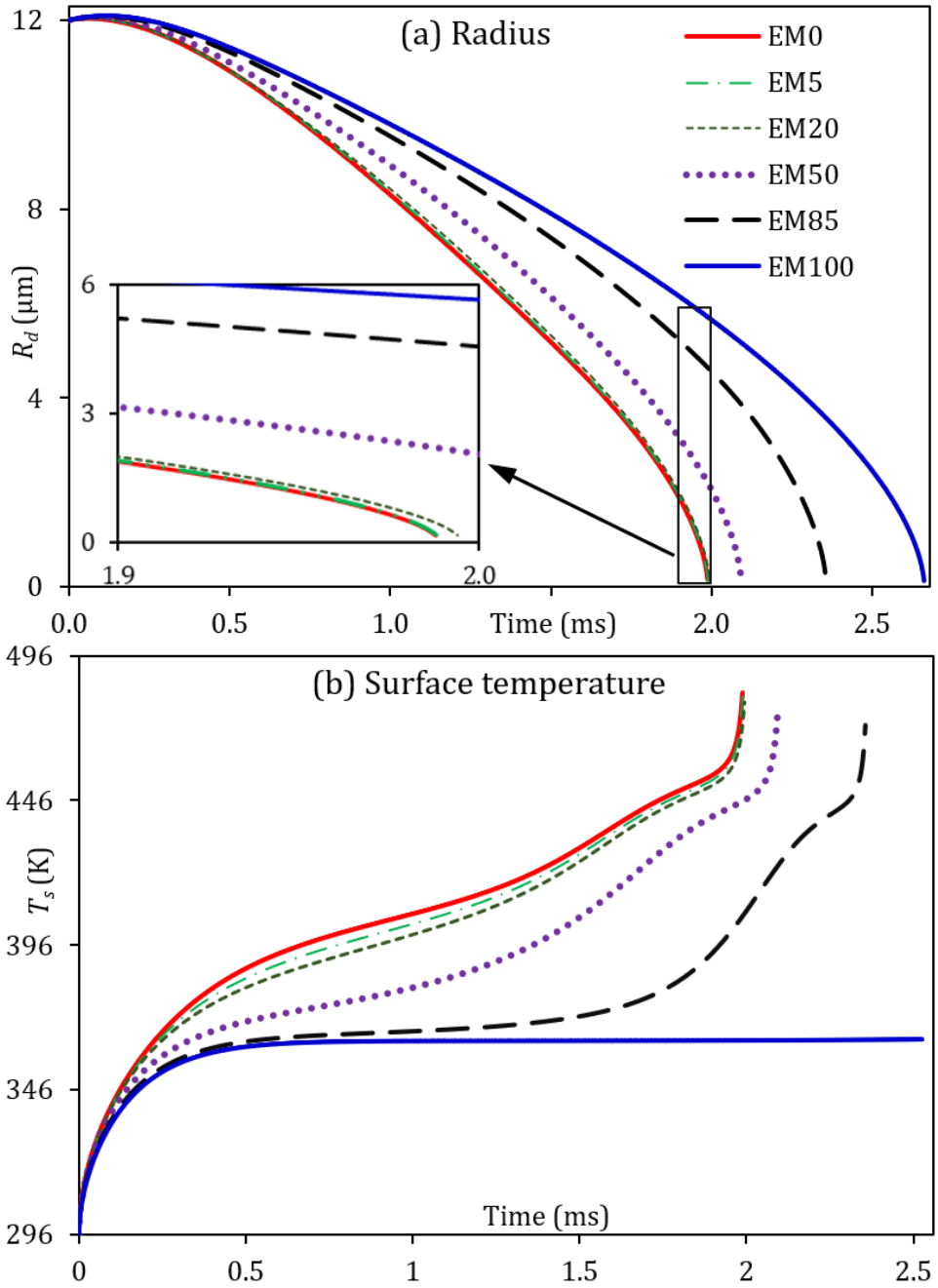

Figure 5. Plots of R_d (a) and T_s (b) versus time for various ethanol/petrol blends. Reproduced with modifications with permission from Energy & Fuels, Vol. 32, Pages 6498–506, "Ethanol/gasoline droplet heating and evaporation: Effects of fuel blends and ambient conditions," by Al Qubeissi et al., copyright (2018) American Chemical Society.

As can be seen from Figure 6, in the case of heavy species their liquid mass fractions at the droplet surface monotonically increase with time at the expense of the lighter species. In the case of the intermediate species (e.g., iso-$C_{10}H_{22}$), their mass fractions at the droplet surface initially increase and then decrease with time. The same trend was predicted in ref. 31. Such complex behaviour of species can have significant impacts on the distributions of species in the liquid (inside droplets) and vapour phases inside the combustion chamber when considering realistic ICE conditions.

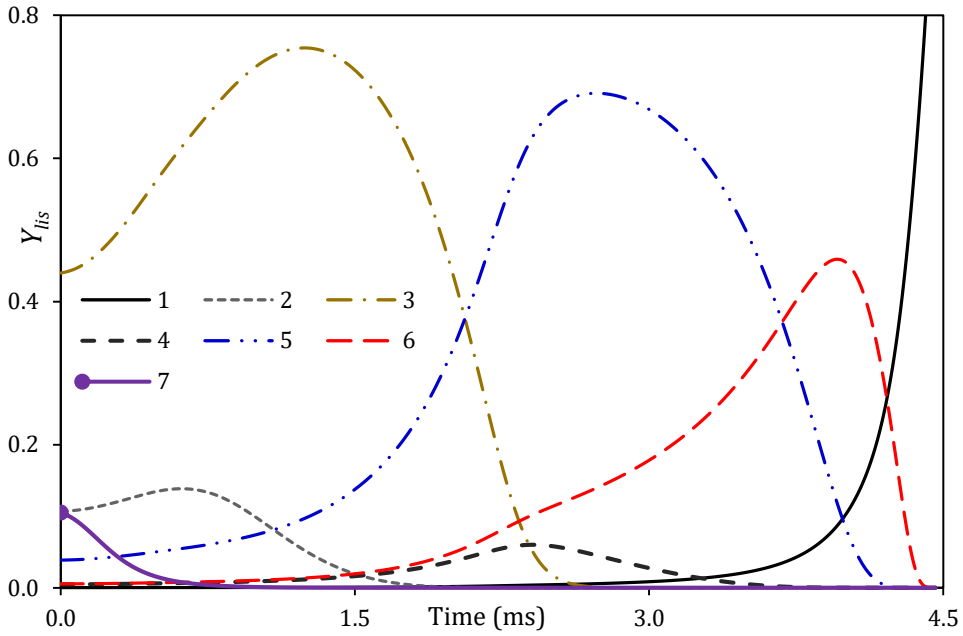

Figure 6. Liquid mass fractions of some representative species of the EM20 fuel blend at the droplet surface, Y_{lis}, versus time. The following components are shown: n-$C_{12}H_{26}$ (1), iso-C_7H_{16} (2), iso-C_8H_{18} (3), iso-$C_{11}H_{24}$ (4), iso-$C_{10}H_{22}$ (5), arom-C_9H_{10} (6) and C_2H_6O (7). Reproduced, with modifications, with permission from Energy & Fuels, Vol. 32, Pages 6498–506, "Ethanol/gasoline droplet heating and evaporation: Effects of fuel blends and ambient conditions," by Al Qubeissi et al., copyright (2018) American Chemical Society.

3.6.2. Impacts of ambient conditions

In ref. 103, a wide range of petrol engine conditions (including in-cylinder pressures, temperatures and radiative effects) were taken into account to improve our understanding of droplet heating and evaporation of EM0–EM100 fuels. The ranges for ambient pressures were 3–30 bar, those for ambient gas temperatures were 400–650 K, and those for radiative temperatures were 1000–2000 K. The model used in ref. 103 took into account the maximal impact of thermal radiation on droplet heating (considering the radiative heating as a surface phenomenon; see Expression (7)). This was different to previous studies (e.g., refs. 42,78), where droplets were assumed to be semi-transparent. Using the DC model described in Sections 3.1–3.3, the impacts of these radiative temperatures on droplet lifetime were investigated. The results are illustrated in Figure 7.

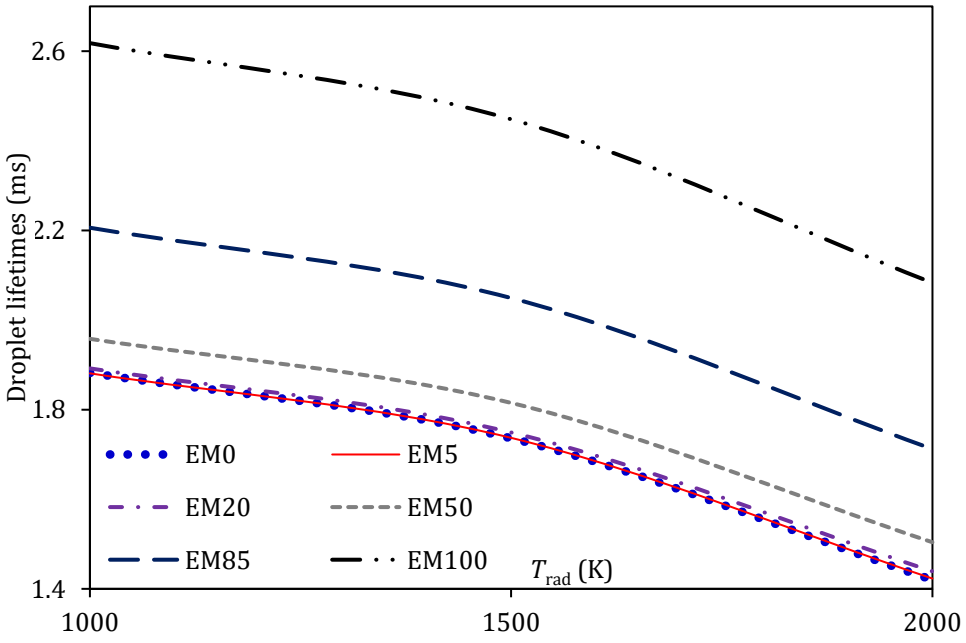

Figure 7. Droplet lifetimes of EM0–EM100 fuel blends versus radiative temperatures T_{rad}, assuming that the radiative heating is a surface phenomenon (see Equation (7)) at 9 bar ambient pressure and 550 K ambient temperature. Reprinted with permission from Energy & Fuels, Vol. 32, Pages 6498–506, "Ethanol/gasoline droplet heating and evaporation: Effects of fuel blends and ambient conditions," by Al Qubeissi et al., copyright (2018) American Chemical Society.

From Figure 7 it follows that higher radiative temperatures led to significant reductions in droplet lifetimes. The impact of radiation was less significant for droplets with higher ethanol/petrol fuel ratios compared to those with more dominant petrol fuel in the mixture. This phenomenon was not directly linked to the radiation effects since the droplet lifetimes of ethanol were the longest (see Figures 8-10). More examples showed the effects of ambient pressures and temperature on EM0–EM100 fuel droplet lifetimes.[103]

The effects of ambient pressures at 650 K ambient temperature are illustrated in Figure 8. As can be seen from this figure, the droplet lifetimes become shorter at higher ambient pressures. It has also been shown that EM100 (pure ethanol) droplets have the longest lifetimes and EM0 (pure petrol) droplets have the shortest lifetimes. The impacts of the ambient temperatures on droplet lifetimes at 3 bar are shown in Figure 9. The trends shown in Figure 9 (decrease in droplet lifetimes with increasing temperatures) are similar to those shown in Figure 8.

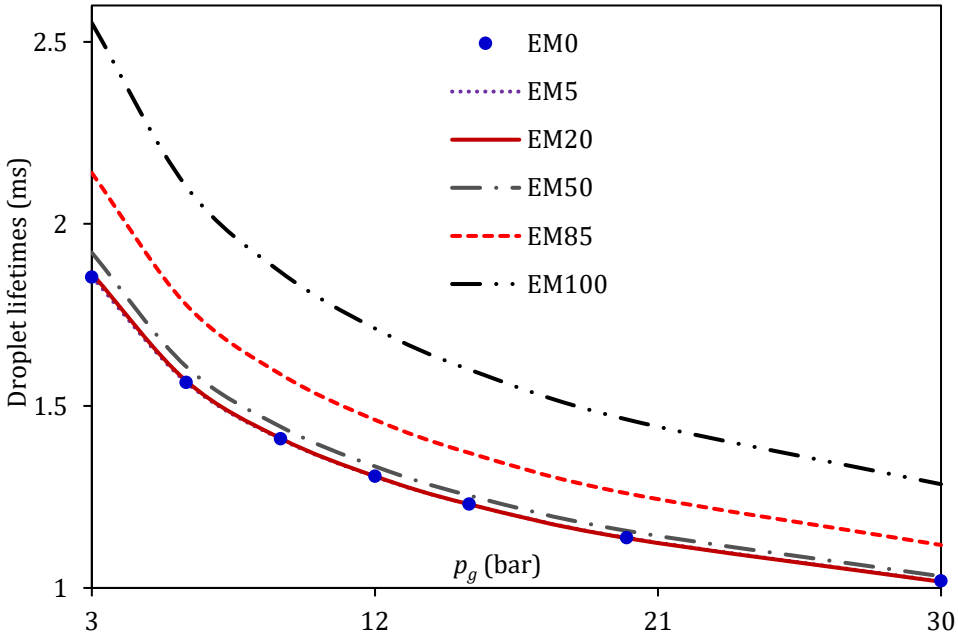

Figure 8. Droplet lifetimes of EM0–EM100 fuel blends versus ambient pressures, estimated using the same model as in Figure 7 but at a constant ambient temperature of 650 K. The effects of thermal radiation are ignored. Reproduced with modifications with permission from Energy & Fuels, Vol. 32, Pages 6498–506, "Ethanol/gasoline droplet heating and evaporation: Effects of fuel blends and ambient conditions", by Al Qubeissi et al., copyright (2018) American Chemical Society.

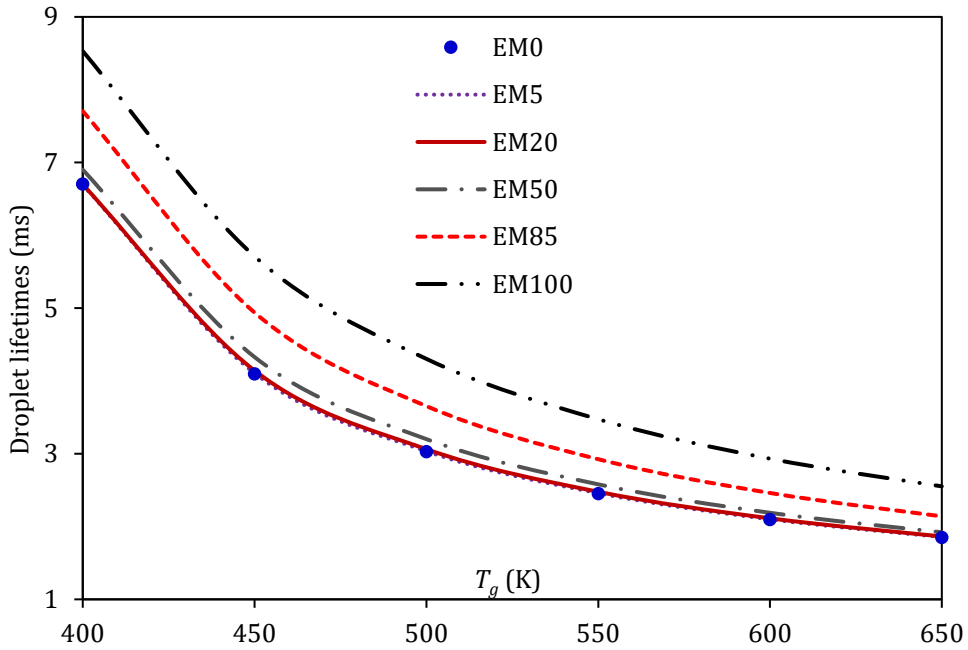

Figure 9. Droplet lifetimes of EM0–EM100 fuel blends versus ambient temperatures, estimated at ambient pressure of 3 bar using the same model as in Figures 7 and 8. The effects of thermal radiation are ignored. Reprinted with permission from Energy & Fuels, Vol. 32, Pages 6498–506, "Ethanol/gasoline droplet heating and evaporation: Effects of fuel blends and ambient conditions," by Al Qubeissi et al., copyright (2018) American Chemical Society.

In Figure 9 one can see that droplet lifetimes are shortened at higher ambient temperatures for all fuel mixtures. It can be concluded that the general trends illustrated in Figures 7–9 are that increasing the ambient pressures, temperatures, or the radiative temperatures always shortens the evaporation times of any ethanol/petrol blend droplet. Pure ethanol (EM100) droplets take longer to evaporate than those mixed with petrol.

3.7. Biodiesel/Diesel fuel blends

Heavy duty ICE are very powerful engines driven mainly by Diesel fuel.[111] These engines, however, have been causing environmental pollution, including the release of carbon oxides. Many attempts (e.g., refs. 112–119) have been made to replace Diesel fuel with alternatives (e.g., Diesel/biofuel blends). Biodiesel fuels are commonly used to replace Diesel fuel due to their several advantages. Both fuels have relatively close Cetane Numbers (CN) and thermodynamic properties. Therefore, some biodiesel/Diesel fuel blends can be used in standard Diesel engines without modification.[113,114] Also, CO_2 emissions from biodiesel fuels are much lower than from Diesel fuel. Their flash point is higher, and production is more sustainable than that of Diesel fuel. According to Tier I and Tier II standards by the U.S. Environmental Protection Agency (see ref. 7 for details), the current FAME fuels meet the requirements for potential health effects of fuel combustion emissions. [120] In this section, the studies of the effects of adding biodiesel and ethanol to Diesel fuel on droplet heating and evaporation and relevant combustion characteristics are summarised.

3.7.1. Impacts of fuel blends

In ref. 45, the DC model, described in Sections 3.1-3.4, was used for the analysis of biodiesel/Diesel fuel droplet heating and evaporation. A droplet of $R_{do} = 12$ μm (initial radius) and $T_o = 360$ K (initial temperature) was moving at constant velocity $U_d = 10$ m.s^{-1}. The ambient pressure and temperature were equal to p_g = 30 bar and T_g = 800 K, respectively. The following biodiesel/(biodiesel + Diesel) fuel blends were considered: B0, B5, B20, B50, B80, and B100 (B# refers to molar fractions #% of biodiesel/(biodiesel + Diesel) fuel blend), using Soybean Methyl Esters (SME) and Waste Cooking Oil

Methyl Ester (WCO) biodiesel fuels. An example of the influence of biodiesel molar fractions in biodiesel/Diesel fuel on the droplet lifetimes was presented in ref. 45 and is reproduced in Table 7. One can see from Table 7 that increasing biodiesel molar fractions from B5 (5% biodiesel and 95% Diesel) to B100 (pure biodiesel) had noticeable impacts on droplet lifetimes for both SME and WCO fuels, compared to the case of B0 (pure Diesel) fuel.

Table 7. Biodiesel/(biodiesel + Diesel) fuel droplet lifetimes (in ms) and the differences between those and that of a B0 droplet (2.25 ms), $\left(\text{Diff \%} = \frac{\text{lifetime}_{B0} - \text{lifetime}_{blend}}{\text{lifetime}_{B0}}\right) \times 100$.[45]

Blends	Biodiesel Fuels			
	SME		WCO	
	Lifetime	Diff %	Lifetime	Diff %
B5	2.236	0.62	2.237	0.57
B20	2.198	2.31	2.194	2.49
B50	2.127	5.47	2.121	5.73
B80	2.055	8.67	2.052	8.80
B100	1.981	11.96	2.002	11.02

In Table 7, one can see that the B100 SME droplet lifetime was 12% shorter than that of pure Diesel fuel (B0). In the case of B5, the reduction in droplet lifetime did not exceed 0.7% compared to the B0 droplet. Also, the WCO biodiesel fuel droplet lifetimes were noticeably close to those of the SME droplets; these were 12% and 0.7% shorter for the B100 and B5 WCO blends, respectively, compared to the B0 droplet lifetime. These differences in droplet lifetimes should not be ignored in most engineering applications. Results of a similar investigation were presented in ref. 46, but for a broad range of biodiesel fuels, considering twenty types of FAME fuel. Some results presented in ref. 46 are reproduced in Table 8, where the droplet lifetimes of these biodiesel/(biodiesel + Diesel) fuel mixtures were compared to that predicted for B0 fuel (2.25 ms). In Table 8, the B100 RME fuel droplet lifetime was 6% shorter than that of B0. In the case of the B5 RME fuel blend, this reduction was less than 0.4% under the same conditions. Also, in the case of TGE biodiesel fuel, the droplet lifetime was close to that of a B0 fuel droplet; it was up to 8% longer for B100 and up to 0.5% longer for B5. For all pure biodiesel fuels (B100), the difference between the lifetimes of droplets of these fuels and those of B0 droplets was the highest for B100 CME fuel (up to 21. 6%), indicating that this fuel would be more difficult to use than B0. The difference was lowest for B100 RME (5.29%), suggesting that it might be better tolerated than B0 in some engineering applications.

Table 8. Biodiesel/Diesel fuel droplet lifetimes (in ms) and the differences between those and that of a pure Diesel fuel (B0) droplet (2.25 ms) $\left(\text{Diff \%} = \frac{\text{lifetime}_{B0} - \text{lifetime}_{blend}}{\text{lifetime}_{B0}}\right) \times 100$.[46]

FAME	B100		B50		B20		B5	
	Lifetime	Diff %	Lifetime	Diff %	Lifetime	Diff %	Lifetime	Diff %
TME	1.967	12.6	2.102	6.6	2.184	2.9	2.232	0.80
LME	1.995	11.3	2.114	6.0	2.190	2.7	2.234	0.71
BME	1.943	13.6	2.089	7.2	2.180	3.1	2.232	0.80
CME	1.765	21.6	2.036	9.5	2.166	3.7	2.229	0.93
PMK	1.846	18.0	2.050	8.9	2.169	3.6	2.230	0.89
PME	1.944	13.6	2.097	6.8	2.183	3.0	2.232	0.80
SFE	1.980	12.0	2.122	5.7	2.195	2.4	2.235	0.67
PTE	2.052	8.8	2.138	5.0	2.199	2.3	2.236	0.62
CSE	2.014	10.5	2.128	5.4	2.197	2.4	2.236	0.62
CNE	2.002	11.0	2.128	5.4	2.197	2.4	2.236	0.62
SNE	2.011	10.6	2.132	5.2	2.200	2.2	2.237	0.58
RME	2.131	5.3	2.188	2.8	2.222	1.2	2.242	0.36
LNE	1.991	11.5	2.141	4.8	2.206	2.0	2.239	0.49

TGE	2.085	7.3	2.160	4.0	2.211	1.7	2.240	0.44
HME1	2.022	10.1	2.138	5.0	2.203	2.1	2.237	0.58
HME2	1.994	11.4	2.135	5.1	2.202	2.1	2.238	0.53
CAN	2.014	10.5	2.130	5.3	2.199	2.3	2.236	0.62
CML	2.064	8.3	2.153	4.3	2.209	1.8	2.239	0.49
JTR	2.047	9.0	2.133	5.2	2.198	2.3	2.236	0.62
YGR	2.077	7.7	2.149	4.5	2.203	2.1	2.237	0.58

3.7.2. Impacts of ambient conditions

Note that in refs. 35,45,121 the radiative effects on the evaporation of droplets were not taken into account. The latter effects were investigated in refs. 64,65, where the full compositions of biodiesel/Diesel fuel blends were considered, using a simplified radiation model (see Equation (7)). In ref. 65, a broad range of SME and WCO biodiesel/(biodiesel + Diesel) fuel blends (B0–B100) were considered in order to investigate the impacts of radiation temperature (in the range 1000 K– 2000 K) on droplet lifetimes. The results of these investigations under a range of Diesel engine injection conditions are presented in Table 9 and illustrated in Figures 10 and 11.

As follows from Table 9, the impacts of radiation on droplet lifetimes become more noticeable at high radiation temperatures, as expected. There were reductions in droplet lifetimes, of up to 19.4% for B0 and up to 23.3% for B100, when the radiation temperature was assumed equal to 2000 K. The impact of radiation temperatures on droplet lifetimes increased as the biodiesel/(biodiesel + Diesel) molar fractions increased. The effects of in-cylinder temperatures and pressures on the estimated droplet lifetimes for B0–B100 fuel blends are illustrated in Figures 10 and 11. In Figure 10, the droplet lifetimes shortened as the ambient pressures increased at 800 K ambient temperature. Similar results were obtained for all fuel blends of SME/Diesel and WCO/Diesel. This effect was attributed to the increased gas density and faster evaporation rates at higher ambient pressures. Similarly, increasing the ambient temperatures at ambient pressure $p_g = 30$ bar shortened the droplet lifetimes (see Figure 11).

Table 9. Blended fuel droplet lifetimes (in ms), taking into account the effects of radiation, and the differences between those and the case when radiation is ignored, $\left(\text{Diff \%} = \frac{\text{lifetime}_{\text{no rad}} - \text{lifetime}_{\text{rad}}}{\text{lifetime}_{\text{no rad}}} \times 100\right)$.[65]

Blends		No radiation	T_{rad}= 1000 K		T_{rad}= 1500 K		T_{rad} = 2000 K	
		Time (ms)	Time (ms)	Diff %	Time (ms)	Diff %	Time (ms)	Diff %
WCO	B0	2.250	2.218	1.42	2.097	6.80	1.814	19.38
	B5	2.237	2.203	1.52	2.082	6.93	1.799	19.54
	B20	2.198	2.162	1.64	2.039	7.23	1.758	20.02
	B50	2.127	2.091	1.70	1.963	7.71	1.683	20.87
	B80	2.052	2.016	1.75	1.889	7.94	1.607	21.69
	B100	2.002	1.964	1.89	1.834	8.40	1.542	22.97
SME	B0	2.250	2.218	1.42	2.097	6.80	1.814	19.38
	B5	2.236	2.204	1.43	2.083	6.84	1.800	19.50
	B20	2.198	2.166	1.46	2.043	7.05	1.761	19.88
	B50	2.127	2.094	1.55	1.968	7.48	1.688	20.64
	B80	2.055	2.021	1.65	1.893	7.88	1.612	21.56
	B100	1.981	1.946	1.77	1.814	8.43	1.520	23.27

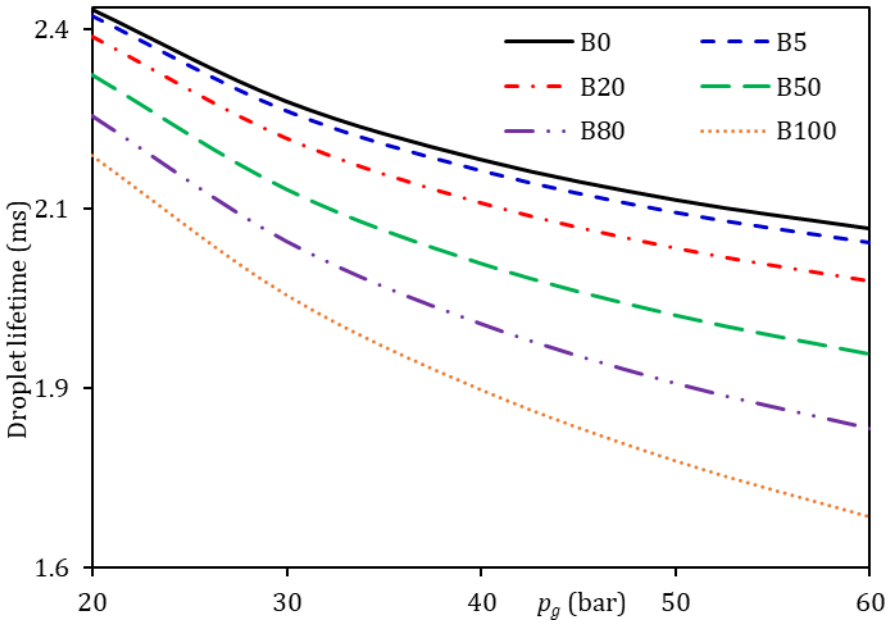

Figure 10. Droplet lifetimes of B0–B100 SME/Diesel fuel blends versus ambient pressures at T_g = 800 K. Reproduced with modifications from ref. 65. Copyright Begellhouse (2018).

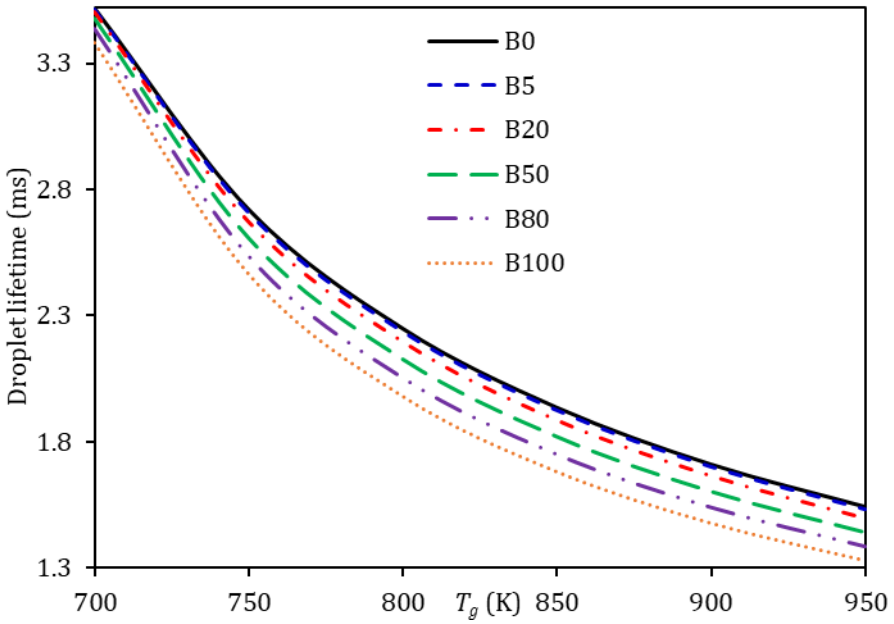

Figure 11. Droplet lifetimes of B0–B100 SME/Diesel fuel blends versus ambient temperatures at p_g = 30 bar. Reproduced with modifications from ref. 65. Copyright Begellhouse (2018).

3.8. Ethanol/biodiesel/Diesel fuel blends

Ethanol has been commonly mixed with Diesel to improve fuel combustion characteristics. Such mixtures require additive (intermediate) agents to attain the required miscibility, control the phase separation, and stabilise the mixture.[112,122] Some attempts were made to use Dimethyl ether (DME) as a mixing agent and to boost the cetane number (CN) of Diesel fuel.[123] Although DME can be a good stabilizer, it cannot be used in Diesel ICE effectively because of its low MM, boiling point, and density, compared to Diesel fuel. It was found that biodiesel can be a chemically-convenient additive agent for the ethanol/Diesel (E/D) fuel blend.[124]

In ref. 112, it was found that adding biodiesel to the E/D blend made a significant contribution to reducing CO and hydrocarbon emissions in real ICE. In ref. 115, the solubility of an

ethanol/biodiesel/Diesel (EBD) blend was good, even with cold injection. A study by Beatrice et al.[125] showed that replacing pure Diesel fuel with a E20/B10/D70 (20% ethanol, 10% biodiesel and 70% Diesel) fuel blend led to significant reduction in the smoke and nitrogen oxide (NO_X) emissions of ICE. Similar results were shown in an experimental study by Fang et al.,[126] where the EBD blend had a significant impact on reducing NO_X emissions.

Similarly, many studies (e.g., refs. 127–131) showed that using EBD in Diesel engines increased CN and produced less NO_x emissions than did Diesel fuel. The results presented in refs. 124,132 showed that a mixture of up to E10/B25/D65 was acceptable in terms of improving the CN, solubility and heating value and reducing toxic emissions compared with pure Diesel fuel. The impacts of such blends on the evolutions of droplet heating and evaporation, using the full fuel compositions, was investigated in a recent study.[64] In this section, the key findings presented in this paper are reviewed. The focus will be on the investigation of the effect of mixing various fractions of EBD blends on droplet lifetimes and surface temperatures.

3.8.1. Cetane number and viscosity

It has long been known that CN is an important parameter for the evaluation of Diesel fuel combustion.[133] Also, fuel viscosity has been shown to have an important influence on fuel atomization and combustion in Diesel engines.[130,134] Biodiesel fuel was recommended as an addition to the E/D mixture to compensate for the decrease in CN and viscosity in this mixture.[122] In ref. 135, the feasibility of using EBD fuel in Diesel engines was investigated in terms of replicating the pre-combustion features, including CN and viscosity. Following ref. 136, the CN of EBD fuel was predicted. The CN of Diesel fuel (CN_D) was predicted as:[137]

$$CN_D = \frac{\sum_i v_i \beta_i CN_i}{\sum_i v_i \beta_i}, \quad (35)$$

where i is the index of the chemical group or species, and CN_i, v_i and β_i are the cetane number, total volume fraction and blending parameter of that group, respectively. CNs of individual components are inferred from refs. 137–140. In ref. 35, due to the similar physical properties of iso-alkane and n-alkane groups, they were merged into one group of alkanes. In ref. 135, these two groups were accounted for individually for the calculation of their CN, due to the influence of chemical structures (straight or branched chain) on this value. Using Expression (35), the predicted CN_D are presented in Table 10. In ref. 135, the three groups of Diesel fuel with small molar fractions (0.66%, 1.56%, 1.224%)[35] were ignored.

Table 10. Volume fractions and β_i of each group of Diesel fuel components and the predicted CN_D.[135]

Groups	v_i	β_i
n-alkanes	15.94	0.5212
iso-alkanes	31.32	7.3717
cycloalkanes	15.99	0.0727
bicycloalkanes	7.53	0.0727
aromatics	12.84	3.1967
tetralines	10.39	3.1967
naphthalenes	5.97	0.0727
$CN_D = 54.5$		

The biodiesel fuel CNs of individual methyl esters were calculated based on their numbers of carbon atoms and double-bonds.[141] The total biodiesel fuel CN (CN_B) was calculated using the following formulae:[142]

$$CN_B = 1.068 \sum (CN_i y_i) - 6.747, \quad (36)$$

where y_i is the mass fraction of the i^{th} methyl ester. The latter formula predicts that adding 1% vol. of some biodiesel fuels can increase the CN of the blend by 0.55, which can compensate for the 0.6 units decrease in that CN if the same amount of ethanol (1% vol.) is added. The finding that the reduction in CN caused by ethanol can be compensated for cannot, however, be generalised to all types of biodiesel fuels. It was noted in ref. 135 that the CN_B was dependent on the molecular structures of individual methyl esters. For example, a very low CN ($\approx$ 23) was shown for methyl lineolate ($C_{19}H_{34}O_2$). Hence, adding biodiesel fuels with small fractions of methyl lineolate, e.g., SME, can be an appropriate means of boosting the CN of the blend. A typical example showing the impact of different EBD volume fractions on their CN is illustrated in Table 11.

In the same study,[135] the EBD CN was predicted as:[136]

$$CN_{EBD} = CN_D - 0.59v_E + 0.55v_B, \quad (37)$$

where v_E and v_B are the volume fractions of ethanol and biodiesel, respectively. The results predicted by Expression (37) were verified using the predictions of CN for EBD blends.[143]

The approach of ref. 95 for the calculation of EBD viscosity was based on species and structures, using the UNIFAC–VISCO method. This was described as a 'rigorous approach',[135] given by the following formula:

$$\ln \mu_m = \sum_i x_i \ln(\mu_i V_i) - \ln V_m + \frac{\Delta^* g^{EC}}{RT} + \frac{\Delta^* g^{RC}}{RT}, \quad (38)$$

where μ_m is the viscosity of the mixture and μ_i is the viscosity of the i^{th} component, V_m and V_i are the critical (molar) volumes of the mixture ($cm^3 \cdot mol^{-1}$) and the i^{th}component, respectively, $\frac{\Delta^* g^{EC}}{RT} = \sum_i x_i \ln \frac{\Phi_i}{X_i} + \frac{z}{2} \sum_i x_i q_i \ln \frac{\theta_i}{\Phi_i}$, and $\frac{\Delta^* g^{ER}}{RT} = -\sum_i x_i \ln \gamma_i^{*R}$. All the terms and parameters in Expression (38) are the same as those in the UNIFAC model (Section 3.4). The results of the application of Expression (38) to predict EBD viscosity are summarised in Table 12.

Table 11. Predicted CN of biodiesel, Diesel, ethanol, and their blends.[135]

EBD vol.%	CN [143]	CN [136]
D100	54.5	54.5
B100	56.4	56.4
E100	8.0	8.0
E10/D90	49.8	48.6
E5/B5/D90	52.3	54.4
E5/B15/D90	52.5	55.0

Table 12. Viscosities of Diesel, biodiesel, ethanol, and their blends, calculated at $T = 40$ °C.[135]

EBD vol.%	μ_m (cP)
D100	3.51
B100	3.59
E100	0. 81
E10/D90	3.27
E5/B5/D90	3.46
E5/B15/D80	3.44

One can see from Tables 11 and 12 that adding up to 5% ethanol and 15% biodiesel (E5/B15/D80) can lead to reductions in the CN and viscosity of up to 0.2% and 2%, respectively, compared to those of pure Diesel (D100). The addition of biodiesel fuel to the mixture, however, compensates for the reduction in the CN and viscosity caused by ethanol. This is noticeable for the cases of E/D blends

without biodiesel additions. For example, E10/D90 has 10.8% smaller CN and 7% smaller viscosity, compared to those of D100.

3.8.2. Heating value

In ref. 135, the impacts of EBD blends on their heating values (HV) were investigated based on the following formula:[144]

$$\mathrm{HV}_{\mathrm{blend}} = \frac{v_B \mathrm{HV}_D \rho_D + v_B \mathrm{HV}_B \rho_B + v_E \mathrm{HV}_E \rho_E}{\rho_{\mathrm{blend}}}, \tag{39}$$

where HV_E, HV_B and HV_D are the HV of ethanol, biodiesel and Diesel fuels (in MJ/kg), respectively, v_E, v_B and v_D are the corresponding volume fractions of EBD components, and ρ_E, ρ_B, ρ_D and ρ_{blend} are the corresponding densities and the density of the blend, respectively. In ref. 135, the predictions of (39) were compared to the experimental data.[112] The results are illustrated in Figure 12.

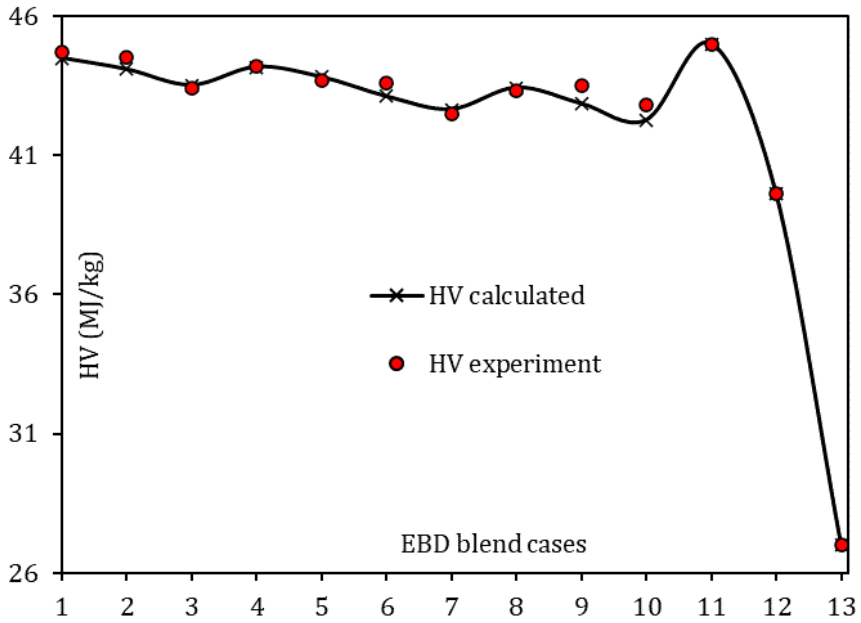

Figure 12. Predicted[135] and experimentally measured[112] heating values, for EBD blends: 1) B10/D90, 2) E5/B5/D90, 3) E10/D90, 4) B15/D85, 5) E5/B10/D85, 6) E10/B5/D85, 7) E15/D85, 8) E5/B15/D80, 9) E10/B10/D80, 10) E15/B5/D80, 11) D100, 12) B100 and 13) E100. Reproduced with permission from Energies, Vol. 12, "The impact of biodiesel fuel on ethanol/diesel blends," by Al-Esawi et al; published by MDPI (2019).

As shown in Figure 12, the HV predicted using (38) agree very well with those experimentally measured[112] for all EBD fuel blends. In the case of pure ethanol (case 13) the HV is the lowest due to the relatively simple structure of this fuel. However, the biodiesel fuel addition compensates for this loss. For example, in the case of E10/D90 (case 3) HV is 3% lower than that of D100, but in the case of E5/B5/D90 (case 2) HV is only 0.5% lower than that of D100.

4. Multi-dimensional quasi-discrete model

The MDQDM ('Multi-Dimensional Quasi-Discrete Model' introduced in ref. 35) was a generalisation of the Quasi-Discrete (QD) model (introduced in ref. 33). The QD model was applicable to a single group of hydrocarbons within fuels, while the MDQDM was applicable to a realistic number of groups within fuels. In what follows the main features of both models are summarised.

4.1. Quasi-discrete model

In the original quasi-discrete model,[33,34] the contribution of n-alkane components was described by the distribution function:

$$f_m(n) = C_m(n_0, n_f)\frac{(\mathrm{MM}(n)-\gamma)^{\alpha-1}}{\beta^{\alpha}\,\Gamma(\alpha)}\,\exp\left[-\left(\frac{\mathrm{MM}(n)-\gamma}{\beta}\right)\right], \tag{40}$$

where MM is the molar mass, n is the number of carbon atoms, $n_0 \le n \le n_f$, subscripts '0' and 'f' indicate the initial and final carbon numbers, α, β and γ are parameters used to determine the distribution function shape, $\Gamma(\alpha)$ is the Gamma function, and C_m is a constant:

$$C_m = \left\{\int_{\mathrm{MM}(n_0)}^{\mathrm{MM}(n_f)} \frac{(\mathrm{MM}-\gamma)^{\alpha-1}}{\beta^{\alpha}\Gamma(\alpha)}\exp\left[-\left(\frac{\mathrm{MM}-\gamma}{\beta}\right)\right] d\mathrm{MM}\right\}^{-1}. \tag{41}$$

This calculation of C_m is based on the condition that:

$$\int_{\mathrm{MM}(n_0)}^{\mathrm{MM}(n_f)} f_m(\mathrm{MM})\, d\mathrm{MM} = 1, \tag{42}$$

The continuous distribution function $f_m(\mathrm{MM})$ or $f_m(n)$ was replaced with a discrete one, based on the assumption that the properties of hydrocarbons in each narrow range of n are the same. The averaged carbon numbers of Quasi-Components (QC) were determined as:

$$\bar{n}_j = \frac{\int_{n_{j-1}}^{n_j} n\, f_m(n)\, \mathrm{d}n}{\int_{n_{j-1}}^{n_j} f_m(n)\, \mathrm{d}n}, \tag{43}$$

and the corresponding molar fractions:

$$X_j = \int_{n_{j-1}}^{n_j} f_m(n)\, \mathrm{d}n, \tag{44}$$

where j is an integer in the range $\left(1 \le j \le N_f\right)$. Note that:

$$\sum_{i=1}^{j=N_f} X_j = 1. \tag{45}$$

The choice of n_j could be arbitrary. It was assumed that all $n_j - n_{j-1}$ were equal, i.e. all Quasi-Components (QC) had the same range of values of n. For the case when $N_f = 1$ this approach reduced the analysis to that of mono-component fuels. These new QC (described by $\bar{n}_j$ in Expression (43)) were not the actual physical hydrocarbon components because $\bar{n}_j$ were not integers in the general case. Therefore, this mathematical approach to representing multiple components in fuels was described as a 'quasi-discrete' model. In the DC model, the QC were treated just like the actual components, including the consideration of their diffusion inside and at the surface of droplets.

4.2. Multi-grouped hydrocarbons

Two main restrictions limit the application of the QD model to multi-group (e.g., Diesel) fuels. Firstly, the contribution of all hydrocarbon groups (not only n-alkanes) was not considered in the QD model; the contribution of these groups cannot be ignored in any realistic multi-group fuel. Secondly, even if the analysis were restricted only to one group (e.g., alkanes), it did not appear to be easy to approximate the distribution of species with a reasonably simple distribution function $f_m(n)$ in Expression (40). In the Multi-Dimensional Quasi-Discrete Model (MDQDM), both these issues were addressed. In the version of MDQDM considered in ref. 35, n-alkanes and iso-alkanes in Diesel fuel (the composition of this fuel was taken from ref. 62) were treated as a single group of alkanes due to the small differences between their thermodynamic and transport properties.

In the MDQDM, the focus was shifted from the distribution function to consider the contributions of individual species. The corresponding molar fractions were described by the matrix X_{nm}, where m is the index number of a particular group (e.g., alkanes) and n refers to the number of carbon atoms within group m. The names of m groups are presented in Table 13.

Table 13. Diesel fuel groups of components.[35]

m	Group	Molar fraction (%)
1	alkanes	40.0556
2	cycloalkanes	14.8795
3	bicycloalkanes	7.6154
4	alkylbenzenes	16.1719
5	indanes & tetralines	9.1537
6	naphthalenes	8.6773
7	tricycloalkane	1.5647
8	diaromatic	1.2240
9	phenanthrene	0.6577

For each m the values of $\bar{n}_{jm}$ of each QC were found as:[35]

$$\left.\begin{aligned}
\bar{n}_{1m} &= \frac{\sum_{n=n_{1m}}^{n=n_{(\varphi_m+1)m}}(nX_{nm})}{\sum_{n=n_{1m}}^{n=n_{(\varphi_m+1)m}}(X_{nm})} \\
\bar{n}_{2m} &= \frac{\sum_{n=n_{(\varphi_m+2)m}}^{n=n_{(2\varphi_m+2)m}}(nX_{nm})}{\sum_{n=n_{(\varphi_m+2)m}}^{n=n_{(2\varphi_m+2)m}}(X_{nm})} \\
\bar{n}_{3m} &= \frac{\sum_{n=n_{(2\varphi_m+3)m}}^{n=n_{(3\varphi_m+3)m}}(nX_{nm})}{\sum_{n=n_{(2\varphi_m+3)m}}^{n=n_{(3\varphi_m+3)m}}(X_{nm})} \\
&\vdots \\
\bar{n}_{\ell m} &= \frac{\sum_{n=n_{((\ell-1)\varphi_m+\ell)m}}^{n=n_{km}}(nX_{nm})}{\sum_{n=n_{((\ell-1)\varphi_m+\ell)m}}^{n=n_{km}}(X_{nm})}
\end{aligned}\right\}, \tag{46}$$

where $n_{1m} = n_{m(\min)}$ is the minimum n for which $X_{nm} \neq 0$, $n_{km} = n_{m(\max)}$ is the maximum n for which $X_{nm} \neq 0$. Parameter φ_m was assumed to be integer; $\varphi_m + 1$ was equal to the number of components used within each Quasi-Component group, except possibly the last group. φ_m was assumed to be the same for all QC within group m. In the general case, $\ell = \text{integer}((k_m + \varphi_m)/(\varphi_m + 1))$. If $\varphi_m = 0$ then $\ell = k_m$ and the number of QC would be equal to the number of actual components. φ_m and k_m were dependent on m. At $\ell = k_m$, the new approach reduced to the conventional DC model. The averaged carbon numbers ($\bar{n}_{im}$) were not integers in the general case; as in the case of the QD model. If mass fractions of C/QC with large carbon numbers were small, however, these C/QC were merged to form a single QC. With the extended dimensions (groups) (identified as m in System (46)), the new model was described as the 'Multi-Dimensional Quasi-Discrete Model' (MDQDM). As in Table 13, the smallest number of $\bar{n}_{im}$ would be the total number of groups (9 groups in the case of Diesel fuel). The molar fractions of C/QC in each group were estimated as:

$$\left.\begin{aligned}
X_{1m} &= \sum_{n=n_{1m}}^{n=n_{(\varphi_m+1)m}} X_{nm} \\
X_{2m} &= \sum_{n=n_{(\varphi_m+2)m}}^{n=n_{(2\varphi_m+2)m}} X_{nm} \\
X_{3m} &= \sum_{n=n_{(2\varphi_m+3)m}}^{n=n_{(3\varphi_m+3)m}} X_{nm} \\
&\vdots \\
X_{\ell m} &= \sum_{n=n_{((\ell-1)\varphi_m+\ell)m}}^{n=n_{km}} X_{nm}
\end{aligned}\right\}, \tag{47}$$

The results of the application of MDQDM to several fuels are reviewed in the following sections.

4.2.1. Diesel fuel

In ref. 35, the MDQDM was applied to the analysis of Diesel fuel droplets. The full composition of Diesel fuel was accounted for (see Section 2.2 for the details). A droplet with initial radius 12.66 μm and temperature 360 K was monitored whilst moving at constant velocity 10 m/s in a still air at pressure and temperature 32 bar and 700 K, respectively. The plots of typical evolutions of Diesel fuel droplet surface temperatures T_s and radii R_d are shown in Figure 13.[35]

The eleven cases in Figure 13 were that the full composition of Diesel fuel (all 98 components) was accounted for using the DC model (indicated as (98)); this composition was approximated with 23, 21, 20, 17, 15, 12, 9, and 7 C/QC using the MDQDM; this composition was approximated with 9 C/QC (corresponding to the 9 groups shown in Table 13) based on the species initial mass fractions (i.e. ignoring their diffusion) using the SC model (indicated as (S9)); this composition was approximated with 7 C/QC using the SC model (indicated as (S7)); this composition was replaced with only 20 hydrocarbons of alkane, and these alkanes were approximated with a single component of an averaged carbon number ($C_{14.763}H_{31.526}$; indicated as (SA)). It was found that the 15 C/QC approximation, made good predictions of droplet lifetime with less than 3% error compared to that considering all 98 components, using the DC model. At the same time, the use of the MDQDM with 15 C/QC reduced the CPU time by five sixths compared with the CPU time required by the DC model considering all 98 components (see Figure 14). In all cases, the errors were higher and CPU times shorter for smaller numbers of C/QC, and these errors were smaller and CPU times longer for higher numbers of C/QC.

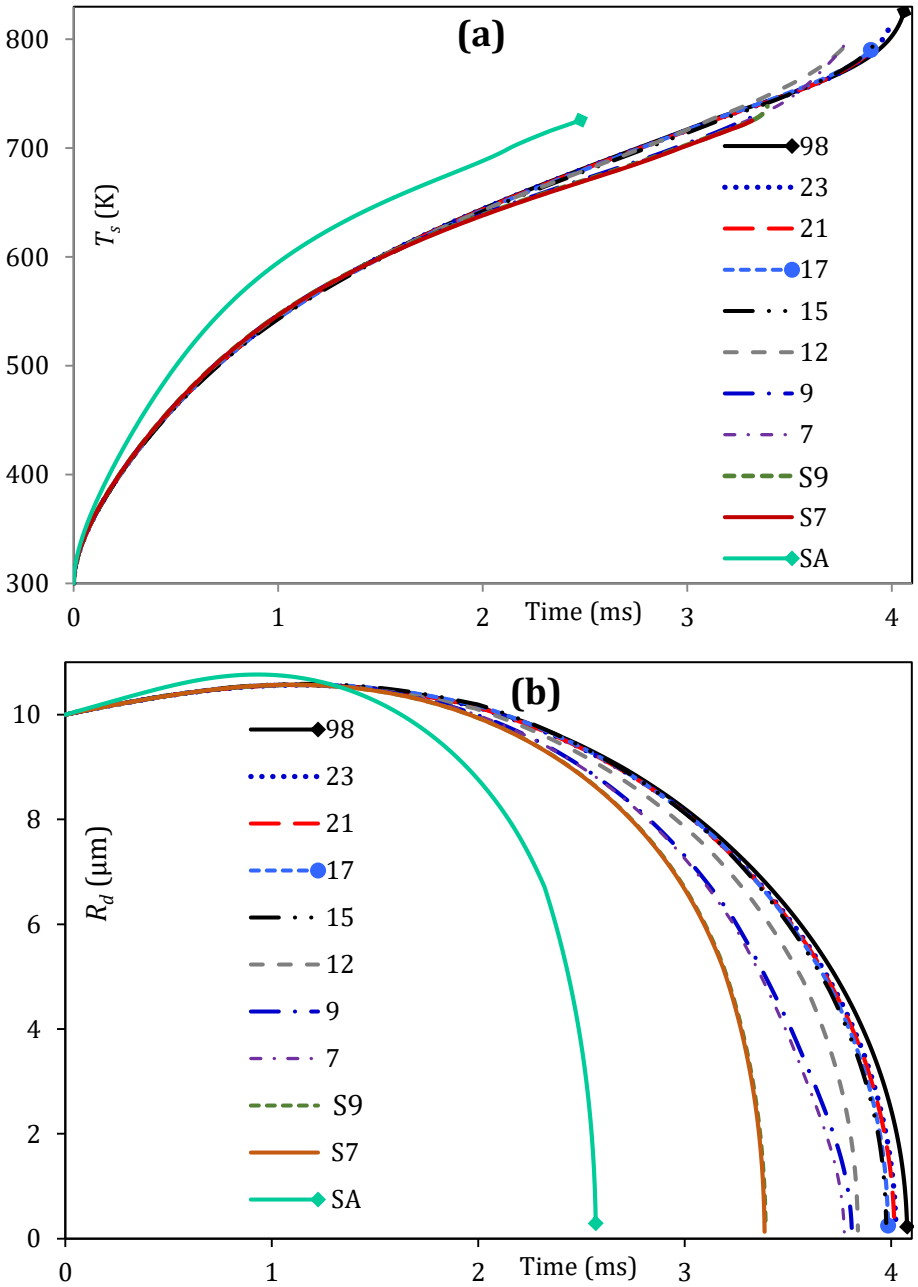

Figure 13. Plots of T_s **(a)** and R_d **(b)** of Diesel fuel droplets versus time, predicted using the DC model for all 98 components, the approximations by 23, 21, 20, 17, 15, 12, 9, and 7 Components/Quasi-Components (C/QC) using the MDQDM, and the approximations by 9 QC (indicated as 'S9'), 7 QC (indicated as 'S7') and 1 alkane QC (indicated as 'SA') using the SC model, which refer to the case when diffusion between these QC is not allowed so that their mass fractions remain equal to the initial mass fractions. Reprinted from Fuel, Volume 154, Pages 238–266, "A multi-dimensional quasi-discrete model for the analysis of Diesel fuel droplet heating and evaporation", by Sazhin et al., copyright Elsevier (2014).

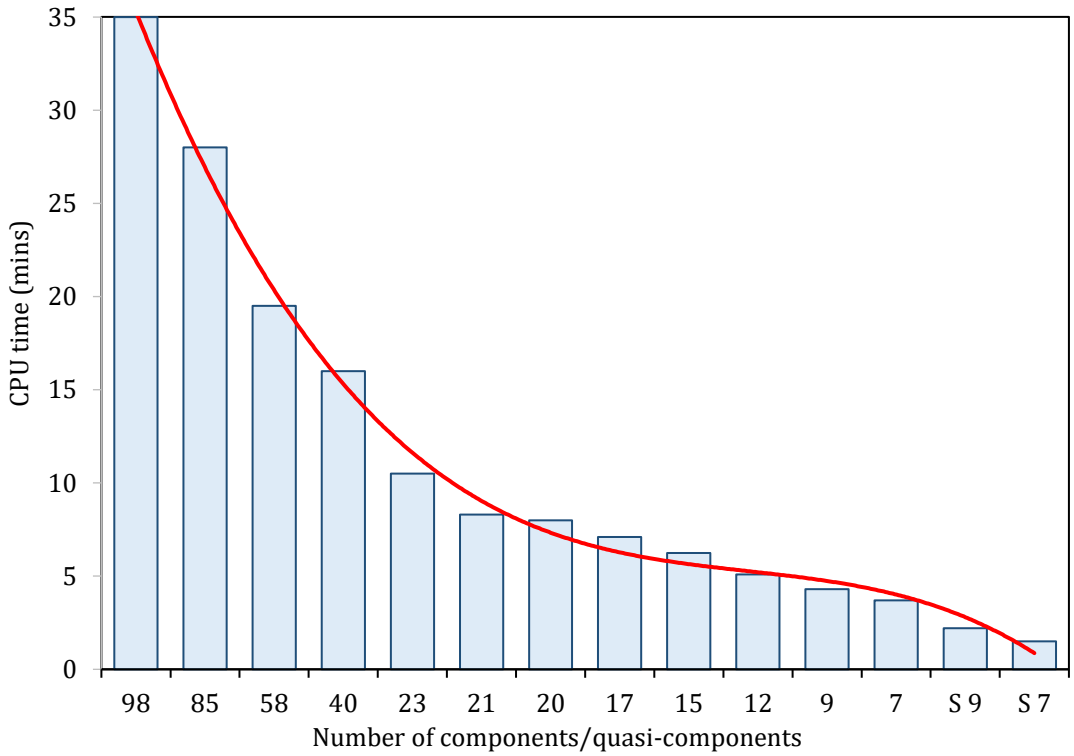

Figure 14. CPU time spent for the calculation of Diesel fuel droplet heating and evaporation, using the same parameters as in Figure 13. Reprinted from Fuel, Volume 154, Pages 238–266, "A multi-dimensional quasi-discrete model for the analysis of Diesel fuel droplet heating and evaporation", by Sazhin et al., copyright Elsevier (2014).

4.2.2. Petrol fuel

In ref. 36, the MDQDM was applied to the analysis of six groups of petrol fuel (described in Section 2.1). Three of these groups were approximated by individual components, while QC were generated for three remaining groups: n-alkanes (n-paraffins), iso-alkanes (i-paraffins) and aromatics. This model was applied to the analysis of heating and evaporation of a droplet with 12 μm initial radius and 300 K initial temperature, moving at 20 m/s in still air. Ambient pressure and temperature were equal to 1 MPa and 550 K, respectively. Examples of the evolutions of the droplet surface temperatures T_s and radii R_d for petrol FACE C fuel are presented in Figure 15.

The results shown in Figure 15 were prepared for the following cases:[36] all 20 components were considered, using the DC model (indicated as '20 components'); the approximation of 20 components with 6 QC ($C_{8.032}H_{18.064}$, $C_{8.936}H_{11.872}$, $C_{5.242}H_{12.484}$, $C_{11.091}H_{24.182}$, $C_{6.181}H_{14.36}$, $C_{10.111}H_{14.222}$), using the MDQDM (indicated as '6 C/QC'); the approximation of 20 components with 5 QC ($C_{10.111}H_{14.222}$, $C_{5.242}H_{12.484}$, $C_{11.091}H_{24.182}$, $C_{7.407}H_{16.814}$, $C_{8.936}H_{11.872}$), using the MDQDM (indicated as '5 C/QC'); the approximation of 20 components with 4 QC ($C_{10.111}H_{14.222}$, $C_{5.242}H_{12.484}$, $C_{7.402}H_{16.803}$, $C_{8.936}H_{11.872}$), using the MDQDM (indicated as '4 C/QC'); and the approximation of 20 components with 3 QC ($C_{5.247}H_{12.494}$, $C_{7.402}H_{16.803}$, $C_{9.072}H_{18.144}$), using the MDQDM (indicated as '3 C/QC'). The MDQDM and DC model were compared in terms of predicted droplet lifetimes and surface temperatures. The errors in droplet lifetimes and surface temperature when replacing 20 components with 6 C/QC were less than 1.73% and 0.7%, respectively. Tolerating such small errors allowed the authors of ref. 36 to achieve a 73% reduction in CPU time, compared to the case when all 20 components were considered.

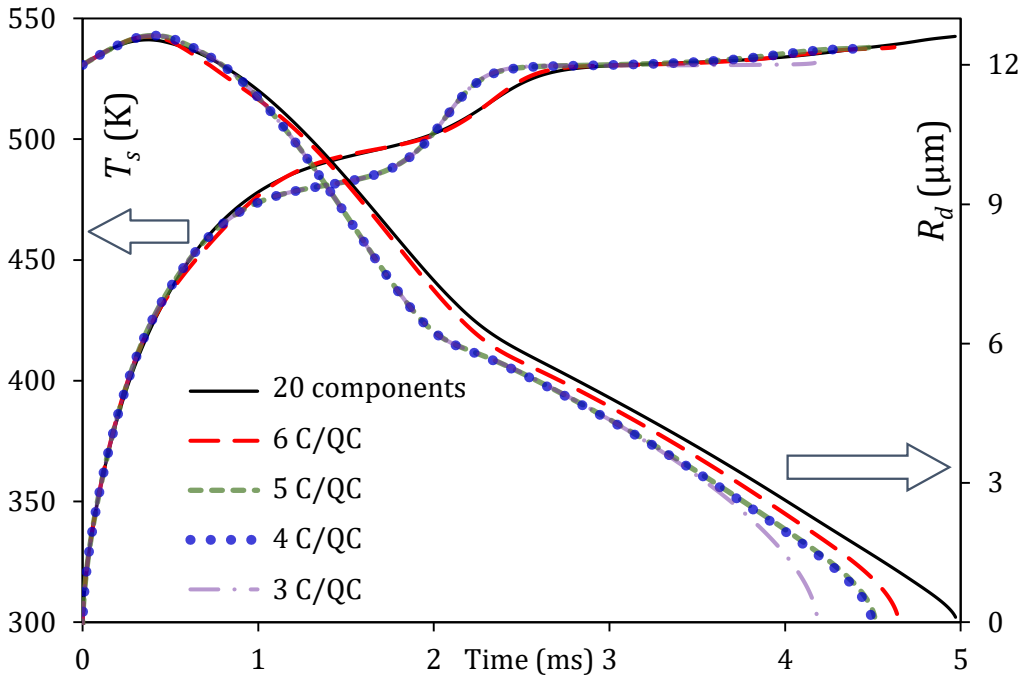

Figure 15. Plots of T_s and R_d of petrol fuel droplets versus time, predicted using the DC model (indicated as 20 components) and their approximations with 6, 5, 4 and 3 Components/Quasi-Components (C/QC) using the MDQDM. Reprinted from Fuel, Volume 159, Pages 373–384, "Modelling of gasoline fuel droplets heating and evaporation," by Al Qubeissi et al., copyright Elsevier (2015).

4.2.3. Biodiesel fuels

In ref. 46, the MDQDM was applied to the analysis of biodiesel fuel droplets. An example of this analysis for waste cooking oil (WCO) FAME is shown in Figure 16. Using the MDQDM led to replacement of 14 methyl esters in WCO with 5, 4 and 3 Components/Quasi-Components (see Table 14). The initial droplet temperature and radius were assumed equal to 350 K and 10 μm, respectively. The droplet was assumed to be moving at 10 m/s in still air of ambient pressure and temperature equal to 30 bar and 800 K, respectively.

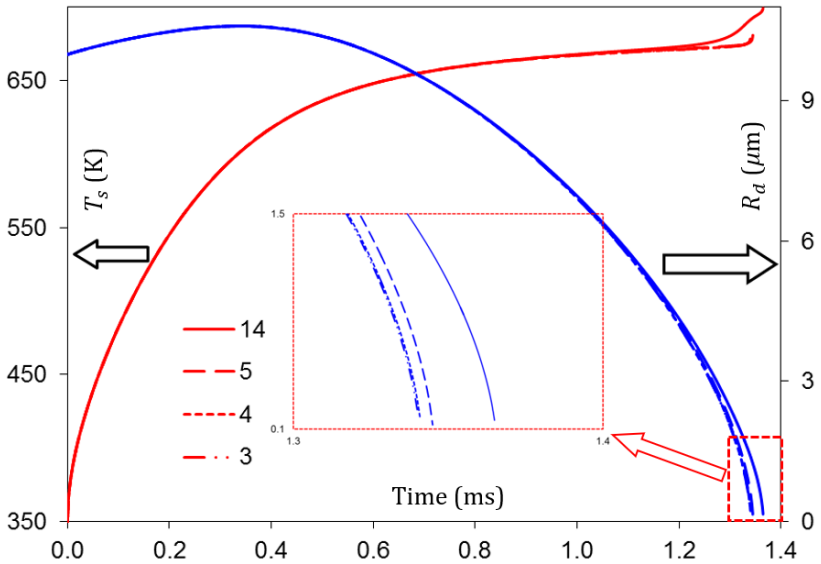

Figure 16. Plot of T_s and R_d of a WCO fuel droplet versus time using the MDQDM, showing the effect of reducing the numbers of Components/Quasi-Components from 14, using the DC model, to 5, 4 and 3 (numbers near the curves; see Table 14). Reprinted from Applied Thermal Engineering, Vol. 136, Pages 260–267, "Predictions of

droplet heating and evaporation: An application to biodiesel, Diesel, gasoline and blended fuels", by Al Qubeissi, copyright Elsevier (2018).

In Figure 16 one can see that replacing the full composition of WCO FAME with 5, 4 and 3 C/QC produced similar plots of the T_s and R_d evolutions for the same conditions. The maximal errors in predicting T_s for all (5, 4, 3) C/QC, using the MDQDM, compared with those taking into account all 14 components were less than 2%. Similarly, the corresponding errors in predicting droplet lifetime were less than 1.83%. At the same time, using the MDQDM reduced the computational time by up to 96% (see Table 14 for more details).

Table 14. Numbers of WCO C/QC using the MDQDM, their formulae, CPU times, and errors when compared to the DC model prediction.[46]

C/QC	FAME	CPU time (ms)	Error%
14 components	See Section 2.3	128	-
5 C/QC	$C_{16.884}H_{33.768}O_2$ $C_{19.597}H_{39.194}O_2$ $C_{19.006}H_{36.012}O_2$ $C_{19}H_{34}O_2$ $C_{19}H_{32}O_2$	55	1.46
4 C/QC	$C_{17.705}H_{35.41}O_2$ $C_{19.006}H_{36.012}O_2$ $C_{19}H_{34}O_2$ $C_{19}H_{32}O_2$	50	1.76
3 C/QC	$C_{17.705}H_{35.41}O_2$ $C_{19.006}H_{36.012}O_2$ $C_{19}H_{34}O_2$	37	1.83

4.2.4. Biodiesel/Diesel fuel blends

In refs. 45,46, the MDQDM was applied to the analysis of blended biodiesel/Diesel fuel droplet heating and evaporation. Both the DC model and MDQDM were considered – accounting for 114 components within 12 groups of hydrocarbons and FAME ($m = 1$ to 3 for FAME groups, and $m = 4$ to 12 for Diesel fuel groups). This model was applied to blends of all 20 types of FAME biodiesel fuel with commercially used Diesel fuel (see Sections 2.2 and 2.3). Droplets were assumed to be moving at 10 m/s in still air; their initial radii and temperatures were 12.66 μm and 360 K, respectively. The ambient air (gas) pressure and temperature were assumed to be equal to 32 bar and 700 K, respectively.

The predicted droplet lifetimes for twenty-two types of biodiesel fuel are shown in Table 8. The B100 RME fuel droplet lifetime was 6% shorter than that of a Diesel fuel droplet. This drop was less than 0.4% for the B5 RME fuel blend. Also, the lifetime of a TGE droplet was 8% shorter for B100, and 0.5% shorter for B5, when compared to that of Diesel fuel. The maximum difference in droplet lifetimes was seen in the case of B100 CME (up to 21.6%). Also, droplet lifetime was always reduced by more than 5.29% for RME when compared to Diesel. Typical examples of the evolutions of T_s and R_d over time, predicted by the DC model and MDQDM for a B5 Diesel-biodiesel fuel blend (5% biodiesel and 95% Diesel) droplet, are shown in Figure 17.

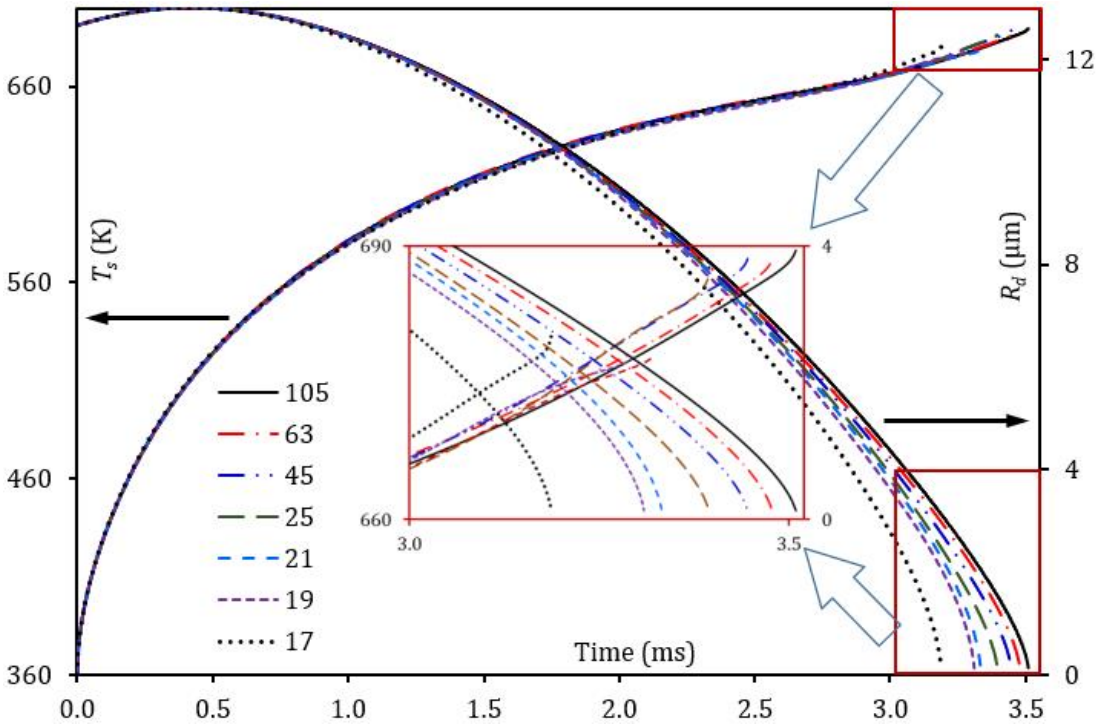

Figure 17. Plots of T_s and R_d versus time for the B5 Diesel-SME blend, using the DC model and MDQDM, with several numbers of C/QC (numbers near the curves). Reprinted from Fuel, Vol. 187, Pages 349–355, "Modelling of blended Diesel and biodiesel fuel droplet heating and evaporation", by Al Qubeissi et al., copyright Elsevier (2017).

In Figure 17 one can see that the approximation of a 105 hydrocarbon/FAME blended fuel with 25, 21 and 17 C/QC caused underpredictions in droplet lifetimes by up to 3.2%, 4% and 4.5%, respectively. The droplet surface temperatures were less affected, with up to 2% error for any approximation. This approximation led to a considerable improvement in the CPU efficiency of computation, as illustrated in Figure 18. As can be seen from Figure 18, the approximation of hydrocarbon and methyl ester species of SME/Diesel B50 blend by 17 C/QC saved more than 83% CPU time in comparison to the case when all 105 components were considered using the DC model. The droplet lifetimes of the B5 and B50 blends using the latter approximation, however, were underpredicted by 4% and 9%, respectively, in comparison to the case when the DC model was used. These errors are acceptable in some engineering applications; toleration of these errors led to considerable improvement in computational efficiency.[45]

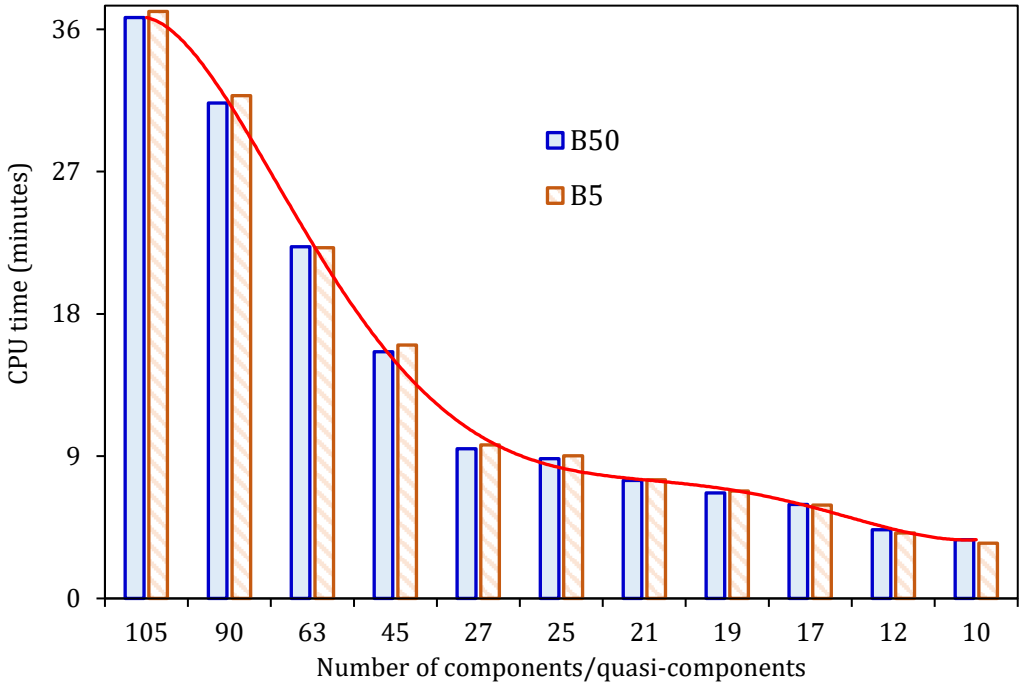

Figure 18. CPU time of the calculation using the MDQDM for B50 and B5 SME/Diesel fuel droplets versus numbers of Components/Quasi-Components, under the same conditions as in Figure 17. Reprinted with modifications with permission from Fuel, Vol. 187, Pages 349–355, "Modelling of blended Diesel and biodiesel fuel droplet heating and evaporation", by Al Qubeissi et al., copyright Elsevier (2017).

4.2.5. Ethanol/petrol/Diesel fuel blends

In some studies,[111,145] Diesel fuels were successfully mixed with ethanol and ethanol/petrol blends for direct use in ICE. In ref. 13, it was shown that mixing 15% ethanol with 85% Diesel is acceptable for standard Diesel engines. In ref. 14, droplets of ethanol/Diesel blend containing up to 20% ethanol were investigated. For higher fractions of ethanol, additives would become essential for the miscibility of ethanol and to attain the required cetane number, stabilise the blend, and control the phase separation.[13,112,117,146–148] The most common blend of Diesel fuel is with flex-fuel (E85, with 15% petrol and 85% ethanol).[111,145,147,149] The addition of petrol can improve the cold start in Diesel engines and reduce nitrogen oxide emissions.[147,150] Previous studies of E85-Diesel blends only considered the ignition delay and exhaust emissions.[111,145,147,149] The influence of such blends, and their detailed properties and the chemical structures of all components, on droplet heating and evaporation had not been considered anywhere in previous studies, until the one presented in ref. 47, to the best of our knowledge.

In ref. 47, the MDQDM was applied to blended E85-Diesel droplets, accounting for the full blended fuel composition (119 components). The impacts of using the MDQDM on the predictions of E85-5 (molar fractions of 95% E85 and 5% Diesel) droplet surface temperatures and radii are illustrated in Figures 19 and 20, respectively. The approximations used in the analysis are 90, 63, 45, 20 and 16 C/QC.

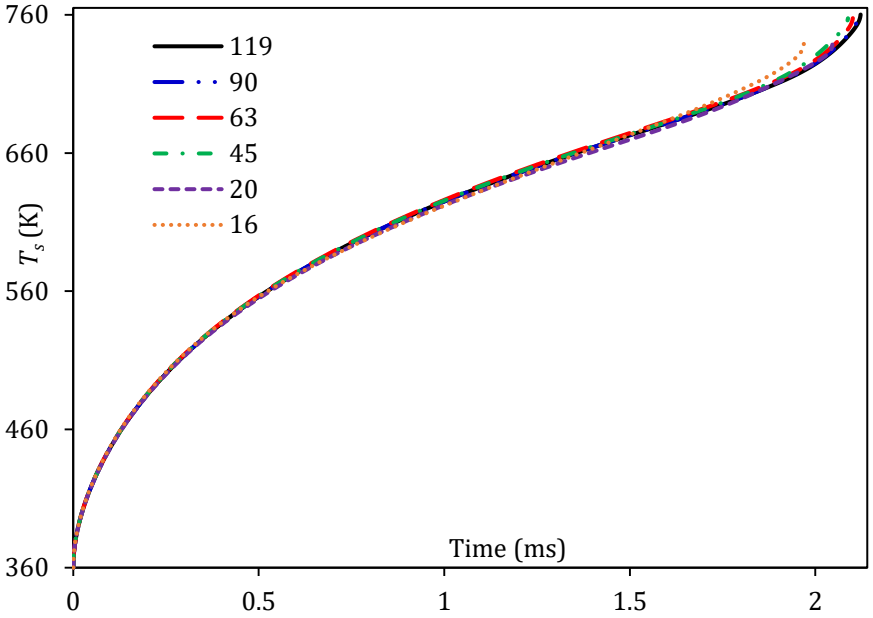

Figure 19. Plots of T_s for E85-5 droplets versus time for six cases: 119 components using the DC model, and approximations of these components by 90, 63, 45, 20, and 16 C/QC (numbers near the curves) using the MDQDM. Reprinted with permission from Energy & Fuels, Vol. 33, Pages 2477–2488, "Blended E85–Diesel fuel droplet heating and evaporation", by Al Qubeissi et al., copyright (2019) American Chemical Society.

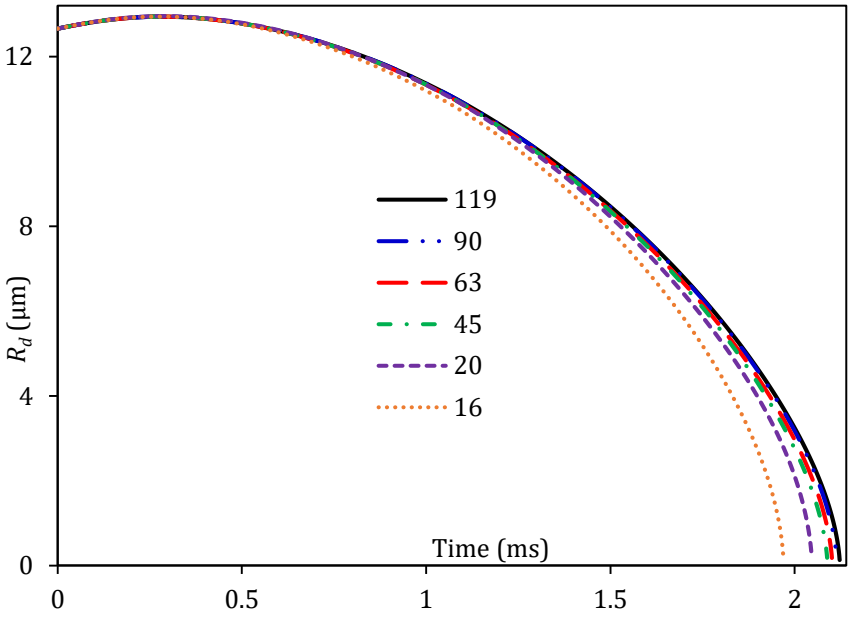

Figure 20. Plots of R_d for E85-5 droplets versus time for six cases: 119 components using the DC model, and approximations of these components by 90, 63, 45, 20 and 16 C/QC (numbers near the curves) using the MDQDM. Reprinted with permission from Energy & Fuels, Vol. 33, Pages 2477–2488, "Blended E85–Diesel fuel droplet heating and evaporation", by Al Qubeissi et al., copyright (2019) American Chemical Society.

In Figures 19 and 20, errors in the case of 90 C/QC were up to 0.26% for droplet surface temperature and up to 0.38% for droplet lifetime, compared with those predicted using the DC model with all 119 components. These errors were up to 0.99% for droplet lifetime and up to 0.39% for droplet surface temperature where the blend was approximated by 63 C/QC. The errors further increased for the case of 16 C/QC, to 7.16% for droplet lifetime and 2.90% for droplet surface temperature. For 20 C/QC, the errors in droplet lifetime and surface temperature were up to 3.58% and 2.90%, respectively. Using the MDQDM achieved a significant improvement in computational efficiency (reduced CPU time), as illustrated in Table 15.

Table 15. CPU time (in s) needed for calculations for six C/QC and the corresponding difference (in percent) in the computational time compared with the case when the DC model was used, Diff= $\frac{|\text{CPU time}_{(C/QC)}-\text{CPU time}_{119}|}{\text{CPU time}_{119}} \times 100$.[47]

Number of C/QC	CPU time	Diff
119	1816	-
90	1360	25.1
63	955	47.4
45	687	62.2
20	314	82.7
16	247	86.4

5. Formulation of fuel surrogates

Fuels used in various practical engineering applications can consist of hundreds of components, mainly hydrocarbons.[133,151] The chemical data and detailed combustion properties of these components are mostly unknown. Therefore, fuel surrogates are widely used to approximate the physical and chemical behaviours of fuels. Fuel surrogates usually include far fewer components than the full composition of commercial fuels such as petrol and Diesel. A wide range of fuel surrogates has been formulated in the past (e.g., refs. 38,139,152–160) to replicate the physical and chemical behaviours of the real fuels using a small number of components. The limitations of researchers' knowledge of the chemistry of combustion processes, and limitations on computational resources, stimulated the approximation of fuels by single components. For example, Diesel and petrol fuels were represented by n-dodecane and iso-octane, respectively.[25,26,161,162] As the reduced chemical mechanisms became more widely available alongside improvements in computational power, surrogates containing more than one component were formulated to match the physical and chemical properties of fuels (including H/C ratio, Research Octane Number (RON) and ignition time delay).

In ref. 37, the DC model was used for the analysis of heating and evaporation of FACE A (A refers to paraffin-rich) petrol fuel (with iso-alkanes accounting for 84 mol%; i.e. research octane number (RON)= 84) droplets and formulation of physical surrogates. Three petrol fuel surrogates from the literature[38,157] were analysed based on their representation of the fuel ignition time delay, research octane number, and H/C ratio. The three surrogates were found to be less than adequate for the analysis of the time evolution of droplet surface temperatures and radii. The study proposed new physical surrogates for FACE A petrol fuel, in which the full composition of this fuel (66 components) was replaced by 19 components. The errors in the predicted droplet lifetimes and surface temperatures of these surrogates were less than 5% and 0.25%, respectively, compared to those predicted using the full fuel composition. Similarly, in ref. 152, the DC model was used for the formulation of physical surrogates of FACE I (a low octane number fuel with RON= 70) petrol. In one set of the formulated surrogates, the 33 hydrocarbons in FACE I petrol fuel were replaced by 8 components, which reproduced the predicted droplet lifetimes and surface temperatures of the full composition of petrol fuel.

A new model was proposed in ref. 40 to formulate fuel surrogates. This model was applied to petrol and Diesel fuels, and their blends with ethanol and biodiesel fuels. The new model, called the 'Complex Fuel Surrogates Model' (CFSM), was based on modification of the MDQDM to allow the generation of, not Quasi-Components, but actual components, or 'Approximate Discrete Components' (ADC). For each ADC in the CFSM, the carbon number was weight averaged by mass fractions as:

$$n_{im} = \left[\frac{\sum_{am}^{bm}(n_{im}\, Y_{im})}{\sum_{am}^{bm} Y_{im}}\right], \tag{48}$$

where, as in Section 4, m referred to the hydrocarbon group number, i referred to the carbon numbers of the i^{th} species in group m, Y_{im} was the mass fraction of the i^{th} species in group m, am and bm were

the first and last components in the group, respectively; am for the 2nd group of components was $bm_{\text{previous}} + 1$.

Unlike the original MDQDM (in which the QC carbon numbers were non-integers in the general case, see Section 4), the nearest integer carbon number was determined from (48). Also, in CFSM, mass fractions Y_{im} were used (instead of the molar fractions in MDQDM) for the calculation of the averaged carbon number n_{im} within each ADC group. Using the mass fractions, instead of molar fractions in Equation (48), was justified in ref. 40 to take into account the importance of heavy components for the prediction of droplet lifetimes. For example, alkane hydrocarbons (the heaviest group in Diesel fuel) accounted for 44.53% of Diesel fuel mass fractions (only 41.48% of Diesel fuel molar fractions). Thus, the dominance of some heavy components was ensured at the expense of the lighter ones, such as alkylbenzenes of initial mass fraction 13.62% (molar fraction 16.75) and naphthalenes of initial mass fraction 7.46% (molar fraction 9%).

5.1. Diesel fuel surrogates

New physical surrogates of Diesel fuel were introduced in ref. 40, using the CFSM. The physical characteristics of these surrogates were compared with those predicted for the full and reduced compositions of fuel, using the DC model and MDQDM, respectively. The evolutions of droplet surface temperatures and radii predicted by the MDQDM[35] and CFSM[40] were compared with those predicted for the full composition of Diesel fuel using the DC model (Figure 21). In ref. 40, the Diesel fuel droplet, of $R_{d0} = 12.66$ μm (initial radius) and $T_{d0} = 360$ K (initial temperature), was moving at $U_d = 10$ m · s^{-1} in air at 800 K temperature and 30 bar pressure. In Table 16, an example is shown to illustrate the effect of approximation of the full composition of Diesel fuel (98 hydrocarbons) with 6 QC (produced using MDQDM) and 6 ADC (produced using CFSM).[40]

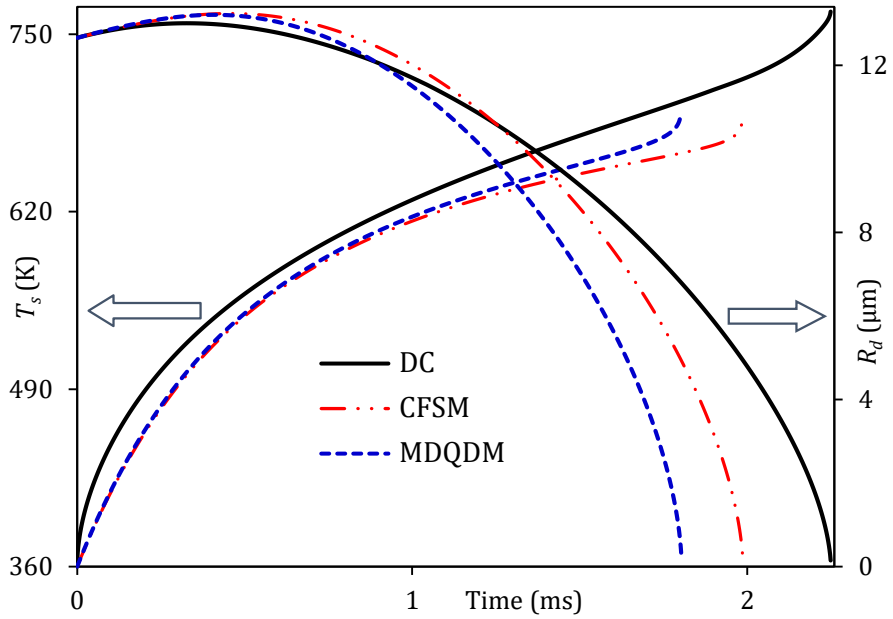

Figure 21. Plots of T_s and R_d versus time for the full compositions of Diesel fuel (98 components) using the DC model, 6 Approximate Discrete Components using the CFSM, and 6 QC using the MDQDM. Reprinted from Fuel, Vol. 283, "A new approach to formulation of complex fuel surrogates", by Al-Esawi & Al Qubeissi, copyright Elsevier (2021).

Table 16. Approximate Diesel fuel composition based on Quasi-Components (QC), produced using the MDQDM, and Approximate Discrete Components (ADC), produced using the CFSM, representing the groups of species in Diesel fuel.[40]

Group	Molar fractions (%)	QC	Mass fractions (%)	ADC

n-alkane	41.48	$C_{14.763}H_{31.526}$	44.53	$C_{16}H_{34}$
cycloalkane	15.41	$C_{15.364}H_{30.728}$	17.05	$C_{17}H_{34}$
bicycloalkane	7.89	$C_{14.743}H_{27.486}$	8.29	$C_{16}H_{30}$
alkylbenzene	16.75	$C_{11.726}H_{17.452}$	13.62	$C_{13}H_{20}$
tetraline	9.48	$C_{13.832}H_{19.664}$	9.05	$C_{15}H_{22}$
naphthalene	8.99	$C_{12.392}H_{12.784}$	7.46	$C_{13}H_{14}$

Examples of comparison between the predictions of the two models (MDQDM and CFSM) for droplet surface temperatures and radii, at time instants $t = 1$ ms and $t = 2$ ms, are shown in Figures 22 and 23, respectively. In Figures 21-23, the predictions of the CFSM look more accurate than those obtained using the MDQDM for this example, especially for small numbers (≤10) of ADC and C/QC. The predicted evolutions of droplet temperatures and radii, using the CFSM approximation of 98 components with 10 ADC, were subject to up to 4% errors, compared with the evolutions predicted using the DC model. The data illustrated in Figures 21-23 matched the trends described in Sections 3 and 4 of this review. Both physical and chemical features of the surrogates produced using the CFSM (Sur1[40]) and those from the literature (Sur2[163] and Sur3[164]) were compared with those for the full composition of Diesel fuel.[47] Table 17 summarises the molar fractions of the components of Sur1 and those of the other two surrogates from the literature (Sur2, Sur3).

The evolutions of Diesel fuel droplet radii and temperatures were analysed using three surrogates (Sur1, Sur2 and Sur3), and compared to those predicted using the DC model. The results shown in Figure 24 refer to a droplet with initial radius 12.66 μm and temperature $T_{d0} = 296$ K, moving at 10 m/s in a still air at 32 bar and temperature 700 K.

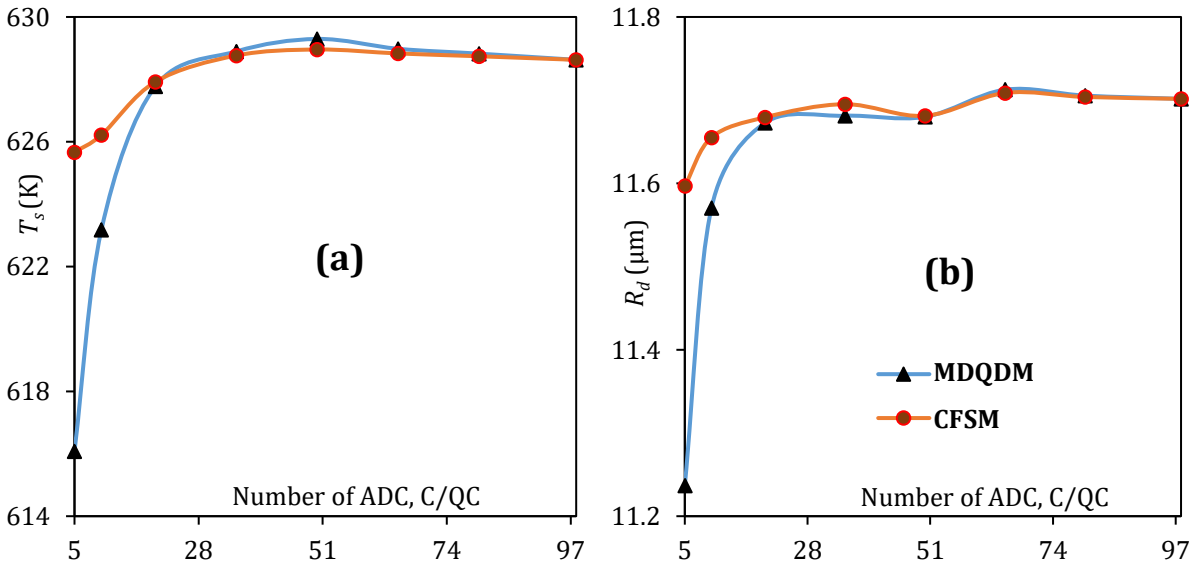

Figure 22. Plots of T_s **(a)** and R_d **(b)** versus the numbers of ADC and C/QC at time instant 1 ms. Reprinted from Fuel, Vol. 283, "A new approach to formulation of complex fuel surrogates", by Al-Esawi & Al Qubeissi, copyright Elsevier (2021).

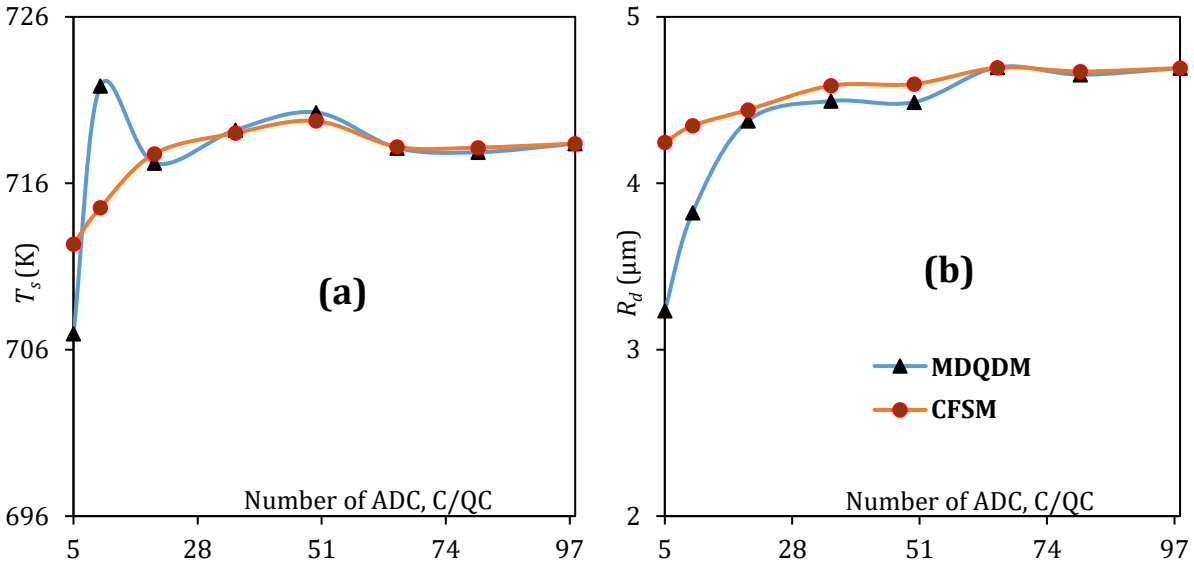

Figure 23. Plots of T_s **(a)** and R_d **(b)** versus the numbers of ADC and C/QC at time instant 2 ms. Reprinted from Fuel, Vol. 283, "A new approach to formulation of complex fuel surrogates", by Al-Esawi & Al Qubeissi, copyright Elsevier (2021).

Table 17. Molar fractions of the components of three surrogates (Sur1, Sur2, and Sur3) of Diesel fuel.[40]

Component	Chemical formula	Molar fractions (%)		
		Sur1[40]	Sur2[163]	Sur3[164]
n-hexadecane	$C_{16}H_{34}$	42.89	41.3	0.88
iso-cetane	$C_{16}H_{34}$	-	36.8	7.48
n-butylcyclohexane	$C_{10}H_{20}$	-	-	29.66
n-pentylcyclododecane	$C_{17}H_{34}$	16.43	-	-
bicyclohexane	$C_{12}H_{24}$	-	-	25.26
bicyclooctane	$C_{16}H_{30}$	7.88	-	-
toluene	C_7H_8	-	-	10.94
heptylbenzene	$C_{13}H_{20}$	13.12	-	-
decalin	$C_{10}H_{18}$	-	-	25.78
1-dimethyl-4-iso-propyltetralin	$C_{15}H_{22}$	8.72	-	-
naphthalene	$C_{11}H_{10}$	-	21.9	-
1-methyl-2-ethyl-naphthalene	$C_{13}H_{14}$	10.95	-	-

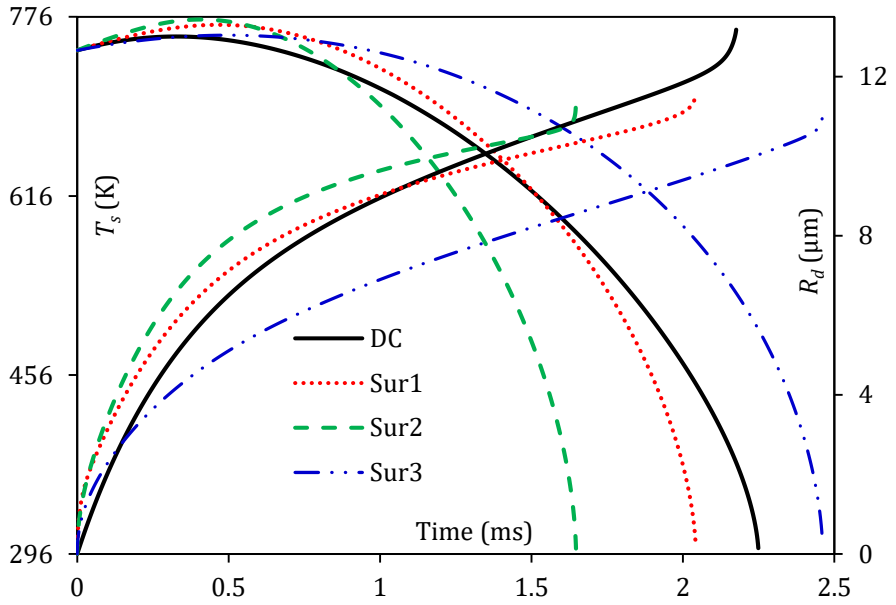

Figure 24. Plots of T_s and R_d for Diesel fuel and the 3 surrogates (Sur1, Sur2 and Sur3). Reprinted from Fuel, Vol. 283, "A new approach to formulation of complex fuel surrogates", by Al-Esawi & Al Qubeissi, copyright Elsevier (2021).

As follows from Figure 24, the time evolutions of the Sur1 droplet radii are the closest to the predictions made for the full composition of Diesel fuel. Droplet lifetime in this case was underpredicted by up to 6.8%. The predicted droplet lifetimes of Sur2 (inferred from ref. 163) and Sur3 (inferred from ref. 164), however, led to errors of 26.8% and 8.4%, respectively. The droplet surface temperatures were underpredicted by 7.3%, 8.4%, and 9.9%, respectively, when Sur1, Sur2 and Sur3 were used.

In ref. 40, the Cetane Number (CN) was investigated for the 3 surrogates. The original composition of Diesel fuel presented in ref. 35 was based on the assumption that n-alkanes and iso-alkanes were part of one group (alkanes) due to the similarity in their chemical properties. For the calculation of CN, however, these two groups were treated separately due to their different CNs.[40] This was due to the different structures of the components – normal (straight chains) or isomers (branched chains).[64] In addition, the viscosities of the three surrogates were also compared to the viscosity of the full composition of Diesel fuel. The viscosity of Sur1 was predicted using the UNIFAC–VISCO method.[95] It was found that the CN of Sur1 mimicked that of Diesel fuel with less than 3% error. At the same time, the viscosity of the proposed Sur1 closely matched that of the full composition of Diesel fuel, with less than 0.8% error. Overall, when taking into account the key features of fuel surrogates (e.g., fuel viscosity, CN and droplet temperatures and lifetimes), Sur1 was found to be the best representative of Diesel fuel when compared to Sur2 and Sur3.

5.2. Petrol fuel surrogates

In ref. 40, the calculations of droplet surface temperatures and lifetimes for the full composition of FACE C petrol fuel were based on the assumption that Raoult's law is valid. In ref. 90, the impact of the activity coefficient on saturated vapour pressure was considered, using the UNIFAC model. In this section, a comparison is made between the physical characteristics of droplets using the full composition of fuel[36,103], surrogates inferred from CFSM (Sur4)[40], and the two previously suggested surrogates (Sur5[38] and Sur6[157]). The compositions of these three surrogates are shown in Table 18.

The predicted time evolutions of droplet radii and surface temperatures for the full composition of fuel and the three surrogates are presented in Figure 25. A droplet of initial radius $R_{d0} = 12$ μm and initial temperature $T_{d0} = 296$ K was assumed to be moving at a constant velocity $U_d = 24$ m · s^{-1} in still air with $p_g = 9$ bar and $T_g = 545$ K.

Table 18. Compositions of the three surrogates (Sur4, Sur5 and Sur6) of petrol fuel.[40]

Component	Molar fractions (%)		
	Sur4[40]	Sur5[38]	Sur6[157]
n-butane	-	17.0	18.4
n-pentane	29.184	-	-
n-heptane	-	11.0	12.5
n-undecane	0. 022	-	-
iso-pentane	10.737	8.0	5.0
iso-heptane	-	5.0	4.7
iso-octane	55.231	56.0	54.6
iso-decane	0.483	-	-
toluene	-	3.0	4.8
iso-propylbenzene	4.343	-	-

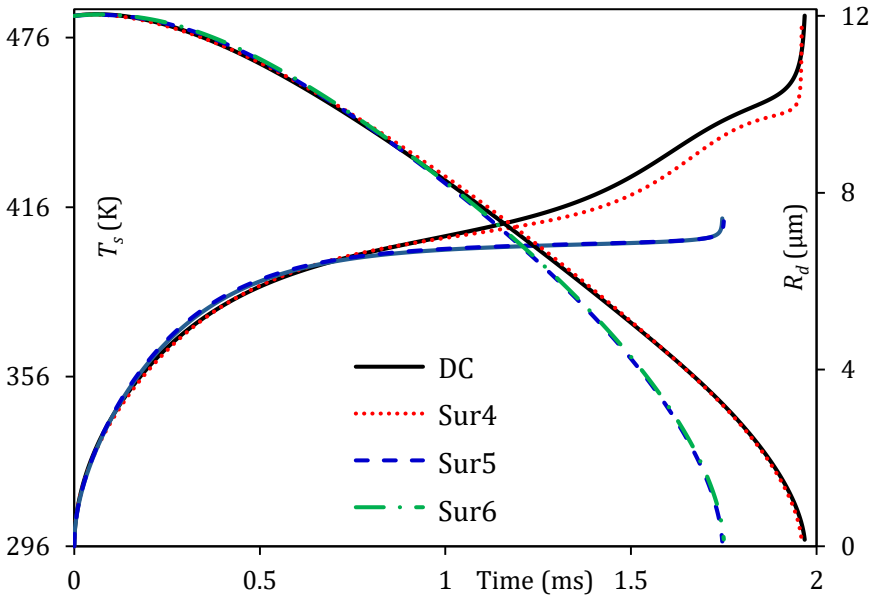

Figure 25. Plots of T_s and R_d versus time for the full composition of petrol fuel and its 3 surrogates: Sur4 (obtained using the CFSM)[40], Sur5[38] and Sur6[157]. Reprinted from Fuel, Vol. 283, "A new approach to formulation of complex fuel surrogates", by Al-Esawi and Al Qubeissi, Copyright Elsevier (2021).

As can be seen in Figure 25, the droplet surface temperatures and radii predicted using the CFSM differ by less than 0.71% and 0.41%, respectively, from those predicted using the full composition of petrol fuel (DC model). It follows from this figure that the corresponding errors in predicting droplet lifetimes for surrogates Sur5 and Sur6 were 15% and 11.3%, respectively. The Sur4 densities were inferred from ref. 165. It was shown in ref. 40 that the densities of all three surrogates were in agreement with those calculated for the full petrol fuel composition. The vapour pressures of the alternative surrogates (Sur5[38] and Sur6[157]) did not match those of the full petrol fuel composition; the corresponding errors were up to 59.1% for Sur5 and 53.0% for Sur6. The physical properties of the fuel were well approximated in the case of Sur4, with less than 4.4% error for vapour pressure prediction. If the molar mass (MM) and H/C ratio of surrogates were made consistent with those of the actual fuel, it was expected that the diffusivity and flame speed would also be consistent with those of the actual fuel.[166] Likewise, the ignition time delay of surrogates could be matched to that of the actual fuel if their RON were close.[38] The H/C ratio, RON, and MM of Sur4 were evaluated and compared with those for the full petrol fuel composition in ref. 40. In the latter study, the H/C ratio was inferred from ref. 157 and RON was inferred from ref. 167. The results of the relevant calculations are presented in Table 19.

Table 19. H/C ratios, RONs and MM (in $g \cdot mole^{-1}$) of petrol fuel and its surrogates.[40]

Fuel	RON	H/C ratio	MM
petrol	84.7	2.27	97.2
Sur4[40]	85.8	2.24	97.8
Sur5[38]	85.3	2.25	98.4
Sur6[157]	85.3	2.23	98.1

5.3. Ethanol/petrol fuel surrogates

Several studies (e.g., refs. 46,54,103,104,108) were focused on heating and evaporation of droplets of biodiesel, ethanol, ethanol/petrol blends and biodiesel/Diesel blends, but without considering the surrogates of these fuels. The first attempt to formulate surrogates of these fuel blends was made in terms of their droplet heating and evaporation.[40] The molar fractions of E20 (20% ethanol and 80% petrol) fuel blend components in two surrogates, the one obtained using the CFSM (Surr7)[40] and the surrogate of ref. 168 (Sur8), are shown in Table 20.

Table 20. Molar fractions of the Sur7 and Sur8 surrogates of E20 fuel.[40]

Component	Molar fractions (%)	
	Sur7[40]	Sur8[168]
n-hexane	18.13	-
n-heptane	-	11.82
iso-pentane	6.64	-
iso-octane	34.17	25.28
iso-decane	2.99	-
toluene	-	25.81
iso-propylbenzene	3.1	-
ethanol	38.13	37.08

The time evolutions of droplet radii and surface temperatures for Sur7,[40] Sur8,[168] and the full composition of the E20 blend are shown in Figure 26. As follows from this figure, using Sur7 leads to a good agreement with the prediction of the DC model using the full composition of E20. The errors in droplet surface temperatures and lifetimes were up to 4% and 2.1%, respectively, compared to those predicted using the full composition of E20. Also, insignificant errors were observed for Sur8 droplet lifetime, compared to the prediction of the model based on the full composition of E20. However, using Sur8 led to a significant deviation in the predicted droplet surface temperature compared to the prediction of the model based on the full composition of E20 (up to 14%). The applicability of surrogates predicted by CFSM was demonstrated for E50 and E85 fuel blends; these were Sur9 and Sur10, respectively (see Table 21).

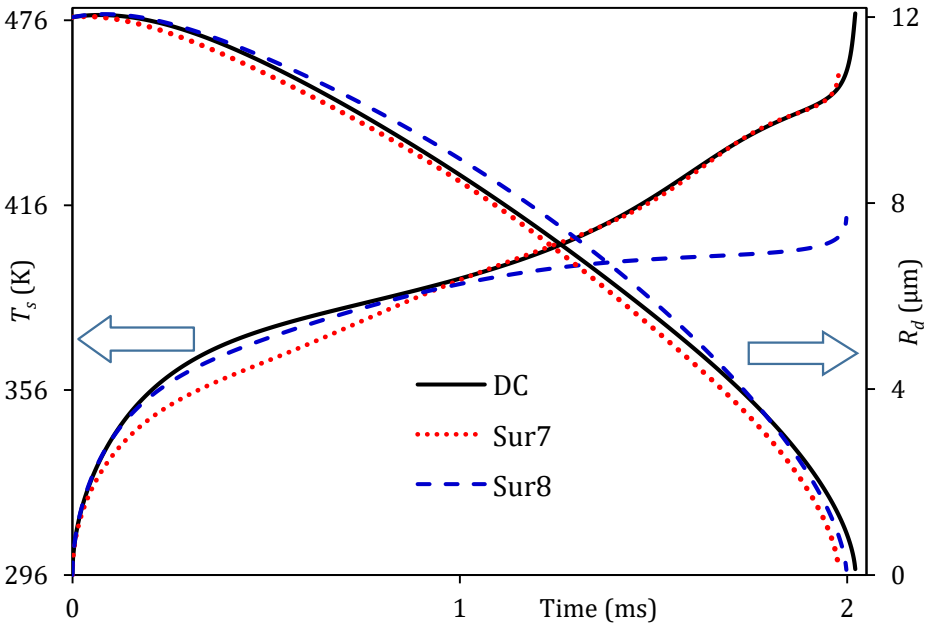

Figure 26. Plots of T_s and R_d versus time predicted by the model using the full compositions of E20 (DC) and surrogates Sur7,[40] and Sur8.[168] Reprinted from Fuel, Vol. 283, "A new approach to formulation of complex fuel surrogates", by Al-Esawi & Al Qubeissi, copyright Elsevier (2021).

Table 21. Molar fractions of the components in Sur9 (surrogates of E50) and Sur10 (surrogates of E85).[40]

Component	Molar fractions (%)	
	Sur9 (E50)	Sur10 (E85)
n-hexane	8.54	1.98
iso-pentane	3.09	0.72
iso-octane	14.54	3.37
iso-decane	1.32	0.31
iso-propylbenzene	1.45	0.33
ethanol	71.15	93.29

In the same study,[40] droplet lifetimes and surface temperatures were analysed for the Sur9 and Sur10 surrogates and the full compositions of E50 and E85 fuels (see Figure 27). The MM, H/C ratios and RON of these fuels and their surrogates (Sur9 and Sur10) are shown in Table 22. It was found that the formulated surrogates for both E50 and E85 blends reproduced the key features of E50 and E85 fuels.

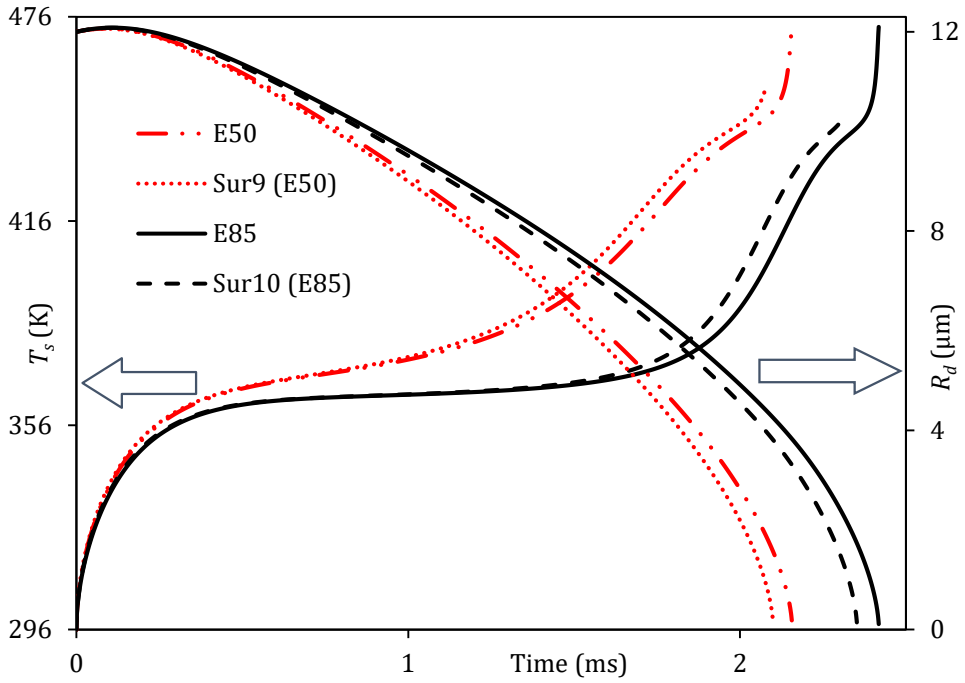

Figure 27. Plots of T_s and R_d versus time for the full compositions of E50 and E85 and their surrogates (Sur9 and Sur10). Reprinted from Fuel, Vol. 283, "A new approach to formulation of complex fuel surrogates", by Al-Esawi and Al Qubeissi, copyright Elsevier (2021).

Table 22. RONs, H/C ratios and MM (in g · mole^{-1}) of E50 and E85 fuel blends and their surrogates.[40]

Fuel	RON	H/C	MM
E50	100.1	2.55	61.03
Sur9 (E50)	102.7	2.58	61.4
E85	106	2.85	49.55
Sur10 (E85)	107	2.85	49.61

5.4. Biodiesel/Diesel fuel surrogates

Biodiesel/Diesel blends are commonly based on WCO biodiesel fuel.[169] As per the UK Department for Transport statistics (2019)[170], about 80% of UK biodiesel (115 million litres) was produced from used cooking oil. The impact of adding biodiesel on droplet lifetime and surface temperature was investigated by the authors of ref. 45. As follows from refs. 64,65, the addition of 10%, biodiesel to Diesel fuel does not necessitate the modification of Diesel engines. In ref. 40, the same ambient conditions and input parameters as in Section 3 of this review were used to analyse the surrogates of B10 (10% vol. biodiesel and 90% vol. Diesel fuel blend, Sur11), B20 (Sur12) and B50 (Sur13). The WCO fuel used in ref. 40 consisted of two unsaturated components of 31.5 mol.% with two double bonds, four unsaturated components of 44.4 mol.% with one double bond, and eight saturated components of 24.1 mol.%. The model predictions for Sur11, Sur12 and Sur13 were compared with those obtained using the full composition of the corresponding fuels in terms of droplet radii and temperatures. The results are shown in Figure 28. The molar fractions of the components in these surrogates are shown in Table 23. In refs. 64,65, the composition of WCO biodiesel fuel was inferred from ref. 63.

The droplet lifetimes and temperatures of the surrogates were underpredicted by less than 7.1% and 8.7%, respectively, compared with those for droplets of the full composition of B10. The CN of Sur9 (to replace B10) was 53.9, which showed consistency with that of the actual fuel (55.1). Therefore, using the results for droplet lifetimes, surface temperatures and CN, we can conclude that the characteristics of droplets of Surr11 for the B10 blend closely match the characteristics of droplets of the full composition of the blend.

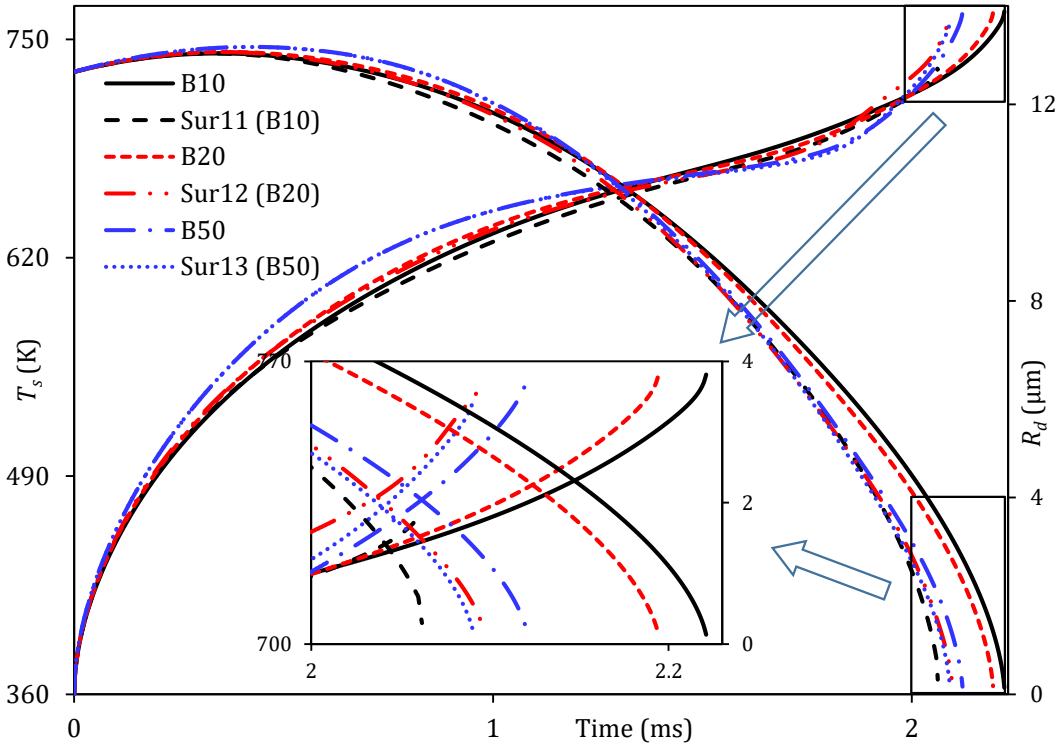

Figure 28. Plots of T_s and R_d versus time for the full compositions of B10, B20 and B50, predicted by the DC model, and Sur11, Sur12 and Sur13, using the CFSM. Reprinted from Fuel, Vol. 283, "A new approach to formulation of complex fuel surrogates", by Al-Esawi and Al Qubeissi., copyright Elsevier (2021).

Table 23. Molar fractions of the B10 (Sur11), B20 (Sur12) and B50 (Sur13) fuel surrogates.[40]

Component	Chemical formula	Molar fractions (%)		
		Sur11 (B10)	Sur12 (B20)	Sur13 (B50)
n-hexadecane	$C_{16}H_{34}$	38.60	34.31	21.44
n-pentylcyclododecane	$C_{17}H_{34}$	14.79	13.15	8.22
bi-cyclooctane	$C_{16}H_{30}$	7.09	6.30	3.94
heptylbenzene	$C_{13}H_{20}$	11.81	10.49	6.56
1-dimethyl-4-isopropyltetralin	$C_{15}H_{22}$	7.85	6.97	4.36
1-methyl-2-ethylnaphthalene	$C_{13}H_{14}$	9.86	8.78	5.48
1-methyl-oleate	$C_{19}H_{36}O_2$	5.85	11.71	29.25
1-methyl-linoleate	$C_{19}H_{34}O_2$	4.15	8.29	20.75

6. Auto-selection of quasi-components

The auto-selection (or auto-generation) of Components/Quasi-Components (C/QC) is essential for the implementation of the MDQDM (see Section 4 of this review) into CFD codes. In ref. 41, a new algorithm, described as the 'Transient Multi-Dimensional Quasi-Discrete' (TMDQD) approach, was suggested. In contrast to the original MDQDM, the new algorithm did not require direct user interference in the formulation of C/QC. Instead, changes in the number of C/QC were allowed during the droplet heating and evaporation process. The initial number of components was assumed equal to the total number of components. At the next timesteps of the droplet heating and evaporation process, the C/QC were generated within each group of components, as in the original MDQDM. Unlike the original MDQDM, however, the number of C/QC within each group was not initially defined by the programmer but was calculated by the code at each timestep. This algorithm automatically allowed the reduction in C/QC numbers from their initial values to smaller numbers. This reduction was controlled by the mass fraction of group i (G_i) at a given timestep. The latter increased or decreased compared with its value at the previous timestep $\left(G_{i_{\text{old}}}\right)$.

In the TMDQD algorithm, it was taken into account that the mass fractions of species (G_i) were better descriptors of their contributions than were molar fractions, which justified their use in the new algorithm.[41] If the change in G_i (ΔG_i) was greater than a small number K (in ref. 41, K was assumed equal to 0.1), the number of C/QC within each group (N_i) would be reduced from this number at the previous timestep ($N_{i_{\text{old}}}$) by the reduction factor F (in ref. 41, F was assumed equal to 0.75).

The QC were formed of the components with the smallest molar fractions (usually the largest carbon numbers) in any group i. In the following timesteps, the relevant sets of C/QC were selected to form new C/QC, the number of which was $N_{i_{\text{new}}} = \text{integer}(N_i/2)$. If the reduction in G_i was small (i.e. $\Delta G_i \leq K$), the number of C/QC at the previous timestep would remain unchanged (i.e. $N_i = N_{i_{\text{old}}}$ and $F = 1$). Using this algorithm, users were able to control the final N_i, with a built-in option at the final stage of the algorithm where feasibility for further reduction is limited. For example, if the end-user sets the final minimum number of C/QC as $N_{i_{\text{final}}} = 10$ but the remaining number of C/QC at the previous timestep (before reaching the final change ΔG_i) is $N_{i_{\text{old}}} = 15$, the auto-reduction is calculated as $N_i = \text{integer}(0.75 \times 15) = 11$ C/QC, and the further reduction of 11 C/QC would result in less than 10 C/QC $\left(\text{i.e. } N_{i_{\text{final}}} = \text{integer}(0.75 \times 11) = 8\right)$, which is not acceptable. Hence, 11 C/QC would only auto-reduce to 10 C/QC.

6.1. Application of the algorithm

In ref. 41, the analysis of droplet heating and evaporation of Diesel fuel and its E85 blend was performed using the TMDQDM. Based on ref. 47, a droplet of initial radius $R_{d0} = 12.66\ \mu$m, and initial temperature $T_{d0} = 298$ K was assumed to be moving at a constant speed of $U_d = 10\ \text{m} \cdot \text{s}^{-1}$. The ambient air temperature and pressure were assumed to be constant and equal to $T_g = 800$ K and $p_g = 30$ bar, respectively. The time evolutions of the droplet radii and surface temperatures predicted by the TMQDM, DC model and MDQDM are shown in Figures 29 and 30, respectively.

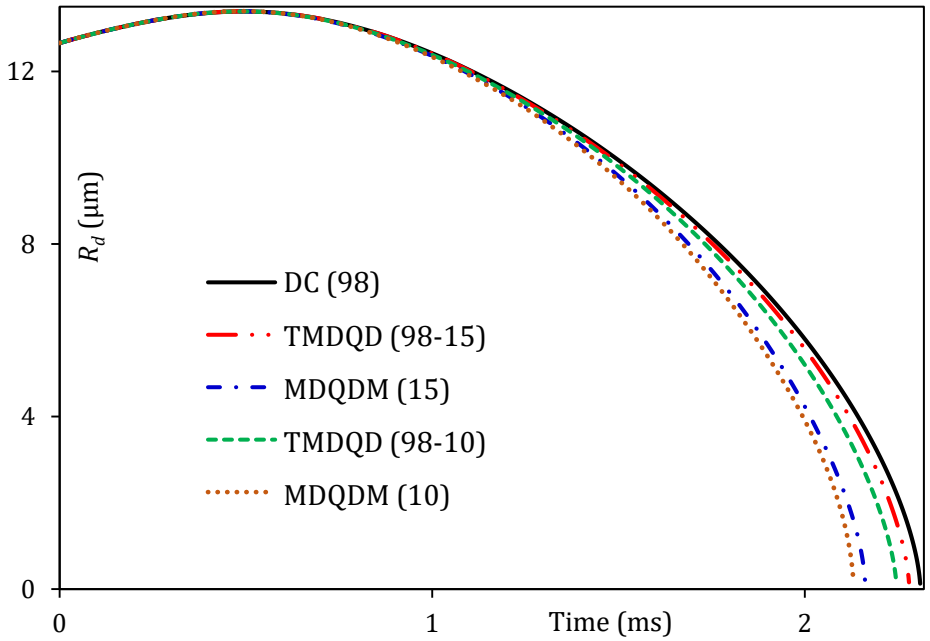

Figure 29. Plots of R_d versus time for Diesel fuel (98 hydrocarbons) droplets, using the DC model, the MDQDM and the TMDQD algorithm. Reprinted from Fuel, Vol. 294, "Auto-selection of quasi-components/components in the multi-dimensional quasi-discrete model", by Al Qubeissi et al., copyright Elsevier (2021).

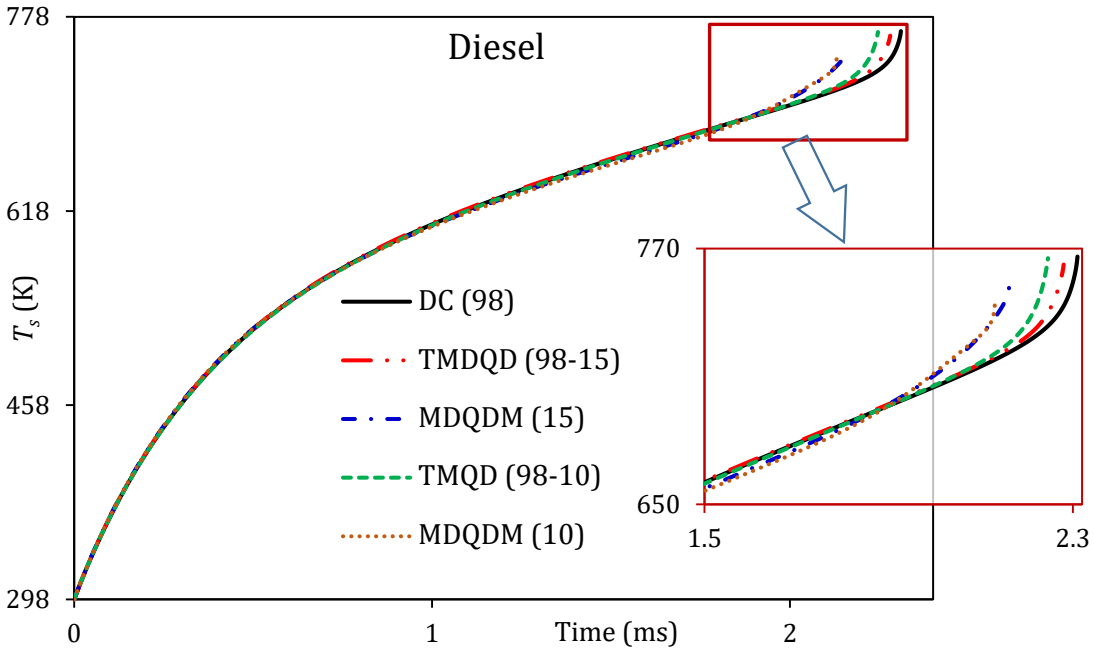

Figure 30. The same as Figure 29, but for T_s. Reprinted with modification from Fuel, Vol. 294, "Auto-selection of quasi-components/components in the multi-dimensional quasi-discrete model", by Al Qubeissi et al., copyright Elsevier (2021).

In Figures 29 and 30, the following cases were considered: the contributions of all 98 components were taken into account, using the DC model (shown as DC (98)); the 98 components were reduced to 15 C/QC, using the original MDQDM (shown as MDQDM (15)); the 98 components were reduced to 10 C/QC, using the original MDQDM (shown as MDQDM (10)); the 98 components were auto-reduced to 15 (or 10) C/QC using the TMDQD algorithm (shown as TMDQD (98-15) and TMDQD (98-10)). TMDQD 98-15 showed the nearest droplet radius evolution to that predicted using the DC model. This was followed by those predicted using TMDQD 98-10. The application of TMDQD (98-15 (98-10)) produced 74 C/QC at time instant 0.300 ms, 56 C/QC at 0.450 ms, 42 C/QC at 0.599 ms, 32 C/QC at 0.782 ms, 24 C/QC at 1.162 ms, 18 C/QC at 1.687 ms, 15 C/QC at 1.887 ms and 10 C/QC at 2.009 ms. Similar trends were seen in the evolutions of droplet surface temperatures (see Figure 30).

One can see from Figures 29 and 30 that the predictions based on the TMDQD algorithm were close to those predicted using the DC model based on the full composition. The evolutions of droplet radii and surface temperature of several other E85/Diesel blends were also investigated in ref. 41, and showed the same trends as those presented in Figures 29 and 30 (see Table 24).

Table 24. Droplet lifetimes (ms) (first column in each cell) relative differences in droplet lifetimes (second column in each cell) for Diesel (98 hydrocarbons), E85/Diesel blends (119 hydrocarbons) and E85 (21 hydrocarbons) fuels, predicted by the TMDQD algorithm and the original MDQDM for 20, 10 and 5 C/QC: $\Delta\text{time} = (\text{time}_{DC} - \text{time}_{model}) \times 100\% \,/\text{time}_{DC}$, where time_{DC} is always greater than time_{model}.[41]

Model	Diesel	Δtime	E85-5	Δtime	E85-20	Δtime	E85-50	Δtime	E85	Δtime
DC	2.310	0	2.186	0	2.026	0	1.817	0	1.220	0
TMDQD (20)	2.280	1.3	2.173	0.4	2.018	0.4	1.812	0.3	-	-
MDQDM (20)	2.160	6.4	2.092	4.1	1.960	3.4	1.769	2.6	-	-
TMDQD (10)	2.246	2.8	2.164	0.8	2.010	0.8	1.809	0.4	1.218	0.2
MDQDM (10)	2.130	7.8	1.990	8.8	1.850	8.6	1.698	6.6	1.990	1.2
TMDQD (5)	2.217	4.0	2.144	1.9	1.998	1.4	1.799	1.0	1.211	0.7
MDQDM (5)	1.985	14.1	1.888	13.6	1.839	9.2	1.681	7.5	1.195	2.1

In Table 24, the errors of predictions when the MDQDM and TMDQD algorithm were used decreased in most cases, and the droplet lifetimes became shorter when the ratios of E85/Diesel increased. Noticeable improvement was indicated in the general trends for the predictions of droplet lifetimes using the TMDQD algorithm, compared to the original MDQDM (with 5, 10 and 20 C/QC). For instance, in the case of E85 fuel, reducing 21 components to 5 C/QC near the end of droplet evaporation, using the TMDQD algorithm, under-forecast the droplet lifetime by less than 0.7%. Using the MDQDM with 5 C/QC increased the error to 2.1%. Remembering that time preceding the combustion processes in ICEs is very short, the accuracy of droplet lifetime predictions becomes crucial. Hence, the application of the TMDQD algorithm for the analysis of these processes was recommended for such applications.[41] For example, processes preceding the onset of combustion are in the range 2– 6 ms during the idle speed range of ICE;[171,172] this range is shorter (0.1 − 1.5 ms) in rapid compression Diesel engines.[173] The CPU times and relevant errors are illustrated in Figure 31.

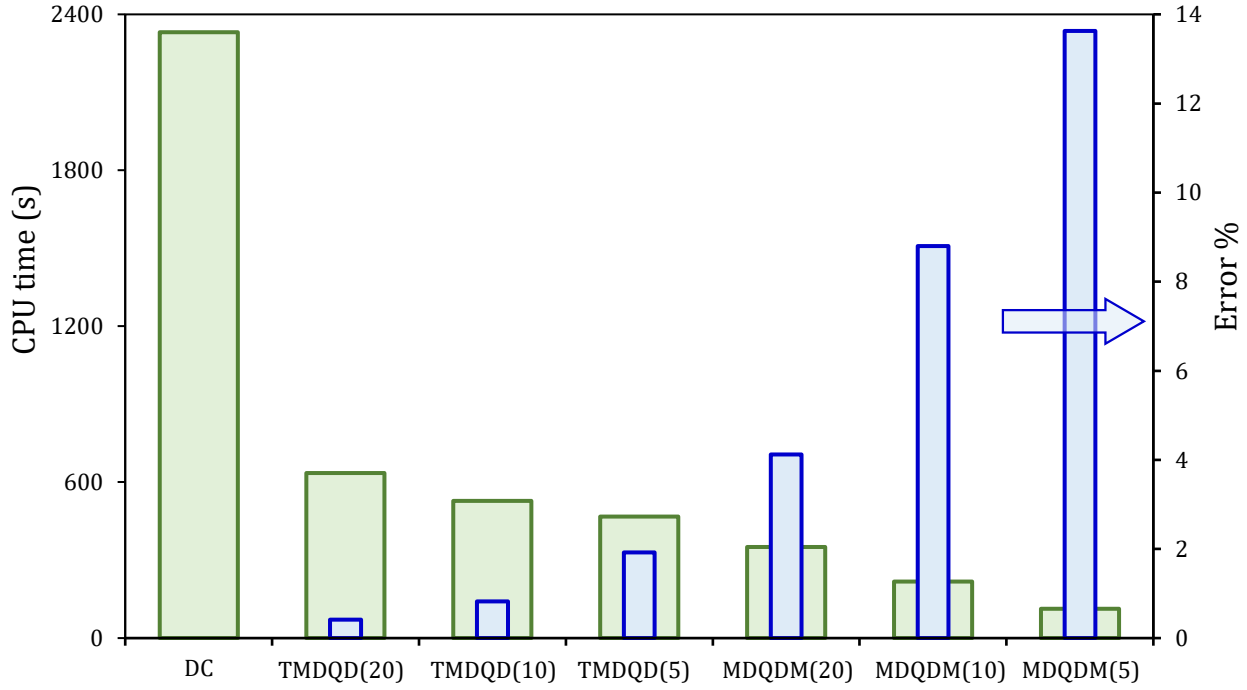

Figure 31. Computational (CPU) times (wide bars) and prediction errors (narrow bars) of six modelling approaches,[41] compared with those predicted using the DC model for E85-5 fuel. Reproduced with modifications from Fuel, Vol. 294, "Auto-selection of quasi-components/components in the multi-dimensional quasi-discrete model", by Al Qubeissi et al., copyright Elsevier (2021).

As can be seen from Figure 31, a significant improvement was achieved in modelling accuracy using the TMDQD algorithm, compared with the results of the MDQDM, and in the corresponding computational efficiency of the TMDQD algorithm, compared with the application of the DC model. For example, using the TMDQD algorithm for 5 C/QC saved 80% of CPU time, compared with the DC model.

7. Spray and full cycle modelling

In ref. 50, the models described in Sections 3 were implemented as user-defined functions (UDF) (see refs. 71,72 for details about the UDFs used in the analysis) into CONVERGE (a commercial Computational Fluid Dynamics (CFD) code).[174]

As with most commercial CFD codes, the model built into the original version of CONVERGE is the ITC/ID model described in Section 3. In the customised version of CONVERGE, this model was replaced with the ETC/ED model using the analytical solutions to the heat transfer and species diffusion equations described in Section 3.[71,72] The thermodynamic and transport properties were calculated at the average temperatures inside droplets using Simpson's rule. These temperatures were updated at

each time-step, which was taken equal to 10^{-5} s. The droplet radius was discretised into 500 layers used to find q_n in Solution (8) for temperature distribution inside droplets and q_{in} in Solution (30) for species mass fraction distribution inside droplets. In both cases, the eigenvalues were found as the solutions to the corresponding equations using the bisection method with an accuracy of 10^{-12}. The customised version of CONVERGE (using the UDF) was validated against experimental data for isolated droplets.[175] The customised version was also used for hollow-cone spray simulations of PRF65. This version was validated against experimental data described in refs. 180, 181.

A hollow cone spray of PRF65 fuel (Primary reference fuel: 65% iso-octane/35% n-heptane) was investigated using the conventional CONVERGE code based on the Amsden et al. combustion (including a particle-based liquid wall film) model[177,178] and the customised version of this software. The full-cycle simulation of a partially premixed compression ignition (PPCI) engine was conducted. The results for the late injection timings were calculated using the customised version of the software which included the new droplet heating and evaporation models and algorithms.

Following ref. 175, the initial droplet radius was assumed equal to 743 μm; the initial droplet composition had the following component mass fractions: 21.3% n-heptane and 78.7% n-decane; the constant droplet velocity and initial temperature were assumed equal to 3.1 m/s and 294 K, respectively; the ambient pressure and temperature were equal to 0.101 MPa and 348 K, respectively. The results predicted by CONVERGE were compared with those predicted using the same software but with the models described in Sections 3–6 of this review (using a user-defined-function described in refs. 177,178), and experimental data.[175] The results of this comparison are shown in Figure 32. In refs. 177,178, temperature and species distribution inside droplets were assumed to be homogeneous, although these were allowed to change with time.

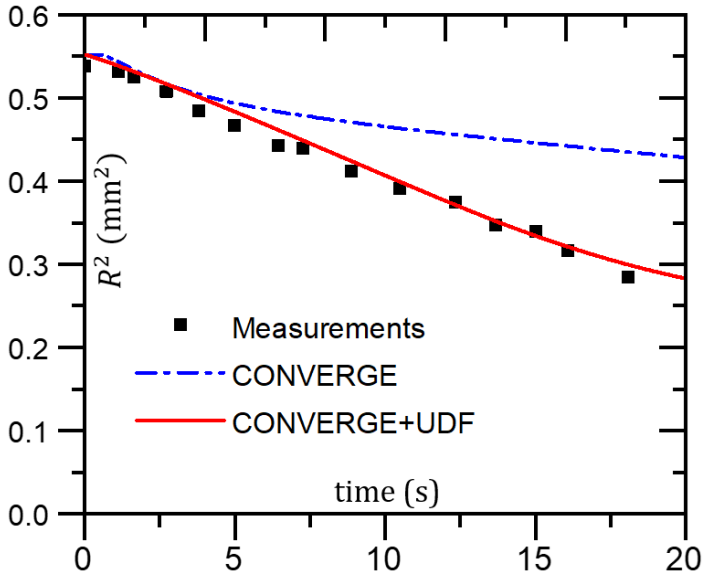

Figure 32. Predicted, using the conventional CONVERGE (dashed-dotted curve)[174] and customised version of CONVERGE (solid curve),[50] and measured (symbols)[175] squared radii of the fuel droplet versus time. Reproduced with permission from Sustainability, Vol. 13, "An improved prediction of pre-combustion processes, using the discrete multicomponent model", by Kabil et al., published by MDPI (2021).

As follows from Figure 32, the predictions made by CONVERGE with the new heating and evaporation model incorporated into it are very close to the experimental data. Also, the predictions of the software with the conventional evaporation model showed lower evaporation rates yielding larger droplets. This clearly demonstrates an improvement in the predictions of CONVERGE when the ETC/ED effects were considered.

The customised version of CONVERGE was used to analyse a PRF65 hollow cone spray. The O'Rourke turbulent dispersion model was used to take into account the turbulence effect on spray droplets. A

dynamic drag model was considered with no-time-counter (NTC) collision to improve the solution accuracy for the post collision regimes.[179]

The effect of the models described in Sections 3–6 of this document on the accuracy of the description of the full engine cycle was investigated using CONVERGE.[50] The simulation results were compared with the results of experiments by Naser et al.,[180] using a PPCI engine with PRF65 fuel. The experiments were conducted on a single cylinder research engine with compression ratio (17:1), 85 mm bore, 90 mm stroke, 138 mm connecting rod length, 100 kPa intake pressure, 298 K intake temperature, 0.51 litre engine displacement, 10 mm bowl depth, and 2 intake and 1 exhaust valves. The intake valve opened at a 30° crank angle (CA) before the top dead centre (BTDC) and closed at 45° CA, after the top dead centre (ATDC), while the exhaust valve opened at a 50° CA, before the bottom dead centre (BBDC), and closed at a 25° CA, after the bottom dead centre (ABDC).

In ref. 50, the impacts of sweeping the start of injection (SOI) between 25 to 20 BTDC were studied to investigate the effect of delayed injection on partially premixed combustion. It was found that accurate modelling of droplet heating and evaporation is crucial to controlling the SOI. Real-life engine dimensions and conditions were used in the geometry inferred from refs. 180,181, with a base grid of 4 mm with fixed Adaptive Mesh Refinement (AMR) at the nozzle exit and dynamic AMR in the fluid flow area. Figure 33 shows the temperature contours and equivalence ratio at various crank angles near the piston. It was shown that at SOI 20 BTDC, the ignition started just at the piston bowl surface, which was attributed to the increased swirling of air inside the bowl and the thermal conductivity of the high temperature piston. Therefore, concentrated fuel vapour (i.e. high equivalence ratio) was seen in this region (point A in Figure 33). Combustion started at point A and spread near the surface of the piston bowl. The predictions were in good agreement with the experimental data (see Figures 33–35). Both, original and customised versions of CONVERGE accurately captured the start of combustion (see Figures 33 and 34). Also, the results of ref. 50 were in good agreement with those based on KIVA-2 simulations for a mono-component Diesel spray,[182] and with those presented in ref. 183. At the early injection stage, larger differences in peak pressure were predicted by the two CONVERGE versions compared to those for late injection, which agreed well with the finding of ref. 158.

Temperature of piston bowl	Equivalence ratio

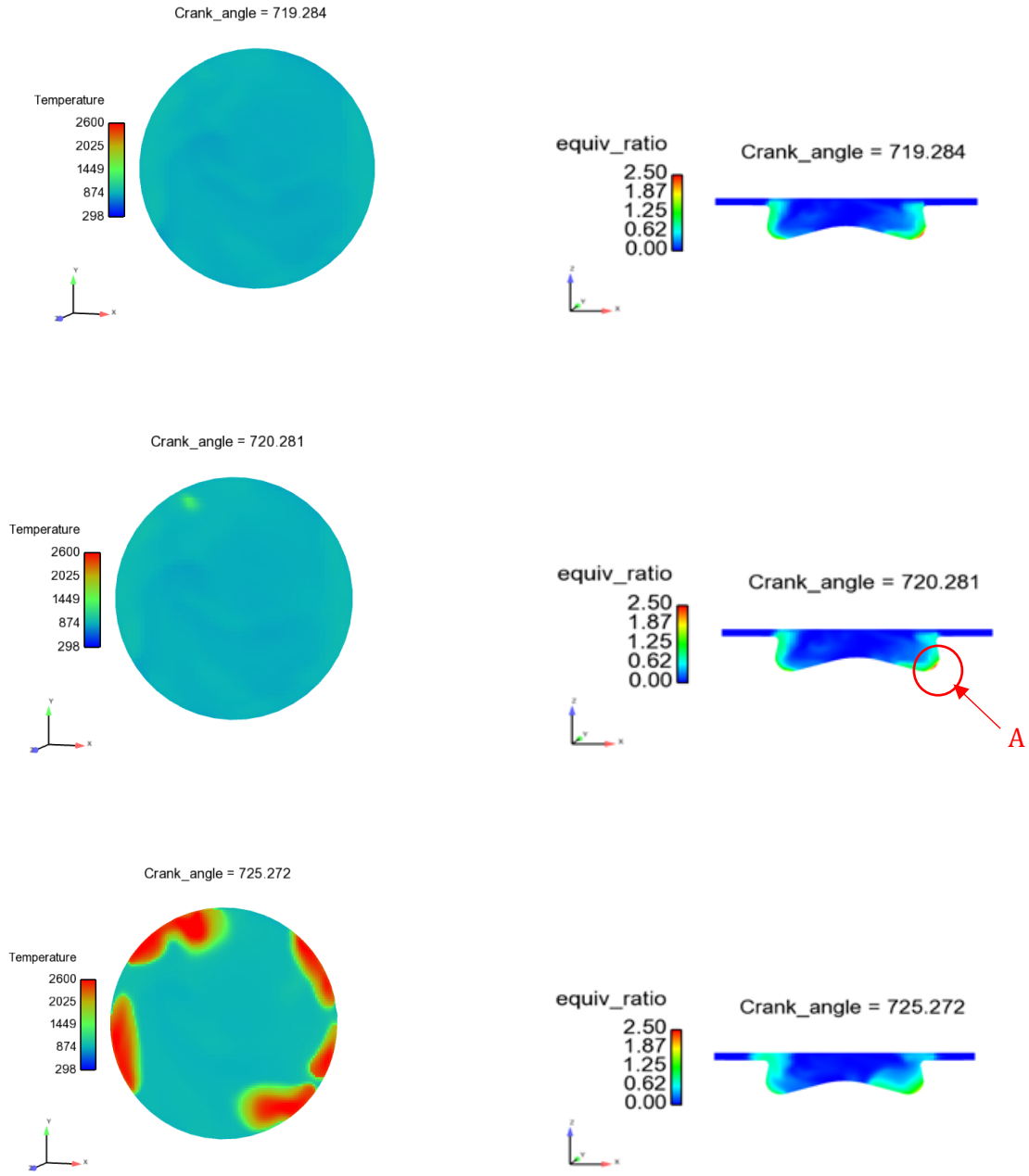

Figure 33. Cross-sections of the engine cylinder, showing the temperatures and equivalence ratios, for the case of SOI 20; the customised version of CONVERGE was used. Reproduced with permission from Sustainability, Vol. 13, "An improved prediction of pre-combustion processes, using the discrete multicomponent model", by Kabil et al., published by MDPI (2021).

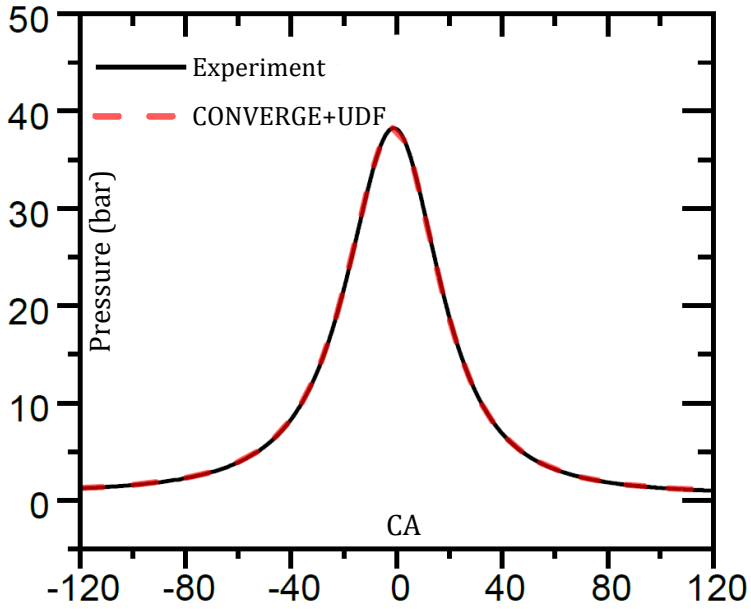

Figure 34. Experimental[180] and predicted (using UDF)[50] in-cylinder pressures versus crank angles (CA). Reproduced with permission from Sustainability, Vol. 13, "An improved prediction of pre-combustion processes, using the discrete multicomponent model", by Kabil et al., published by MDPI (2021).

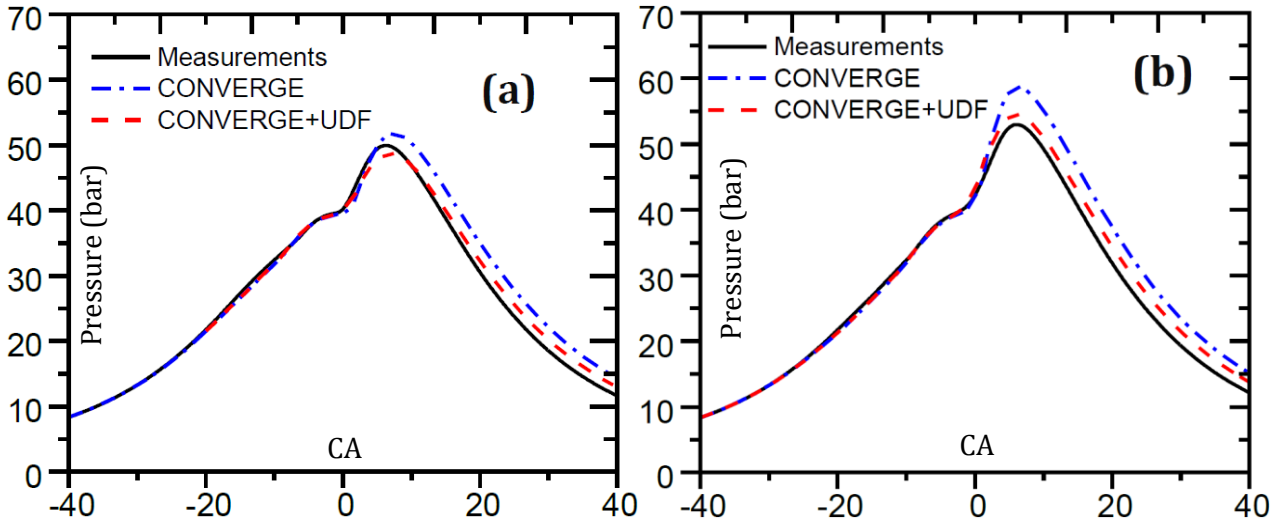

Figure 35. In-cylinder pressures: measured results[180] and those inferred from the simulation using the standard[174] and customised (using UDF)[50] versions of CONVERGE at SOI 20 **(a)** and 25 **(b)** CA BTDC. Reproduced with permission from Sustainability, Vol. 13, "An improved prediction of pre-combustion processes, using the discrete multicomponent model", by Kabil et al., published by MDPI (2021).

8. Research perspectives

In the last two decades, several milestones have been achieved in the experimental and numerical development of fuel droplet heating, evaporation, atomisation, and combustion applications, including those for multi-component and blended fuels. Substantial research advancements in the modelling of droplet heating and evaporation, and their implementation into commercial CFD codes have been reported. Full engine cycle simulations have been addressed. The recent developments support the need to formulate physical and chemical fuel surrogates. The developed models have also addressed the need to take into account detailed processes inside droplets with careful consideration of computational efficiency and accuracy, using CFSM and the TMDQD algorithm. The key findings summarised in this review are presented in Table 25. Some phenomena, such as moving interfaces [184] and kinetic effects,[185,186] have been ignored in these models due to their minor contribution in most cases.

Table 25. List of key findings, with main advantages and disadvantages identified in the review.

References	Key finding	Key benefit	Main limitation
[19]	ETC/ED models	Accounting for the temperature gradient, recirculation, and species diffusion inside droplets	The models have been tested for a limited range of Peclet numbers. They can correctly describe temperature and species mass fractions only at the droplet surfaces
[84,85,187,188]	DC model based on the analytical solutions to the heat transfer and species diffusion equations	The implementation of the analytical solutions to the heat transfer and species diffusion equations into the numerical codes makes these codes more CPU efficient compared with the case when the numerical solutions to these equations are used in these codes	Computationally expensive for large numbers of components
[44,63,66,46,47,65,90,135]	Application of the DC model to realistic fossil fuels, biofuels, and their blends	Highly accurate predictions of droplet heating and evaporation. In depth understanding of the physics associated with droplet heating and evaporation	Computationally expensive, chemical reactions were not considered
[37,48,49,152]	Application of the DC model to the formulation of fuel surrogates	A new approach to the formulation of surrogates for liquid fuel heating and evaporation and combustion of fuel vapour/air mixtures	Focused on the physical surrogates, chemical reactions were not well investigated
[33,34]	Reduced compositions using the quasi-discrete (QD) model	Fuel composition is replaced with a smaller number of quasi-components, which reduces CPU time	Only one group of components can be considered in this approach
[35,36,45]	Reduced compositions using the multi-dimensional quasi-discrete model (MDQDM)	Fuel composition is reduced to a much smaller number of components using a wide range of groups of components, which reduces CPU time	The selection of components and quasi-components (C/QC) requires user-input, which makes it difficult to implement this model into CFD codes
[41]	The auto-selection of quasi-components in the MDQDM using the Transient Multi-Dimensional Quasi-Discrete (TMDQD) algorithm	The C/QC are automatically selected in a transient manner, which makes the code directly implementable into CFD codes	Increase in CPU time, compared to the MDQDM
[40]	Formulation of complex fuel surrogates using the	Formulation of physical surrogates of any type of fuel	Based on the approximation of quasi-

	MDQDM and TMDQD algorithm		components to the nearest integer carbon numbers
[50,71,72]	Implementation into CFD codes and application of these codes to full cycle simulations	Improved CFD models taking into account new effects	Simplified assumptions used in the modified versions of the codes including the assumption that droplets are spherical

Some important processes are still being investigated. For example, the reviewed models were based on the assumption that droplets are spherical. However, the real-life geometries of these droplets can be far from spherical. Additionally, droplets were assumed to be isolated, ignoring the effects of surrounding droplets. It is anticipated that future research will focus on a number of cases not investigated in detail so far, including the following:

- Non-spherically symmetric droplets can be modelled using the DC model. Mathematical modelling of a spheroidal droplet was presented in ref. 189. The results presented in the latter paper, however, can be considered as preliminary. Further investigation in this direction is anticipated.
- The impact of radiation on the heating and evaporation of a semi-transparent droplet should be considered, taking into account full compositions of fuels. This effect was considered in refs. 78,190, but for a very limited number of fuels and cases.
- The impacts of the kinetic region in the vicinity of the droplet interface should be investigated. Thus far, increasing the number of components beyond two for such a complicated model has been challenging.[191]
- The micro-explosion of droplets appears to improve their evaporation rate.[192] This has not been considered for full fuel compositions and blends and could be a potential future research direction.
- There is a need to apply the models described in Section 3 to a wider range of applications than those considered in this review.

Some other research findings relevant to the abovementioned perspective research, which have not been discussed in this review, are presented in Table 26.

Table 26. Future research directions.

Research directions	References	Current position
Emulsion (water/n-decane) droplet combustion	[193]	Has not been investigated for multi-component fuels
Puffing/micro-explosion	[192,194]	Not used for the analysis of the processes in IC engines
Semi-transparent droplets	[57,78,190]	Applied to the analysis of a limited number of fuels
Non-spherical droplets	[189,195,196]	Applied to the analysis of a limited number of shapes (spheroid)
Kinetic effects	[185,186]	Computationally expensive, with small effects on the accuracy
Sprays used in gas turbines	[197]	Limited research on application of the DC model to turbines

9. Conclusions

This review has summarised recent investigations into the heating and evaporation, and some of the combustion characteristics, of multi-component hydrocarbon droplets and sprays. Findings concerning the application of the Discrete Component (DC) model, Multi-Dimensional Quasi-Discrete

model (MDQDM), Approximate Discrete model (ADM), Transient MDQD algorithm (TMDQD algorithm) and Complex Fuel Surrogates Model (CFSM) to the analysis of droplets of petrol, Diesel, biodiesel, ethanol, and their common blends were reviewed. Approaches to estimating the activity coefficient were described. The results of investigation of the impacts of a wide range of ambient conditions, including ambient and radiative temperatures, pressure, and molar fractions of components in blended fuels on droplet heating and evaporation were described. It was shown that the assumption of a unity activity coefficient (AC = 1) based on the validity of Raoult's law could lead to 5.7% errors in the predictions of droplet lifetimes, compared to predictions based on the transient UNIFAC approach.

It was shown that droplet lifetimes were up to 33.9% longer for the balanced ethanol/petrol molar fractions, than for those of pure petrol or pure ethanol fuels. Also, it was shown that the predicted ethanol droplet surface temperature was 24.3% lower than that predicted for a petrol fuel droplet. This was attributed to the lower boiling and critical temperatures and saturated vapour pressure, and the higher density of ethanol than of petrol fuel. The addition of ethanol to petrol fuel made the latter less volatile. It was shown that increasing the ambient pressure, radiative temperature, or ambient temperature, led to shorter droplet lifetimes (faster evaporation), regardless of the blending fractions in ethanol/petrol fuels. It was also shown that E85/Diesel blended fuel droplets had shorter lifetimes than those of pure Diesel. Application of an E85/Diesel blend led to shortening of the droplet lifetime by up to 49.5% and reduced the surface temperature by up to 23.4%, compared with pure Diesel fuel droplets. The approximation of 119 components of E85/Diesel fuel by 20 C/QC saved up to 83% of CPU time but led to 3.6% and 2.9% errors in predicting droplet lifetimes and surface temperatures, respectively.

The effects of mixtures of ethanol/biodiesel/Diesel on the key parameters, including viscosity, Cetane Number (CN), heating value and droplet heating and evaporation characteristics, were demonstrated, using the DC model. It was shown that the presence of 5% ethanol and 5% biodiesel (instead of only 10% ethanol) in the mixtures of ethanol/biodiesel/Diesel compensated for the reduced heating value, viscosity, CN, and droplet surface temperatures and lifetimes (observed when ethanol alone was added to Diesel). In the case of an E5/B15/D80 (5% ethanol, 15% biodiesel and 80% Diesel) fuel blend, the heating value, viscosity, CN, and droplet lifetime were reduced by only 2.2%, 2%, 0.2%, 1.2%, respectively, compared to the same values for the case when pure Diesel fuel (D100) was used.

The development of the Complex Fuel Surrogate Model (CFSM) and its usefulness for the formulation of physical and chemical surrogates of a broad range of fuels and their blends (e.g., Sur1 for Diesel, Sur4 for petrol, Sur7 for E20, and Sur9 for B10) were described. The time evolutions of radii and surface temperatures of droplets of the above-mentioned surrogates and actual fuels were described alongside their chemical properties (e.g., research octane numbers for petrol and ethanol/petrol fuels, cetane numbers for Diesel and biodiesel/Diesel fuels, and H/C ratio). Physical and chemical characteristics of the suggested surrogates and their comparisons with those recommended in the literature were described. The chemical and physical behaviours of droplets of four surrogates suggested by the authors were shown to be in reasonably close agreement with those predicted for droplets of the full compositions of fuels. Although the usefulness of surrogates predicted by the CFSM was clearly demonstrated, the selection of components and quasi-components (C/QC) in this model is based on trial and error. Hence, at present, input from experienced end-users is still required to run this mode.

In contrast to the original MDQDM and CFSM, the recently suggested Transient Multi-Dimensional Quasi-Discrete (TMDQD) algorithm was shown to be a powerful approach to auto-updating C/QC to consider the transient diffusions of species. This algorithm was used for the analyses of droplets of a wide range of fuel blends. Its predictions were compared to those of the earlier developed MDQDM in terms of accuracy and computational competency. The usefulness of the TMDQD algorithm was demonstrated by reducing the full compositions of E85-Diesel fuel (119 species) down to 10 C/QC, sacrificing only up to 1.82% error in predicting droplet lifetimes and temperatures. The application of

this algorithm was shown to have saved about 88% of the CPU time that would be needed if the full composition of fuel was used.

The MDQDM was successfully implemented into the commercial CFD software CONVERGE via user defined functions (UDF). The results predicted by the modified version of CONVERGE were shown to be nearer to experimental data than those produced using the original version of CONVERGE. The two versions also produced similar trends. The results of simulation of a partially premixed compression ignition engine at late fuel injection timings were summarised. It was found that the modified version of CONVERGE, using the new models, leads to more accurate prediction of the combustion characteristics compared with the conventional version of CONVERGE.

Author biographies

Mansour Al Qubeissi is an Assistant Professor of thermo-fluid mechanics and Course Director for Master of Engineering (MEng – mechanical, automotive and motorsport) programmes at Coventry University, UK. He is a Fellow of the Higher Education Academy, a Chartered Engineer, and a Community Buddy in the British Science Association. He received his PgCert HE (1st) from Coventry University in 2016, PhD in engineering from the Sir Harry Ricardo Laboratories, University of Brighton, in 2015, MPhil in engineering from Rolls-Royce UTC – TFMRC, Sussex University, in 2012, and MSc (1st) of power generation in 2005 and BSc (Hons) in 2002 from Mechanical Engineering Department, University of Technology – Baghdad. He is experienced of computational thermo-fluid mechanics, combustion, and energy systems.

Sergei S. Sazhin is a Professor of Thermal Physics at the University of Brighton (UK). He received his PhD (Physics) from St Petersburg State University (Russia) in 1977. He is a Fellow of the Institute of Physics (UK) since 1994, an Awardee of the Leadership in Research Excellence from the University of Brighton in 2017, and a member of the Scientific Council of the International Centre for Heat and Mass Transfer (ICHMT) since 2018. He has authored more than 550 publications, including 4 monographs and more than 250 papers in international refereed journals.

Nawar Al-Esawi is a Lecturer in engineering at the University of Northampton, UK. He received his BSc in chemical engineering from the University of Baghdad (2012) and MSc in chemical process engineering from the University of Leeds (2015). During 2017 to 2020, he conducted his PhD thesis about "blended fuel droplets heating, evaporation and combustion" at Coventry University, UK. His research interests are blended fuels and modelling of heat and mass transfer processes.

Ruslana Kolodnytska is an Associate Professor of automotive engineering at Zhytomyr Polytechnic State University, Ukraine. She received her PhD (with Award of the best PhD paper) in Solid Mechanics from Ternopil State Technical University, Ukraine in 1998, and MSc (Hons) in mechanical engineering from Kiev University in 1981. In 2012, she was winner of the best Award from the Ministry of Education and Science – Ukraine for the pioneering project "Biofuel spray and evaporation modelling". She is author of more than 100 publications and monographs in automotive engineering. Her main field of interest is alternative fuels.

Bidur Khanal is an Assistant Professor of aerospace engineering at Coventry University, and a Visiting Fellow to the National Flying Laboratory Centre at Cranfield University, since 2018. Prior to that, he was a Lecturer in Complex Weapons at Cranfield University's Centre for Defence Engineering (2015-2018), an aerodynamic methods and tools engineer at GE Power (2013-15), a Research Fellow in turbomachinery at Rolls-Royce UTC, University of Oxford (2010-2013). He is a Chartered Engineer, member of the Royal Aeronautical Society, and Associate Fellow of the Higher Education Academy, UK. He received his BEng (1st) in Aeromechanical Systems Engineering in 2004 from the Royal Military College of Science, Cranfield University, MPhil in Computational Aeroacoustics from the University of Southampton in 2016, and PhD in aerodynamics from Cranfield University in 2010. His research focuses on the development of CFD methods for complex fluid flow problems.

Mohammed Ghaleeh is a Senior Lecturer in Engineering at the University of Northampton. He received his PhD in thermo-mechanical engineering from Heriot-Watt University in 2014. He is experienced of FEA, FEM modelling, material design engineering, materials and structural analyst in Oil & Gas, and automotive industry.

Ahmed Elwardany is an Associate Professor of Combustion at Egypt-Japan University of Science and Technology. Prior to that, during 2015–2018, he was an Assistant Professor at Alexandria University, Egypt. He received his BSc in 2005 and MSc in 2009 from mechanical engineering department, Alexandria University, Egypt, and his PhD from the University of Brighton in 2012. In July 2012, he joined the Clean Combustion Research Centre at King Abdullah University of Science and Technology as a research fellow. His role was measuring kinetics targets for fuels using shock tube.

Acknowledgment

This research was funded by the European Commission, KA107 British Council grant numbers: 2018-1-UK01-KA107-047386 (M.AQ., R.K.) and 2020-1-UK01-KA107-078517 (M.AQ.), and the Russian Science Foundation, grant number: 21-19-00876 (S.S.S.).

Abbreviations

AC	Activity Coefficient
ADC	Approximate Discrete Components
B#	#% Biodiesel/(biodiesel+Diesel) molar fraction
BME	Butter Methyl Ester
C/QC	Components/Quasi-Components
CAN	Canola Methyl Ester
CFD	Computational Fluid Dynamics
CFSM	Complex Fuel Surrogate Model
CME	Coconut Methyl Ester
CML	Camelina Methyl Ester
CN	Cetane Number
CNE	Corn Methyl Ester
CO	Carbon Monoxide
CO_2	Carbon Dioxide
CPU	Central Processing Unit
CSE	Cottonseed Methyl Ester
DB	Double Bond
Diff	Difference
DLM	Diffusion Limit Model
DMCM	Discrete Multi-Component Model
E#	Ethanol/(ethanol+gasoline) volume fraction
EM#	Ethanol/(ethanol+gasoline) mass fraction
EBD	Ethanol/Biodiesel/Diesel
ED	Effective Diffusivity
E/D	Ethanol/Diesel
ETC	Effective Thermal Conductivity
FACE	Fuel used in Advanced Combustion Engines
FAME	Fatty Acid Methyl Ester
HC	Hydrocarbons
H/C	Hydrogen/Carbon
HME1	Hempseed oil Methyl Ester, Produced in Ukraine
HME2	Hempseed oil Methyl Ester, Produced in the EU
HV	Heating Value

ICE	Internal Combustion Engine
ID	Infinite Diffusivity
ITC	Infinite Thermal Conductivity
JTR	Jatropha Methyl Ester
LME	Lard Methyl Ester
LNE	Linseed Methyl Ester
MDQDM	Multi-Dimensional Quasi-Discrete Model
MM	Molar Mass
MON	Motor Octane Number
NO_x	Nitrogen Oxides
Nu	Nusselt Number
NRTL	Non-Random Two Liquids
ON	Octane Number
Pe	Peclet Number
PME	Palm Methyl Ester
PMK	Palm Kernel Methyl Ester
Pr	Prandtl Number
RMM	Rapid Mixing Model
PTE	Peanut Methyl Ester
QDM	Quasi-Discrete Model
Re	Reynolds Number
RME	Rapeseed Methyl Ester
RON	Research Octane Number
Sc	Schmidt Number
SCM	Single Component Model
SFE	Safflower Methyl Ester
Sh	Sherwood Number
SME	Soybean Methyl Ester
SNE	Sunflower Methyl Ester
Sur#	Surrogate Number
TGE	Tung Methyl Ester
TMDQDM	Transient Multi-Dimensional Quasi-Discrete Model
TME	Tallow Methyl Ester
UNIFAC	Universal Quasi-Chemical Functional–group Activity Coefficient
WCO	Waste Cooking Oil
YGR	Yellow Grease Methyl Ester

Nomenclature

Symbols	Definition	Units
B_M	Spalding mass transfer number	-
B_T	Spalding heat transfer number	-
c	Specific heat capacity	$J \cdot K^{-1}$
C_F	Friction drag coefficient	-
c_{pv}	Specific heat capacity of the fuel vapour at constant pressure	$J \cdot K^{-1}$
D	Diffusion coefficient	-
$F(B_M)$	Mass film thickness correction factor	-
$F(B_T)$	Heat film thickness correction factor	-
G	Group mass fraction	-
h	Convective heat transfer coefficient	$W \cdot m^{-2} \cdot K^{-1}$
h_{OT}	Parameter introduced in Equation 8	-
h_{OY}	Parameter introduced in Equation 30	-

k	Thermal conductivity	$W \cdot m^{-1} \cdot K^{-1}$
L	Latent heat of evaporation	J
Le	Lewis number	-
m	Hydrocarbon group number	-
$\dot{m}$	Evaporation rate of droplets	$kg \cdot s^{-1}$
n	Carbon number	-
N	Number of atoms	-
p	Pressure	Pa
q	Sum of the group area parameter	-
q_n	Parameter introduced in Equation 8	-
Q	Molecular Van der Waals surface	Å
Q_L	Power spent on droplet heating	W
r	Sum of the group volume parameter	-
R	Droplet Radius (or molecular van der Waals volume)	m
$\dot{R}$	Rate of change in droplet radius	$m \cdot s^{-1}$
t	Time	s
T	Temperature	K
U	Velocity	$m \cdot s^{-1}$
v	Volume fraction	-
v_n	Parameter introduced in Equation 8	-
V	Volume	m^3
W	Weight	kg
x	Molar fraction	-
y	Mass fraction	-

Greek Symbols

α	Parameter defined by Equation (27)	-
β	Parameter value for octane or cetane numbers	-
γ	Activity coefficient	-
θ	Area fraction	-
ϵ	Evaporation rate of species	-
ε	Error	-
κ	Effective thermal diffusivity	$m^2 \cdot s^{-1}$
μ	Dynamic viscosity	$Pa \cdot s$
ν	Kinematic viscosity	$m^2 \cdot s^{-1}$
ρ	Density	$kg \cdot m^{-3}$
$\tilde{\rho}$	Relative density	-
ν	Number of structure groups in molecule i	-
ψ	Group interaction parameter	-
Γ	Group residual activity coefficient	-
Φ	Segment fraction	-
ϕ	Equivalence ratio	-
φ	Parameter introduced in Equation (27) or fugacity coefficient	-
τ	Time instant in transient states or ignition time delay	s
σ	Stefan-Boltzmann constant	$W \cdot m^{-2} \cdot K^{-4}$
λ	Eigenvalues	-
χ	Recirculation coefficient	-
Δ	Difference	-

Subscripts

av	Average
b	Boiling

B	Biodiesel
c	Critical
C	Carbon
d	Droplet
D	Diesel
E	Evaporation or Ethanol
eff	Effective
g	Gas
H	Hydrogen
i	Index of individual components
ign	Ignition
iso	Isolated
j	Molecular group of mixed type
k, m, n	Molecular group of one type used in the UNIFAC model
l	Liquid
m	Mixture
r	Reduced
rad	Radiation
s	Surface
T	Temperature
v	Vapour
∞	Far from the droplet surface

Superscripts

C	Combinatorial term
R	Residual term
Sat	Saturation
$*$	Modified values

References

(1) Kalghatgi, G. Is It Really the End of Internal Combustion Engines and Petroleum in Transport? *Applied Energy* **2018**, *225*, 965–974. https://doi.org/10.1016/j.apenergy.2018.05.076.

(2) *Renewable Energy - Resources, Challenges and Applications*; Al Qubeissi, M., El-kharouf, A., Serhad Soyhan, H., Eds.; IntechOpen, 2020. https://doi.org/10.5772/intechopen.81765.

(3) Kalghatgi, G.; Levinsky, H.; Colket, M. Future Transportation Fuels. *Progress in Energy and Combustion Science* **2018**, *69*, 103–105. https://doi.org/10.1016/j.pecs.2018.06.003.

(4) Ali, O.; Mamat, R.; Najafi, G.; Yusaf, T.; Safieddin Ardebili, S. Optimization of Biodiesel-Diesel Blended Fuel Properties and Engine Performance with Ether Additive Using Statistical Analysis and Response Surface Methods. *Energies* **2015**, *8* (12), 14136–14150. https://doi.org/10.3390/en81212420.

(5) Qasim, M.; Ansari, T. M.; Hussain, M. Combustion, Performance, and Emission Evaluation of a Diesel Engine with Biodiesel Like Fuel Blends Derived From a Mixture of Pakistani Waste Canola and Waste Transformer Oils. *Energies* **2017**, *10* (7), 1023. https://doi.org/10.3390/en10071023.

(6) *Biofuels - Challenges and Opportunities*; Al Qubeissi, M., Ed.; IntechOpen, 2019. https://doi.org/10.5772/intechopen.76490.

(7) EPA, U. US Environmental Protection Agency http://www.epa.gov/ (accessed 2017 -11 -15).

(8) Masum, B. M.; Masjuki, H. H.; Kalam, M. A.; Rizwanul Fattah, I. M.; Palash, S. M.; Abedin, M. J. Effect of Ethanol–Gasoline Blend on NOx Emission in SI Engine. *Renewable and Sustainable Energy Reviews* **2013**, *24*, 209–222. https://doi.org/10.1016/j.rser.2013.03.046.

(9) Pure European Renewavle Ethanol https://epure.org/ (accessed 2020 -01 -05).

(10) Energy Policy Act of 1992. U.S. Department of Energy October 24, 1992.

(11) D02 Committee. *Specification for Biodiesel Fuel Blend Stock (B100) for Middle Distillate Fuels*; ASTM International. https://doi.org/10.1520/D6751-20A.

(12) Alternative Fuels Data Center. U.S. Department of Energy: Energy Efficiency and Renewable Energy http://www.afdc.energy.gov (accessed 2017 -02 -12).

(13) Torres-Jimenez, E.; Jerman, M. S.; Gregorc, A.; Lisec, I.; Dorado, M. P.; Kegl, B. Physical and Chemical Properties of Ethanol–Diesel Fuel Blends. *Fuel* **2011**, *90* (2), 795–802. https://doi.org/10.1016/j.fuel.2010.09.045.

(14) Padala, S.; Woo, C.; Kook, S.; Hawkes, E. R. Ethanol Utilisation in a Diesel Engine Using Dual-Fuelling Technology. *Fuel* **2013**, *109*, 597–607. https://doi.org/10.1016/j.fuel.2013.03.049.

(15) Al Qubeissi, M. *Heating and Evaporation of Multi-Component Fuel Droplets*; WiSa: Stuttgart, 2015.

(16) Department for Transport, UK. New regulations to double the use of sustainable renewable fuels by 2020 https://www.gov.uk/government/news/new-regulations-to-double-the-use-of-sustainable-renewable-fuels-by-2020 (accessed 2019 -02 -22).

(17) Eller, D. Trump administration gives final approval for year-round E15 use https://eu.desmoinesregister.com/story/money/agriculture/2019/05/31/trump-administration-approves-year-round-e-15-use-biofuels-ethanol/1297055001/ (accessed 2019 -08 -16).

(18) Agarwal, A. K.; Dhar, A.; Gupta, J. G.; Kim, W. I.; Choi, K.; Lee, C. S.; Park, S. Effect of Fuel Injection Pressure and Injection Timing of Karanja Biodiesel Blends on Fuel Spray, Engine Performance, Emissions and Combustion Characteristics. *Energy Conversion and Management* **2015**, *91*, 302–314. https://doi.org/10.1016/j.enconman.2014.12.004.

(19) Sirignano, W. A. *Fluid Dynamics and Transport of Droplets and Sprays*; Cambridge University Press: Cambridge, U.K, 2010.

(20) Stojkovic, B. D.; Sick, V. Evolution and Impingement of an Automotive Fuel Spray Investigated with Simultaneous Mie/LIF Techniques: *Appl Phys B* **2001**, *73* (1), 75–83. https://doi.org/10.1007/s003400100598.

(21) Ott, L. S.; Smith, B. L.; Bruno, T. J. Composition-explicit distillation curves of waste lubricant oils and resourced crude oil: A diagnostic for re-refining and evaluation. *American Journal of Environmental Sciences* **2010**, *6* (6), 523–534. https://doi.org/10.3844/ajessp.2010.523.534.

(22) Smith, B. L.; Bruno, T. J. Advanced Distillation Curve Measurement with a Model Predictive Temperature Controller. *Int J Thermophys* **2006**, *27* (5), 1419–1434. https://doi.org/10.1007/s10765-006-0113-7.

(23) Abdel-Qader, Z.; Hallett, W. L. H. The Role of Liquid Mixing in Evaporation of Complex Multicomponent Mixtures: Modelling Using Continuous Thermodynamics. *Chemical Engineering Science* **2005**, *60* (6), 1629–1640. https://doi.org/10.1016/j.ces.2004.10.015.

(24) Zhu, G.-Sh.; Reitz, R. D. A Model for High-Pressure Vaporization of Droplets of Complex Liquid Mixtures Using Continuous Thermodynamics. *International Journal of Heat and Mass Transfer* **2002**, *45* (3), 495–507. https://doi.org/10.1016/S0017-9310(01)00173-9.

(25) Davidson, D. F.; Shao, J. K.; Choudhary, R.; Mehl, M.; Obrecht, N.; Hanson, R. K. Ignition Delay Time Measurements and Modeling for Gasoline at Very High Pressures. *Proceedings of the Combustion Institute* **2018**. https://doi.org/10.1016/j.proci.2018.08.032.

(26) Sazhina, E. M.; Sazhin, S. S.; Heikal, M. R.; Babushok, V. I.; Johns, R. J. R. A Detailed Modelling of the Spray Ignition Process in Diesel Engines. *Combustion Science and Technology* **2000**, *160* (1), 317–344. https://doi.org/10.1080/00102200008935806.

(27) Sazhin, S. S.; Krutitskii, P. A. A Conduction Model for Transient Heating of Fuel Droplets. In *proceedings of the 3rd ISAAC Congress*; World Scientific: River Edge, NJ, 2003; pp 1231–1240.

(28) Hallett, W. L. H.; Legault, N. V. Modelling Biodiesel Droplet Evaporation Using Continuous Thermodynamics. *Fuel* **2011**, *90* (3), 1221–1228. https://doi.org/10.1016/j.fuel.2010.11.035.

(29) Saha, K.; Abu-Ramadan, E.; Li, X. Multicomponent Evaporation Model for Pure and Blended Biodiesel Droplets in High Temperature Convective Environment. *Applied Energy* **2012**, *93*, 71–79. https://doi.org/10.1016/j.apenergy.2011.05.034.

(30) Sazhin, S. S.; Elwardany, A.; Krutitskii, P. A.; Castanet, G.; Lemoine, F.; Sazhina, E. M.; Heikal, M. R. A Simplified Model for Bi-Component Droplet Heating and Evaporation. *International Journal of Heat and Mass Transfer* **2010**, *53* (21–22), 4495–4505. https://doi.org/10.1016/j.ijheatmasstransfer.2010.06.044.

(31) Sazhin, S. S. *Droplets and Sprays*; Springer: London, 2014.

(32) Sazhin, S. S. Modelling of Fuel Droplet Heating and Evaporation: Recent Results and Unsolved Problems. *Fuel* **2017**, *196*, 69–101. https://doi.org/10.1016/j.fuel.2017.01.048.

(33) Sazhin, S. S.; Elwardany, A. E.; Sazhina, E. M.; Heikal, M. R. A Quasi-Discrete Model for Heating and Evaporation of Complex Multicomponent Hydrocarbon Fuel Droplets. *International Journal of Heat and Mass Transfer* **2011**, *54* (19–20), 4325–4332. https://doi.org/10.1016/j.ijheatmasstransfer.2011.05.012.

(34) Elwardany, A. E.; Sazhin, S. S. A Quasi-Discrete Model for Droplet Heating and Evaporation: Application to Diesel and Gasoline Fuels. *Fuel* **2012**, *97*, 685–694. https://doi.org/10.1016/j.fuel.2012.01.068.

(35) Sazhin, S. S.; Al Qubeissi, M.; Nasiri, R.; Gun'ko, V. M.; Elwardany, A. E.; Lemoine, F.; Grisch, F.; Heikal, M. R. A Multi-Dimensional Quasi-Discrete Model for the Analysis of Diesel Fuel Droplet Heating and Evaporation. *Fuel* **2014**, *129*, 238–266. https://doi.org/10.1016/j.fuel.2014.03.028.

(36) Al Qubeissi, M.; Sazhin, S. S.; Turner, J.; Begg, S.; Crua, C.; Heikal, M. R. Modelling of gasoline fuel droplets heating and evaporation. *Fuel* **2015**, *159*, 373–384. https://doi.org/10.1016/j.fuel.2015.06.028.

(37) Elwardany, A. E.; Sazhin, S. S.; Im, H. G. A New Formulation of Physical Surrogates of FACE A Gasoline Fuel Based on Heating and Evaporation Characteristics. *Fuel* **2016**, *176*, 56–62. https://doi.org/10.1016/j.fuel.2016.02.041.

(38) Sarathy, S. M.; Kukkadapu, G.; Mehl, M.; Wang, W.; Javed, T.; Park, S.; Oehlschlaeger, M. A.; Farooq, A.; Pitz, W. J.; Sung, C.-J. Ignition of Alkane-Rich FACE Gasoline Fuels and Their Surrogate Mixtures. *Proceedings of the Combustion Institute* **2015**, *35* (1), 249–257. https://doi.org/10.1016/j.proci.2014.05.122.

(39) Mueller, C. J.; Cannella, W. J.; Bays, J. T.; Bruno, T. J.; DeFabio, K.; Dettman, H. D.; Gieleciak, R. M.; Huber, M. L.; Kweon, C.-B.; McConnell, S. S.; Pitz, W. J.; Ratcliff, M. A. Diesel Surrogate Fuels for Engine Testing and Chemical-Kinetic Modeling: Compositions and Properties. *Energy Fuels* **2016**, *30* (2), 1445–1461. https://doi.org/10.1021/acs.energyfuels.5b02879.

(40) Al-Esawi, N.; Al Qubeissi, M. A New Approach to Formulation of Complex Fuel Surrogates. *Fuel* **2021**, *283*, 118923. https://doi.org/10.1016/j.fuel.2020.118923.

(41) Al Qubeissi, M.; Al-Esawi, N.; Sazhin, S. S. Auto-Selection of Quasi-Components/Components in the Multi-Dimensional Quasi-Discrete Model. *Fuel* **2021**, *294*, 120245. https://doi.org/10.1016/j.fuel.2021.120245.

(42) Sazhin, S. S.; Krutitskii, P. A.; Abdelghaffar, W. A.; Sazhina, E. M.; Mikhalovsky, S. V.; Meikle, S. T.; Heikal, M. R. Transient Heating of Diesel Fuel Droplets. *International Journal of Heat and Mass Transfer* **2004**, *47* (14–16), 3327–3340. https://doi.org/10.1016/j.ijheatmasstransfer.2004.01.011.

(43) Sazhin, S. S. Advanced Models of Fuel Droplet Heating and Evaporation. *Progress in Energy and Combustion Science* **2006**, *32* (2), 162–214. https://doi.org/10.1016/j.pecs.2005.11.001.

(44) Sazhin, S. S.; Al Qubeissi, M.; Kolodnytska, R.; Elwardany, A. E.; Nasiri, R.; Heikal, M. R. Modelling of Biodiesel Fuel Droplet Heating and Evaporation. *Fuel* **2014**, *115*, 559–572. https://doi.org/10.1016/j.fuel.2013.07.031.

(45) Al Qubeissi, M.; Sazhin, S. S.; Elwardany, A. E. Modelling of Blended Diesel and Biodiesel Fuel Droplet Heating and Evaporation. *Fuel* **2017**, *187*, 349–355. https://doi.org/10.1016/j.fuel.2016.09.060.

(46) Al Qubeissi, M. Predictions of Droplet Heating and Evaporation: An Application to Biodiesel, Diesel, Gasoline and Blended Fuels. *Applied Thermal Engineering* **2018**, *136* (C), 260–267. https://doi.org/10.1016/j.applthermaleng.2018.03.010.

(47) Al-Esawi, N.; Al Qubeissi, M.; Whitaker, R.; Sazhin, S. S. Blended E85–Diesel Fuel Droplet Heating and Evaporation. *Energy & Fuels* **2019**, *33* (3), 2477–2488. https://doi.org/10.1021/acs.energyfuels.8b03014.

(48) Poulton, L.; Rybdylova, O.; Zubrilin, I. A.; Matveev, S. G.; Gurakov, N. I.; Al Qubeissi, M.; Al-Esawi, N.; Khan, T.; Gun'ko, V. M.; Sazhin, S. S. Modelling of Multi-Component Kerosene and Surrogate Fuel Droplet Heating and Evaporation Characteristics: A Comparative Analysis. *Fuel* **2020**, *269*, 117115. https://doi.org/10.1016/j.fuel.2020.117115.

(49) Pinheiro, A. P.; Rybdylova, O.; Zubrilin, I. A.; Sazhin, S. S.; Sacomano Filho, F. L.; Vedovotto, J. M. Modelling of Aviation Kerosene Droplet Heating and Evaporation Using Complete Fuel Composition and Surrogates. *Fuel* **2021**, *305*, 121564. https://doi.org/10.1016/j.fuel.2021.121564.

(50) Kabil, I.; Al Qubeissi, M.; Badra, J.; Abdelghaffar, W.; Eldrainy, Y.; Sazhin, S. S.; Im, H. G.; Elwardany, A. An Improved Prediction of Pre-Combustion Processes, Using the Discrete Multicomponent Model. *Sustainability* **2021**, *13* (5), 2937. https://doi.org/10.3390/su13052937.

(51) Elwardany, A. E.; Sazhin, S. S.; Farooq, A. Modelling of Heating and Evaporation of Gasoline Fuel Droplets: A Comparative Analysis of Approximations. *Fuel* **2013**, *111*, 643–647. https://doi.org/10.1016/j.fuel.2013.03.030.

(52) Teng, S. T.; Williams, A. D.; Urdal, K. Detailed Hydrocarbon Analysis of Gasoline by GC-MS (SI-PIONA). *J High Resolution Chromat.* **1994**, *17* (6), 469–475. https://doi.org/10.1002/jhrc.1240170614.

(53) Sawyer, R. F. Trends in Auto Emissions and Gasoline Composition. *Environ Health Perspect* **1993**, *101* (Suppl 6), 5–12.

(54) Bader, A.; Keller, P.; Hasse, C. The Influence of Non-Ideal Vapor–Liquid Equilibrium on the Evaporation of Ethanol/Iso-Octane Droplets. *International Journal of Heat and Mass Transfer* **2013**, *64*, 547–558. https://doi.org/10.1016/j.ijheatmasstransfer.2013.04.056.

(55) Ma, X.; Jiang, C.; Xu, H.; Ding, H.; Shuai, S. Laminar Burning Characteristics of 2-Methylfuran and Isooctane Blend Fuels. *Fuel* **2014**, *116*, 281–291. https://doi.org/10.1016/j.fuel.2013.08.018.

(56) Paxson, F. L. *The Last American Frontier*; Simon Publications LLC, 2001.

(57) Sazhin, S. S.; Kristyadi, T.; Abdelghaffar, W. A.; Begg, S.; Heikal, M. R.; Mikhalovsky, S. V.; Meikle, S. T.; Al-Hanbali, O. Approximate Analysis of Thermal Radiation Absorption in Fuel Droplets. *Journal of Heat Transfer* **2007**, *129* (9), 1246. https://doi.org/10.1115/1.2740304.

(58) Pitz, W. J.; Cernansky, N. P.; Dryer, F. L.; Egolfopoulos, F. N.; Farrell, J. T.; Friend, D. G.; Pitsch, H. *Development of an Experimental Database and Chemical Kinetic Models for Surrogate Gasoline Fuels*; SAE Technical Paper 2007-01–0175; SAE International: Warrendale, PA, 2007.

(59) Yaws, C. L. *The Yaws Handbook of Physical Properties for Hydrocarbons and Chemicals: Physical Properties for More than 54,000 Organic and Inorganic Chemical Compounds, Coverage for C1 to C100 Organics and Ac to Zr Inorganics*, Second edition.; Elsevier: Oxford, UK, 2015.

(60) García-Miaja, G.; Troncoso, J.; Romaní, L. Excess Properties for Binary Systems Ionic Liquid+ethanol: Experimental Results and Theoretical Description Using the ERAS Model. *Fluid Phase Equilibria* **2008**, *274* (1–2), 59–67. https://doi.org/10.1016/j.fluid.2008.09.004.

(61) NIST http://webbook.nist.gov/chemistry/fluid/ (accessed 2017 -07 -28).

(62) Gun'ko, V. M.; Nasiri, R.; Sazhin, S. S.; Lemoine, F.; Grisch, F. A Quantum Chemical Study of the Processes during the Evaporation of Real-Life Diesel Fuel Droplets. *Fluid Phase Equilibria* **2013**, *356*, 146–156. https://doi.org/10.1016/j.fluid.2013.07.022.

(63) Al Qubeissi, M.; Sazhin, S. S.; Crua, C.; Turner, J.; Heikal, M. R. Modelling of Biodiesel Fuel Droplet Heating and Evaporation: Effects of Fuel Composition. *Fuel* **2015**, *154*, 308–318. https://doi.org/10.1016/j.fuel.2015.03.051.

(64) Al-Esawi, N.; Al Qubeissi, M.; Kolodnytska, R. The Impact of Biodiesel Fuel on Ethanol/Diesel Blends. *Energies* **2019**, *12* (9), 1804. https://doi.org/10.3390/en12091804.

(65) Al-Esawi, N.; Al Qubeissi, M.; Sazhin, S. S. The Impact of Fuel Blends and Ambient Conditions on the Heating and Evaporation of Diesel and Biodiesel Fuel Droplets. In *International Heat Transfer Conference 16*; Begellhouse: Beijing, China, 2018; pp 6641–6648. https://doi.org/10.1615/IHTC16.mpf.020772.

(66) Sazhin, S. S.; Al Qubeissi, M.; Heikal, M. R. Modelling of Biodiesel and Diesel Fuel Droplet Heating and Evaporation. In *15th International Heat Transfer Conference*; Begellhouse: Kyoto, Japan, 2014; Vol. IHTC15-8936. https://doi.org/10.1615/IHTC15.evp.008936.

(67) Ra, Y.; Reitz, R. D. A Vaporization Model for Discrete Multi-Component Fuel Sprays. *International Journal of Multiphase Flow* **2009**, *35* (2), 101–117. https://doi.org/10.1016/j.ijmultiphaseflow.2008.10.006.

(68) Maqua, C.; Castanet, G.; Lemoine, F. Bicomponent Droplets Evaporation: Temperature Measurements and Modelling. *Fuel* **2008**, *87* (13–14), 2932–2942. https://doi.org/10.1016/j.fuel.2008.04.021.

(69) Zhang, L.; Kong, S.-Ch. Vaporization Modeling of Petroleum–Biofuel Drops Using a Hybrid Multi-Component Approach. *Combustion and Flame* **2010**, *157* (11), 2165–2174. https://doi.org/10.1016/j.combustflame.2010.05.011.

(70) Al Qubeissi, M.; Sazhin, S. S. Models for Droplet Heating and Evaporation: An Application to Biodiesel, Diesel and Gasoline Fuels. *International Journal of Engineering Systems Modelling and Simulation* **2017**, *9* (1), 32. https://doi.org/10.1504/IJESMS.2017.10002565.

(71) Rybdylova, O.; Al Qubeissi, M.; Braun, M.; Crua, C.; Manin, J.; Pickett, L. M.; Sercey, G. de; Sazhina, E. M.; Sazhin, S. S.; Heikal, M. A Model for Droplet Heating and Its Implementation into ANSYS Fluent. *International Communications in Heat and Mass Transfer* **2016**. https://doi.org/10.1016/j.icheatmasstransfer.2016.05.032.

(72) Rybdylova, O.; Poulton, L.; Al Qubeissi, M.; Elwardany, A. E.; Crua, C.; Khan, T.; Sazhin, S. S. A Model for Multi-Component Droplet Heating and Evaporation and Its Implementation into ANSYS Fluent. *International Communications in Heat and Mass Transfer* **2018**, *90*, 29–33. https://doi.org/10.1016/j.icheatmasstransfer.2017.10.018.

(73) Al Qubeissi, M. Proposing a Numerical Solution for the 3D Heat Conduction Equation; IEEE, 2012; pp 144–149. https://doi.org/10.1109/AMS.2012.10.

(74) Carslaw, H. S. *Conduction of Heat in Solids*, 2nd ed.; Clarendon Press; Oxford University Press: Oxford: New York, 1986.

(75) Kartashov, E. M. *Analytical Methods in Heat Transfer Theory in Solids*; Vysshaya Shkola: Moscow, 2001.

(76) Abramzon, B.; Sirignano, W. A. Droplet Vaporization Model for Spray Combustion Calculations. *International Journal of Heat and Mass Transfer* **1989**, *32* (9), 1605–1618. https://doi.org/10.1016/0017-9310(89)90043-4.

(77) Elwardany, A. E. Modelling of Multi-Component Fuel Droplets Heating and Evaporation. PhD thesis, University of Brighton, UK, 2012.

(78) Abramzon, B.; Sazhin, S. S. Convective Vaporization of a Fuel Droplet with Thermal Radiation Absorption. *Fuel* **2006**, *85* (1), 32–46. https://doi.org/10.1016/j.fuel.2005.02.027.

(79) Maqua, C.; Castanet, G.; Grisch, F.; Lemoine, F.; Kristyadi, T.; Sazhin, S. S. Monodisperse Droplet Heating and Evaporation: Experimental Study and Modelling. *International Journal of Heat and Mass Transfer* **2008**, *51* (15–16), 3932–3945. https://doi.org/10.1016/j.ijheatmasstransfer.2007.12.011.

(80) Sazhin, S. S.; Elwardany, A. E.; Krutitskii, P. A.; Deprédurand, V.; Castanet, G.; Lemoine, F.; Sazhina, E. M.; Heikal, M. R. Multi-Component Droplet Heating and Evaporation: Numerical Simulation versus Experimental Data. *International Journal of Thermal Sciences* **2011**, *50* (7), 1164–1180. https://doi.org/10.1016/j.ijthermalsci.2011.02.020.

(81) Spalding, D. B. *Convective Mass Transfer: An Introduction*; Edward Arnold Publ. Ltd: London, 1963.

(82) Sazhin, S. S. Modelling of Fuel Droplet Heating and Evaporation: Recent Results and Unsolved Problems. *Fuel* **2017**, *196*, 69–101. https://doi.org/10.1016/j.fuel.2017.01.048.

(83) Sazhin, S. S.; Al Qubeissi, M.; Xie, J.-F. Two Approaches to Modelling the Heating of Evaporating Droplets. *International Communications in Heat and Mass Transfer* **2014**, *57*, 353–356. https://doi.org/10.1016/j.icheatmasstransfer.2014.08.004.

(84) Sazhin, S. S.; Elwardany, A.; Krutitskii, P. A.; Castanet, G.; Lemoine, F.; Sazhina, E. M.; Heikal, M. R. A Simplified Model for Bi-Component Droplet Heating and Evaporation. *International Journal of Heat and Mass Transfer* **2010**, *53* (21–22), 4495–4505. https://doi.org/10.1016/j.ijheatmasstransfer.2010.06.044.

(85) Sazhin, S. S.; Abdelghaffar, W. A.; Krutitskii, P. A.; Sazhina, E. M.; Heikal, M. R. New Approaches to Numerical Modelling of Droplet Transient Heating and Evaporation. *International Journal of Heat and Mass Transfer* **2005**, *48* (19–20), 4215–4228. https://doi.org/10.1016/j.ijheatmasstransfer.2005.04.007.

(86) Sirignano, W. A. *Fluid Dynamics and Transport of Droplets and Sprays*; Cambridge University Press: Cambridge, U.K, 1999.

(87) Continillo, G.; Sirignano, W. A. Unsteady, Spherically-Symmetric Flame Propagation Through Multicomponent Fuel Spray Clouds. In *Modern Research Topics in Aerospace Propulsion*; Angelino, G., Luca, L. D., Sirignano, W. A., Eds.; Springer New York, 1991; pp 173–198.

(88) Faeth, G. M. Evaporation and Combustion of Sprays. *Progress in Energy and Combustion Science* **1983**, *9* (1–2), 1–76. https://doi.org/10.1016/0360-1285(83)90005-9.

(89) Sazhin, S. S.; Al Qubeissi, M. Modelling of Automotive Fuel Droplet Heating and Evaporation: Mathematical Tools and Approximations. *J. Phys.: Conf. Ser.* **2016**, *727*, 012015. https://doi.org/10.1088/1742-6596/727/1/012015.

(90) Al-Esawi, N.; Al Qubeissi, M.; Sazhin, S. S.; Whitaker, R. The Impacts of the Activity Coefficient on Heating and Evaporation of Ethanol/Gasoline Fuel Blends. *International Communications in Heat and Mass Transfer* **2018**, *98*, 177–182. https://doi.org/10.1016/j.icheatmasstransfer.2018.08.018.

(91) Al Qubeissi, M.; Sazhin, S.; Al-Esawi, N. Models for Automotive Fuel Droplets Heating and Evaporation; Universitat Politècnica València, 2017. https://doi.org/10.4995/ILASS2017.2017.4754.

(92) Al Qubeissi, M.; Al-Esawi, N.; Sazhin, S. S. Droplets Heating and Evaporation: An Application to Diesel-Biodiesel Fuel Mixtures; Universitat Politècnica València, 2017. https://doi.org/10.4995/ILASS2017.2017.4644.

(93) Brenn, G.; Deviprasath, L. J.; Durst, F.; Fink, C. Evaporation of Acoustically Levitated Multi-Component Liquid Droplets. *International Journal of Heat and Mass Transfer* **2007**, *50* (25–26), 5073–5086. https://doi.org/10.1016/j.ijheatmasstransfer.2007.07.036.

(94) Reid, R. C.; Prausnitz, J. M.; Poling, B. E. *The Properties of Gases and Liquids*, 4th ed.; McGraw-Hill: New York, 1987.

(95) Poling, B. E.; Prausnitz, J. M.; O'Connell, J. P. *The Properties of Gases and Liquids*; McGraw-Hill: New York, 2001.

(96) Bondi, A. Van Der Waals Volumes and Radii. *The Journal of Physical Chemistry* **1964**, *68* (3), 441–451. https://doi.org/10.1021/j100785a001.

(97) Pumphrey, J. A.; Brand, J. I.; Scheller, W. A. Vapour Pressure Measurements and Predictions for Alcohol–Gasoline Blends. *Fuel* **2000**, *79* (11), 1405–1411. https://doi.org/10.1016/S0016-2361(99)00284-7.

(98) Banerjee, R. Numerical Investigation of Evaporation of a Single Ethanol/Iso-Octane Droplet. *Fuel* **2013**, *107*, 724–739. https://doi.org/10.1016/j.fuel.2013.01.003.

(99) Banerjee, R.; Gopinath, R. CFD Analysis to Study Evaporation of a Single Ethanol/Iso-Octane Binary Mixture Droplet; ASME, 2011; pp 2571–2578. https://doi.org/10.1115/AJK2011-10033.

(100) Balabin, R. M.; Syunyaev, R. Z.; Karpov, S. A. Molar Enthalpy of Vaporization of Ethanol–Gasoline Mixtures and Their Colloid State. *Fuel* **2007**, *86* (3), 323–327. https://doi.org/10.1016/j.fuel.2006.08.008.

(101) Oktavian, R.; Amidelsi, V.; Rasmito, A.; Wibawa, G. Vapor Pressure Measurements of Ethanol–Isooctane and 1-Butanol–Isooctane Systems Using a New Ebulliometer. *Fuel* **2013**, *107*, 47–51. https://doi.org/10.1016/j.fuel.2013.02.005.

(102) Kar, K.; Last, T.; Haywood, C.; Raine, R. Measurement of Vapor Pressures and Enthalpies of Vaporization of Gasoline and Ethanol Blends and Their Effects on Mixture Preparation in an SI Engine. *SAE International Journal of Fuels and Lubricants* **2009**, *1*, 132–144.

(103) Al Qubeissi, M.; Al-Esawi, N.; Sazhin, S. S.; Ghaleeh, M. Ethanol/Gasoline Droplet Heating and Evaporation: Effects of Fuel Blends and Ambient Conditions. *Energy & Fuels* **2018**, *32* (6), 6498–6506. https://doi.org/10.1021/acs.energyfuels.8b00366.

(104) Corsetti, S.; Miles, R. E. H.; McDonald, C.; Belotti, Y.; Reid, J. P.; Kiefer, J.; McGloin, D. Probing the Evaporation Dynamics of Ethanol/Gasoline Biofuel Blends Using Single Droplet Manipulation Techniques. *The Journal of Physical Chemistry A* **2015**, *119* (51), 12797–12804. https://doi.org/10.1021/acs.jpca.5b10098.

(105) Ni, Z.; Han, K.; Zhao, C.; Chen, H.; Pang, B. Numerical Simulation of Droplet Evaporation Characteristics of Multi-Component Acetone-Butanol-Ethanol and Diesel Blends under Different Environments. *Fuel* **2018**, *230*, 27–36. https://doi.org/10.1016/j.fuel.2018.05.038.

(106) Ma, X.; Zhang, F.; Han, K.; Yang, B.; Song, G. Evaporation Characteristics of Acetone–Butanol–Ethanol and Diesel Blends Droplets at High Ambient Temperatures. *Fuel* **2015**, *160*, 43–49. https://doi.org/10.1016/j.fuel.2015.07.079.

(107) Al-Esawi, N.; Al Qubeissi, M.; Sazhin, S. S.; Emekwuru, N.; Blundell, M. V. Impact of Corrected Activity Coefficient on the Estimated Droplet Heating and Evaporation. In *Eleven International Conference on Thermal Engineering: Theory and Applications*; Doha, Qatar, 2018.

(108) Járvás, G.; Kontos, J.; Hancsók, J.; Dallos, A. Modeling Ethanol–Blended Gasoline Droplet Evaporation Using COSMO-RS Theory and Computation Fluid Dynamics. *International Journal of Heat and Mass Transfer* **2015**, *84*, 1019–1029. https://doi.org/10.1016/j.ijheatmasstransfer.2014.12.046.

(109) Department for Transport. E10 petrol explained https://www.gov.uk/guidance/e10-petrol-explained (accessed 2021 -04 -10).

(110) Hallett, W. L. H.; Beauchamp-Kiss, S. Evaporation of Single Droplets of Ethanol–Fuel Oil Mixtures. *Fuel* **2010**, *89* (9), 2496–2504. https://doi.org/10.1016/j.fuel.2010.03.007.

(111) Sarjovaara, T.; Larmi, M. Dual Fuel Diesel Combustion with an E85 Ethanol/Gasoline Blend. *Fuel* **2015**, *139*, 704–714. https://doi.org/10.1016/j.fuel.2014.09.049.

(112) Kwanchareon, P.; Luengnaruemitchai, A.; Jai-In, S. Solubility of a Diesel–Biodiesel–Ethanol Blend, Its Fuel Properties, and Its Emission Characteristics from Diesel Engine. *Fuel* **2007**, *86* (7–8), 1053–1061. https://doi.org/10.1016/j.fuel.2006.09.034.

(113) Pan, K.-L.; Li, J.-W.; Chen, C.-P.; Wang, C.-H. On Droplet Combustion of Biodiesel Fuel Mixed with Diesel/Alkanes in Microgravity Condition. *Combustion and Flame* **2009**, *156* (10), 1926–1936. https://doi.org/10.1016/j.combustflame.2009.07.020.

(114) US Department of Energy: Energy Efficiency and Renewable Energy. Biodiesel Blends http://www.afdc.energy.gov/fuels/biodiesel_blends.html (accessed 2017 -07 -29).

(115) Silveira, M. B.; do Carmo, F. R.; Santiago-Aguiar, R. S.; de Sant'Ana, H. B. Ab–Diesel: Liquid–Liquid Equilibrium and Volumetric Transport Properties. *Fuel* **2014**, *119*, 292–300. https://doi.org/10.1016/j.fuel.2013.11.022.

(116) US Department of Energy. Ethanol Blends https://www.eia.gov/energyexplained/index.php?page=biofuel_ethanol_use#tab2 (accessed 2018 -04 -20).

(117) Li, D.; Zhen, H.; Xingcai, L.; Wu-gao, Z.; Jian-guang, Y. Physico-Chemical Properties of Ethanol–Diesel Blend Fuel and Its Effect on Performance and Emissions of Diesel Engines. *Renewable Energy* **2005**, *30* (6), 967–976. https://doi.org/10.1016/j.renene.2004.07.010.

(118) Chin, J.-Y.; Batterman, S. A.; Northrop, W. F.; Bohac, S. V.; Assanis, D. N. Gaseous and Particulate Emissions from Diesel Engines at Idle and under Load: Comparison of Biodiesel Blend and Ultralow Sulfur Diesel Fuels. *Energy & Fuels* **2012**, *26* (11), 6737–6748. https://doi.org/10.1021/ef300421h.

(119) Liu, X.; Wang, H.; Yao, M. Experimental and Modeling Investigations on Soot Formation of Ethanol, *n* -Butanol, 2,5-Dimethylfuran, and Biodiesel in Diesel Engines. *Energy & Fuels* **2017**, *31* (11), 12108–12119. https://doi.org/10.1021/acs.energyfuels.7b01622.

(120) Yuan, W.; Hansen, A. C.; Zhang, Q. Predicting the Physical Properties of Biodiesel for Combustion Modeling. *Transactions of the ASAE* **2003**, *46* (6), 1487–1493. https://doi.org/10.13031/2013.15631.

(121) Al Qubeissi, M.; Sazhin, S. S. Blended Biodiesel/Diesel Fuel Droplet Heating and Evaporation; Brighton, UK, 2016; Vol. DHE-01, p 179.

(122) Pidol, L.; Lecointe, B.; Starck, L.; Jeuland, N. Ethanol–Biodiesel–Diesel Fuel Blends: Performances and Emissions in Conventional Diesel and Advanced Low Temperature Combustions. *Fuel* **2012**, *93*, 329–338. https://doi.org/10.1016/j.fuel.2011.09.008.

(123) Kim, H. J.; Park, S. H. Optimization Study on Exhaust Emissions and Fuel Consumption in a Dimethyl Ether (DME) Fueled Diesel Engine. *Fuel* **2016**, *182*, 541–549. https://doi.org/10.1016/j.fuel.2016.06.001.

(124) Shahir, S. A.; Masjuki, H. H.; Kalam, M. A.; Imran, A.; Fattah, I. M. R.; Sanjid, A. Feasibility of Diesel–Biodiesel–Ethanol/Bioethanol Blend as Existing CI Engine Fuel: An Assessment of Properties, Material Compatibility, Safety and Combustion. *Renewable and Sustainable Energy Reviews* **2014**, *32*, 379–395. https://doi.org/10.1016/j.rser.2014.01.029.

(125) Beatrice, C.; Napolitano, P.; Guido, C. Injection Parameter Optimization by DoE of a Light-Duty Diesel Engine Fed by Bio-Ethanol/RME/Diesel Blend. *Applied Energy* **2014**, *113*, 373–384. https://doi.org/10.1016/j.apenergy.2013.07.058.

(126) Fang, Q.; Fang, J.; Zhuang, J.; Huang, Z. Effects of Ethanol–Diesel–Biodiesel Blends on Combustion and Emissions in Premixed Low Temperature Combustion. *Applied Thermal Engineering* **2013**, *54* (2), 541–548. https://doi.org/10.1016/j.applthermaleng.2013.01.042.

(127) Aydın, F.; Öğüt, H. Effects of Using Ethanol-Biodiesel-Diesel Fuel in Single Cylinder Diesel Engine to Engine Performance and Emissions. *Renewable Energy* **2017**, *103*, 688–694. https://doi.org/10.1016/j.renene.2016.10.083.

(128) Noorollahi, Y.; Azadbakht, M.; Ghobadian, B. The Effect of Different Diesterol (Diesel–Biodiesel–Ethanol) Blends on Small Air-Cooled Diesel Engine Performance and Its Exhaust Gases. *Energy* **2018**, *142*, 196–200. https://doi.org/10.1016/j.energy.2017.10.024.

(129) Tse, H.; Leung, C. W.; Cheung, C. S. Investigation on the Combustion Characteristics and Particulate Emissions from a Diesel Engine Fueled with Diesel-Biodiesel-Ethanol Blends. *Energy* **2015**, *83*, 343–350. https://doi.org/10.1016/j.energy.2015.02.030.

(130) Labeckas, G.; Slavinskas, S.; Mažeika, M. The Effect of Ethanol–Diesel–Biodiesel Blends on Combustion, Performance and Emissions of a Direct Injection Diesel Engine. *Energy Conversion and Management* **2014**, *79*, 698–720. https://doi.org/10.1016/j.enconman.2013.12.064.

(131) Shahir, S. A.; Masjuki, H. H.; Kalam, M. A.; Imran, A.; Ashraful, A. M. Performance and Emission Assessment of Diesel–Biodiesel–Ethanol/Bioethanol Blend as a Fuel in Diesel Engines: A Review. *Renewable and Sustainable Energy Reviews* **2015**, *48*, 62–78. https://doi.org/10.1016/j.rser.2015.03.049.

(132) Mofijur, M.; Rasul, M. G.; Hyde, J.; Azad, A. K.; Mamat, R.; Bhuiya, M. M. K. Role of Biofuel and Their Binary (Diesel–Biodiesel) and Ternary (Ethanol–Biodiesel–Diesel) Blends on Internal Combustion Engines Emission Reduction. *Renewable and Sustainable Energy Reviews* **2016**, *53*, 265–278. https://doi.org/10.1016/j.rser.2015.08.046.

(133) Pitz, W. J.; Mueller, Ch. J. Recent Progress in the Development of Diesel Surrogate Fuels. *Progress in Energy and Combustion Science* **2011**, *37* (3), 330–350. https://doi.org/10.1016/j.pecs.2010.06.004.

(134) Alptekin, E.; Canakci, M. Characterization of the Key Fuel Properties of Methyl Ester–Diesel Fuel Blends. *Fuel* **2009**, *88* (1), 75–80. https://doi.org/10.1016/j.fuel.2008.05.023.

(135) Al-Esawi, N.; Al Qubeissi, M.; Kolodnytska, R. The Impact of Biodiesel Fuel on Ethanol/Diesel Blends. *Energies* **2019**, *12* (9), 1804. https://doi.org/10.3390/en12091804.

(136) Zöldy, M. ETHANOL–BIODIESEL–DIESEL BLENDS AS A DIESEL EXTENDER OPTION ON COMPRESSION IGNITION ENGINES. *TRANSPORT* **2011**, *26* (3), 303–309. https://doi.org/10.3846/16484142.2011.623824.

(137) Ghosh, P.; Jaffe, S. B. Detailed Composition-Based Model for Predicting the Cetane Number of Diesel Fuels. *Industrial & Engineering Chemistry Research* **2006**, *45* (1), 346–351. https://doi.org/10.1021/ie0508132.

(138) Santana, R.; Do, P.; Santikunaporn, M.; Alvarez, W.; Taylor, J.; Sughrue, E.; Resasco, D. Evaluation of Different Reaction Strategies for the Improvement of Cetane Number in Diesel Fuels. *Fuel* **2006**, *85* (5–6), 643–656. https://doi.org/10.1016/j.fuel.2005.08.028.

(139) Qian, Y.; Yu, L.; Li, Z.; Zhang, Y.; Xu, L.; Zhou, Q.; Han, D.; Lu, X. A New Methodology for Diesel Surrogate Fuel Formulation: Bridging Fuel Fundamental Properties and Real Engine Combustion Characteristics. *Energy* **2018**, *148*, 424–447. https://doi.org/10.1016/j.energy.2018.01.181.

(140) Creton, B.; Dartiguelongue, C.; de Bruin, T.; Toulhoat, H. Prediction of the Cetane Number of Diesel Compounds Using the Quantitative Structure Property Relationship. *Energy & Fuels* **2010**, *24* (10), 5396–5403. https://doi.org/10.1021/ef1008456.

(141) Lapuerta, M.; Rodríguez-Fernández, J.; de Mora, E. F. Correlation for the Estimation of the Cetane Number of Biodiesel Fuels and Implications on the Iodine Number. *Energy Policy* **2009**, *37* (11), 4337–4344. https://doi.org/10.1016/j.enpol.2009.05.049.

(142) Tong, D.; Hu, C.; Jiang, K.; Li, Y. Cetane Number Prediction of Biodiesel from the Composition of the Fatty Acid Methyl Esters. *Journal of the American Oil Chemists' Society* **2011**, *88* (3), 415–423. https://doi.org/10.1007/s11746-010-1672-0.

(143) Shinde, S.; Yadav, S. D. Theoretical Properties Prediction of Diesel-Biodiesel-DEE Blend as a Fuel for C.I. Engine With Required Modifications for Optimum Performance. *International Journal of Current Engineering and Technology* **2016**, *6* (5), 1562–1567.

(144) Grabar, I. G.; Kolodnytska, R. V.; Semenov, V. G. *Biofuel Based on Oil for Diesel Engines*; ZDTU: Zhytomyr, 2011.

(145) Tutak, W. Bioethanol E85 as a Fuel for Dual Fuel Diesel Engine. *Energy Conversion and Management* **2014**, *86*, 39–48. https://doi.org/10.1016/j.enconman.2014.05.016.

(146) Satgé de Caro, P. Interest of Combining an Additive with Diesel–Ethanol Blends for Use in Diesel Engines. *Fuel* **2001**, *80* (4), 565–574. https://doi.org/10.1016/S0016-2361(00)00117-4.

(147) Tutak, W.; Lukács, K.; Szwaja, S.; Bereczky, Á. Alcohol–Diesel Fuel Combustion in the Compression Ignition Engine. *Fuel* **2015**, *154*, 196–206. https://doi.org/10.1016/j.fuel.2015.03.071.

(148) He, B.-Q.; Shuai, S.-J.; Wang, J.-X.; He, H. The Effect of Ethanol Blended Diesel Fuels on Emissions from a Diesel Engine. *Atmospheric Environment* **2003**, *37* (35), 4965–4971. https://doi.org/10.1016/j.atmosenv.2003.08.029.

(149) Curran, S.; Hanson, R.; Wagner, R. Effect of E85 on RCCI Performance and Emissions on a Multi-Cylinder Light-Duty Diesel Engine; 2012. https://doi.org/10.4271/2012-01-0376.

(150) Jeuland, N.; Montagne, X.; Gautrot, X. Potentiality of Ethanol As a Fuel for Dedicated Engine. *Oil & Gas Science and Technology* **2004**, *59* (6), 559–570. https://doi.org/10.2516/ogst:2004040.

(151) Sarathy, S. M.; Farooq, A.; Kalghatgi, G. T. Recent Progress in Gasoline Surrogate Fuels. *Progress in Energy and Combustion Science* **2018**, *65*, 67–108. https://doi.org/10.1016/j.pecs.2017.09.004.

(152) Elwardany, A.; Badra, J.; Sim, J.; Khurshid, M.; Sarathy, M.; Im, H. Modeling of Heating and Evaporation of FACE I Gasoline Fuel and Its Surrogates; 2016. https://doi.org/10.4271/2016-01-0878.

(153) Mati, K.; Ristori, A.; Gaïl, S.; Pengloan, G.; Dagaut, P. The Oxidation of a Diesel Fuel at 1–10atm: Experimental Study in a JSR and Detailed Chemical Kinetic Modeling. *Proceedings of the Combustion Institute* **2007**, *31* (2), 2939–2946. https://doi.org/10.1016/j.proci.2006.07.073.

(154) Herbinet, O.; Pitz, W. J.; Westbrook, C. K. Detailed Chemical Kinetic Mechanism for the Oxidation of Biodiesel Fuels Blend Surrogate. *Combustion and Flame* **2010**, *157* (5), 893–908. https://doi.org/10.1016/j.combustflame.2009.10.013.

(155) Westbrook, C. K.; Naik, C. V.; Herbinet, O.; Pitz, W. J.; Mehl, M.; Sarathy, S. M.; Curran, H. J. Detailed Chemical Kinetic Reaction Mechanisms for Soy and Rapeseed Biodiesel Fuels. *Combustion and Flame* **2011**, *158* (4), 742–755. https://doi.org/10.1016/j.combustflame.2010.10.020.

(156) Lin, R.; Tavlarides, L. L. Thermophysical Properties Needed for the Development of the Supercritical Diesel Combustion Technology: Evaluation of Diesel Fuel Surrogate Models. *The Journal of Supercritical Fluids* **2012**, *71*, 136–146. https://doi.org/10.1016/j.supflu.2012.08.003.

(157) Ahmed, A.; Goteng, G.; Shankar, V. S. B.; Al-Qurashi, K.; Roberts, W. L.; Sarathy, S. M. A Computational Methodology for Formulating Gasoline Surrogate Fuels with Accurate Physical and Chemical Kinetic Properties. *Fuel* **2015**, *143*, 290–300. https://doi.org/10.1016/j.fuel.2014.11.022.

(158) Kabil, I.; Sim, J.; Badra, J. A.; Eldrainy, Y.; Abdelghaffar, W.; Mubarak Ali, M. J.; Ahmed, A.; Sarathy, S. M.; Im, H. G.; Elwardany, A. A Surrogate Fuel Formulation to Characterize Heating and Evaporation of Light Naphtha Droplets. *Combustion Science and Technology* **2018**, *190* (7), 1218–1231. https://doi.org/10.1080/00102202.2018.1444037.

(159) Pati, A.; Gierth, S.; Haspel, P.; Hasse, C.; Munier, J. Strategies to Define Surrogate Fuels for the Description of the Multicomponent Evaporation Behavior of Hydrocarbon Fuels; 2018. https://doi.org/10.4271/2018-01-1692.

(160) Kang, D.; Fridlyand, A.; Goldsborough, S. S.; Wagnon, S. W.; Mehl, M.; Pitz, W. J.; McNenly, M. J. Auto-Ignition Study of FACE Gasoline and Its Surrogates at Advanced IC Engine Conditions. *Proceedings of the Combustion Institute* **2018**. https://doi.org/10.1016/j.proci.2018.08.053.

(161) Sazhina, E. M.; Sazhin, S. S.; Heikal, M. R.; Marooney, C. J. The Shell Autoignition Model: Applications to Gasoline and Diesel Fuels. *Fuel* **1999**, *78* (4), 389–401. https://doi.org/10.1016/S0016-2361(98)00167-7.

(162) Sileghem, L.; Alekseev, V. A.; Vancoillie, J.; Van Geem, K. M.; Nilsson, E. J. K.; Verhelst, S.; Konnov, A. A. Laminar Burning Velocity of Gasoline and the Gasoline Surrogate Components Iso-Octane, n-Heptane and Toluene. *Fuel* **2013**, *112*, 355–365. https://doi.org/10.1016/j.fuel.2013.05.049.

(163) Yu, L.; Mao, Y.; Li, A.; Wang, S.; Qiu, Y.; Qian, Y.; Han, D.; Zhu, L.; Lu, X. Experimental and Modeling Validation of a Large Diesel Surrogate: Autoignition in Heated Rapid Compression Machine and Oxidation in Flow Reactor. *Combustion and Flame* **2019**, *202*, 195–207. https://doi.org/10.1016/j.combustflame.2019.01.012.

(164) Huang, Z.; Xia, J.; Ju, D.; Lu, X.; Han, D.; Qiao, X.; Huang, Z. A Six-Component Surrogate of Diesel from Direct Coal Liquefaction for Spray Analysis. *Fuel* **2018**, *234*, 1259–1268. https://doi.org/10.1016/j.fuel.2018.07.138.

(165) Yaws, C. L. *Transport Properties of Chemicals and Hydrocarbons: Viscosity, Thermal Conductivity, and Diffusivity of C1 to C100 Organics and Ac to Zr Inorganics*; William Andrew: Norwich, NY, 2009.

(166) Mannaa, O.; Mansour, M. S.; Roberts, W. L.; Chung, S. H. Laminar Burning Velocities at Elevated Pressures for Gasoline and Gasoline Surrogates Associated with RON. *Combustion and Flame* **2015**, *162* (6), 2311–2321. https://doi.org/10.1016/j.combustflame.2015.01.004.

(167) Ghosh, P.; Hickey, K. J.; Jaffe, S. B. Development of a Detailed Gasoline Composition-Based Octane Model. *Industrial & Engineering Chemistry Research* **2006**, *45* (1), 337–345. https://doi.org/10.1021/ie050811h.

(168) Qian, Y.; Liu, G.; Guo, J.; Zhang, Y.; Zhu, L.; Lu, X. Engine Performance and Octane on Demand Studies of a Dual Fuel Spark Ignition Engine with Ethanol/Gasoline Surrogates as Fuel. *Energy Conversion and Management* **2019**, *183*, 296–306. https://doi.org/10.1016/j.enconman.2019.01.011.

(169) Kuti, O. A.; Sarathy, S. M.; Nishida, K. Spray Combustion Simulation Study of Waste Cooking Oil Biodiesel and Diesel under Direct Injection Diesel Engine Conditions. *Fuel* **2020**, *267*, 117240. https://doi.org/10.1016/j.fuel.2020.117240.

(170) Department for Transport. Renewable Fuel Statistics 2019 https://www.gov.uk/government/collections/renewable-fuel-statistics (accessed 2019 -09 -20).

(171) Efthymiou, P.; Davy, M. H.; Garner, C. P.; Hargrave, G. K.; Rimmer, J. E. T.; Richardson, D.; Harris, J. An Optical Investigation of a Cold-Start DISI Engine Startup Strategy. In *Internal Combustion Engines: Performance, Fuel Economy and Emissions*; Elsevier, 2013; pp 33–52. https://doi.org/10.1533/9781782421849.1.33.

(172) Petrukhin, N. V.; Grishin, N. N.; Sergeev, S. M. Ignition Delay Time – an Important Fuel Property. *Chem Technol Fuels Oils* **2016**, *51* (6), 581–584. https://doi.org/10.1007/s10553-016-0642-0.

(173) Kobori, S.; Kamimoto, T.; Aradi, A. A. A Study of Ignition Delay of Diesel Fuel Sprays. *International Journal of Engine Research* **2000**, *1* (1), 29–39. https://doi.org/10.1243/1468087001545245.

(174) Richards, K. J.; Senecal, P. K.; Pomraning, E. *CONVERGE CFD*; CONVERGE; Convergent Science: Madison, WI, 2021.

(175) Daïf, A.; Bouaziz, M.; Chesneau, X.; Ali Chérif, A. Comparison of Multicomponent Fuel Droplet Vaporization Experiments in Forced Convection with the Sirignano Model. *Experimental Thermal and Fluid Science* **1998**, *18* (4), 282–290. https://doi.org/10.1016/S0894-1777(98)10035-3.

(176) Wang, L.; Badra, J. A.; Roberts, W. L.; Fang, T. Characteristics of Spray from a GDI Fuel Injector for Naphtha and Surrogate Fuels. *Fuel* **2017**, *190*, 113–128. https://doi.org/10.1016/j.fuel.2016.11.015.

(177) Amsden, A. A.; O'Rourke, P. J.; Butler, T. D. *KIVA-II: A Computer Program for Chemically Reactive Flows with Sprays*; LA-11560-MS, 6228444; 1989; p LA-11560-MS, 6228444. https://doi.org/10.2172/6228444.

(178) Amsden, AA. *KIVA-3V, RELEASE 2, IMPROVEMENTS TO KIVA-3V*; KIVA-3V; RELEASE 2; Los Alamos National Laboratory: University of California, 1999.

(179) Post, S. L.; Abraham, J. Modeling the Outcome of Drop–Drop Collisions in Diesel Sprays. *International Journal of Multiphase Flow* **2002**, *28* (6), 997–1019. https://doi.org/10.1016/S0301-9322(02)00007-1.

(180) Naser, N.; Jaasim, M.; Atef, N.; Chung, S. H.; Im, H. G.; Sarathy, S. M. On the Effects of Fuel Properties and Injection Timing in Partially Premixed Compression Ignition of Low Octane Fuels. *Fuel* **2017**, *207*, 373–388. https://doi.org/10.1016/j.fuel.2017.06.048.

(181) An, Y.; Jaasim, M.; Vallinayagam, R.; Vedharaj, S.; Im, H. G.; Johansson, Bengt. Numerical Simulation of Combustion and Soot under Partially Premixed Combustion of Low-Octane Gasoline. *Fuel* **2018**, *211*, 420–431. https://doi.org/10.1016/j.fuel.2017.09.064.

(182) Bertoli, C.; Migliaccio, M. na. A Finite Conductivity Model for Diesel Spray Evaporation Computations. *International Journal of Heat and Fluid Flow* **1999**, *20* (5), 552–561. https://doi.org/10.1016/S0142-727X(99)00044-2.

(183) Abdelghaffar, W. A.; Elwardany, A. E.; Sazhin, S. S. Modeling of the processes in diesel engine-like conditions: Effects of fuel heating and evaporation. *Atomiz Spr* **2010**, *20* (8), 737–747. https://doi.org/10.1615/AtomizSpr.v20.i8.50.

(184) Gusev, I. G.; Krutitskii, P. A.; Sazhin, S. S.; Elwardany, A. E. New Solutions to the Species Diffusion Equation inside Droplets in the Presence of the Moving Boundary. *International Journal of Heat and Mass Transfer* **2012**, *55* (7–8), 2014–2021. https://doi.org/10.1016/j.ijheatmasstransfer.2011.12.001.

(185) Sazhin, S. S.; Shishkova, I. N.; Al Qubeissi, M. A Self-Consistent Kinetic Model for Droplet Heating and Evaporation. *International Journal of Heat and Mass Transfer* **2016**, *93*, 1206–1217. https://doi.org/10.1016/j.ijheatmasstransfer.2015.10.039.

(186) Sazhin, S. S.; Shishkova, I. N.; Al Qubeissi, M. Heating and Evaporation of a Two-Component Droplet: Hydrodynamic and Kinetic Models. *International Journal of Heat and Mass Transfer* **2014**, *79*, 704–712. https://doi.org/10.1016/j.ijheatmasstransfer.2014.08.026.

(187) Sazhin, S. S.; Kristyadi, T.; Abdelghaffar, W. A.; Heikal, M. R. Models for Fuel Droplet Heating and Evaporation: Comparative Analysis. *Fuel* **2006**, *85* (12–13), 1613–1630. https://doi.org/10.1016/j.fuel.2006.02.012.

(188) Sazhin, S. S.; Al Qubeissi, M.; Heikal, M. R. Modelling of Spherical Automotive Droplet Heating and Evaporation: Recent Developments. In *Proceeding of Proceedings of CHT-17 ICHMT International Symposium on Advances in Computational Heat Transfer May 28-June 1, 2017, Napoli, Italy*; Begellhouse: Napoli, Italy, 2017; pp 951–954. https://doi.org/10.1615/ICHMT.2017.1030.

(189) Zubkov, V. S.; Cossali, G. E.; Tonini, S.; Rybdylova, O.; Crua, C.; Heikal, M.; Sazhin, S. S. Mathematical Modelling of Heating and Evaporation of a Spheroidal Droplet. *International Journal of Heat and Mass Transfer* **2017**, *108*, 2181–2190. https://doi.org/10.1016/j.ijheatmasstransfer.2016.12.074.

(190) Abramzon, B.; Sazhin, S. Droplet Vaporization Model in the Presence of Thermal Radiation. *International Journal of Heat and Mass Transfer* **2005**, *48* (9), 1868–1873. https://doi.org/10.1016/j.ijheatmasstransfer.2004.11.017.

(191) Shishkova, I. N.; Sazhin, S. S. A Solution of the Boltzmann Equations in the Presence of Three Components and Inelastic Collisions. *International Journal of Heat and Mass Transfer* **2014**, *71*, 26–34. https://doi.org/10.1016/j.ijheatmasstransfer.2013.11.032.

(192) Antonov, D. V.; Fedorenko, R. M.; Strizhak, P. A.; Castanet, G.; Sazhin, S. S. Puffing/Micro-Explosion of Two Closely Spaced Composite Droplets in Tandem: Experimental Results and Modelling. *International Journal of Heat and Mass Transfer* **2021**, *176*, 121449. https://doi.org/10.1016/j.ijheatmasstransfer.2021.121449.

(193) Kim, H.; Baek, S. W. Combustion of a Single Emulsion Fuel Droplet in a Rapid Compression Machine. *Energy* **2016**, *106*, 422–430. https://doi.org/10.1016/j.energy.2016.03.006.

(194) Zhu, C.; Li, G.; Xing, Y.; Gui, X. Adhesion Forces for Water/Oil Droplet and Bubble on Coking Coal Surfaces with Different Roughness. *International Journal of Mining Science and Technology* **2021**, *31* (4), 681–687. https://doi.org/10.1016/j.ijmst.2021.03.002.

(195) Rimbert, N.; Castrillon Escobar, S.; Meignen, R.; Hadj-Achour, M.; Gradeck, M. Spheroidal Droplet Deformation, Oscillation and Breakup in Uniform Outer Flow. *J. Fluid Mech.* **2020**, *904*, A15. https://doi.org/10.1017/jfm.2020.675.

(196) Tonini, S.; Cossali, G. E. An Analytical Model for the Evaporation of Multi-Component Spheroidal Drops Based on Stefan–Maxwell Equations. *International Journal of Thermal Sciences* **2022**, *171*, 107223. https://doi.org/10.1016/j.ijthermalsci.2021.107223.

(197) Al Qubeissi, M.; Wang, G.; Al-Esawi, N.; Rybdylova, O.; Sazhin, S. S. The Heating, Evaporation and Combustion of Kerosene Droplets in a Gas-Turbine Combustor: CFD Modelling Using the Discrete Component Approach. In *7th International Fuels, Combustion and Fire Conference in Engineering (FCE 19)*; Antalya, Turkey, 2019.